Centro de Estudios Interdisciplinarios

Universidad Nacional de Rosario

Tesis de Doctorado

Alpha-synuclein amyloid aggregation: From basic to translational research

Presentada por Biol. Fiamma Ayelén Buratti

Rosario, Argentina

2024

Alpha-synuclein amyloid aggregation: From basic to translational research

Fiamma Ayelen Buratti
Bióloga
Centro de Estudios Interdisciplinarios
Universidad Nacional de Rosario

Esta tesis es presentada como parte de los requisitos para optar por el grado académico de Doctor en Biociencias Molecular y Biomedicina, de la Universidad Nacional de Rosario. La misma contiene los resultados obtenidos en investigaciones llevadas a cabo en Laboratorio Max Planck de Biología Estructural, Química y Biofísica Molecular de Rosario (MPLbioR, UNR-MPINAT) bajo la dirección de Prof. Dr. Claudio O. Fernández y en el laboratorio de Biología Estructural Traslacional (DZNE) bajo la supervisión de Dr. Markus Zweckstetter.

Affidavit

I hereby declare that the doctoral thesis entitled “Alpha-synuclein amyloid aggregation: From basic to translational research” has been written independently, with no other sources and aids than quoted.

Fiamma Ayelen Buratti Rosario, March 2024

Acknowledgements

I would like to thank Prof. Dr. Claudio Fernandez for his supervision, for giving me the chance to work with his team and learn a wide range of technic in his laboratory, and for always being present in any difficult steps of my PhD. I believe that without his support I wouldn't be where I am. Thanks for your understanding over all these years, and your tireless fight against the bureaucratic system of the two countries (I know it not has been easy to be in charge of all the challenges of the Binational Program). Thanks for believing in me, and always giving me hope about the best way to make science. Thanks for opening your house to us, for being confident, and always willing to help with everything, even our problems outside of work. Thanks for being worried about my development in science. I will always be thankful for your efforts in my trip, scholarship in Germany, and the many problems that we go through together.

I would also like to thank Prof. Dr. Markus Zweckstetter for giving me the chance to join his research group, you pushed me to face many challenges up, that I would never have imagined. I had the best memories of the entire group in the DZNE.

Thanks go as well to Prof. Dr. Reinhard Jahn for his scientific advice and support, and the additional members of my examination board: Dr. Eduardo Ceccarelli, Dr. Lisandro Falomir Lockhart, and Dr. Kai Tittmann.

I would also like to thank Prof. Griesinger and Prof. Dr. Claudio Fernández for establishing the German-Argentine doctoral program, it is a great opportunity for students like me, to be part of the best teams around the world. I am very grateful to have in Argentina a laboratory where I developed my career, at the same level as in Germany. I will always be thankful to live in Göttingen, and to learn more about cultures, language, their food; I loved the city and all the facilities that it offered me. I felt very welcomed, and it was one of my unforgettable experiences.

From Göttingen, I would like to thank Sol and Conny, you were my best support in the team. Thanks for your time and patience in explaining everything in the lab, as well as how to afront the German system.
Conny, I will never forget your interest in knowing if I feel comfortable and your advice for my stay there. Every conversation that we had, every adventure making crafts for the graduated students, or our boat trip, taught me that Germans are not as cold as we believe…
Sol, thank God you speak Spanish! You were my life jacket many times, to be honest, I don't remember the times that I cried in front of you! You pushed me to go on with everything and gave me the exact words from your experience. Thanks for every Thursday's breakfast, for your laugh, and your huge knowledge of science. Thanks for all the adventures together, there are dozens, and in all of them, I remember us very happy.

Thanks Alain, I learnt a lot about science with you, always open to explaining the minimal detail, thanks for giving me your time to sit next to me and teach me, that is invaluable. Thanks also because our talks were not only about science, our discussions about news, history, economics, everything. Finding someone like you, who allowed me to grow up in all aspects, is unique.

A very thanks go to all the people from both labs, for the support, scientific discussions, and recommendations, that have enabled me to achieve my goals. Thanks to Phelippe, Nicola, David, Pijush, Tina, Anton, Lisa, Debdeep, Reshma, Maria, Christian, Matthew, Irina, Zheng, Shannon, Aleksandra, Gonzalo.

Thanks to the valuable administrative support: Laura, you make all the administration stuff easier, and calm down every stressful moment about forms. Thanks as well to Amalia, Petra, Dirk, Ulrike and Daniel.

Thanks as well to all my family in Germany: my Argentinian friends who were very warm, and gave the love necessary to afront being far away from my home country and my family. Thanks to Hugo, Fer, Romi, Fede, Gabi, Sabri, Rodri, Flor, Mati, Sebas.

Thanks also Bioturros, my university friends, it has been more than 10 years and still we are in touch and meeting in our city: Cordoba. Many of us are in the same moment, i.e., thesis defense, and I am very glad to share all the feelings and uncertain future together!
Flor, thanks for living the German experience with me, but special mention for your unconditional support. You are my inspiration, that if I want something, I can get it. Your energy and commitment to fighting for all that you deserve is inspiring to me. I hope to be 10% as you are. Your friendship is one of my most valuable things.

Thanks to my friends from Rosario, Poly and Max, even I was almost two years abroad, they supported me by video call and waited to share more moments in this beautiful city. I know that they don't understand anything about my job, but they always listen and buy me a beer to afront my disappointments and celebrate my achievements.

Thanks to Ana, my English teacher, your energy, passion and empathy, make this way easy. I wouldn't be writing right now without your help. Thanks for this virtual relationship and for not giving up with a student like me.

In the end, but not less importantly, my family. *Mami* and *Lenchu*, it was a hard time for us, we lived in different cities and even countries, and I could only visit a few times during my PhD, but your company during this time is incomparable. Brother, I am here, because you gave me all the necessities to finish my university degree, and because you always believe in me. I hope in the future to help you thousands of times, more than you did. *Papi,* your desire was always to be able to see your children finish university because you didn't have that possibility. I am here, finishing a PhD, and I went further than you could imagine, I hope you are proud of me from the sky. I've done this for you.

Gracias, Thanks, Danke.

Table of Contents

List of Figures

List of tables

List of Abbreviations

2D	Two dimensional
AAO	Age at onset
ac-Lys	Acetylated lysines
AFM	Atomic force microscopy
aSyn	Alpha-synuclein
CBP	CREB-binding protein
CCPN	Collaborative Computing Project for NMR
CD	Circular dichroism
D_2O	Deuterated water
DAPI	4′,6-diamidino-2-phenylindole
DMEM	Dulbecco's Modified Eagles Medium
DMSO	Dimethyl sulfoxide
DNA	Deoxyribonucleic acid
DOPC	1,2-dioleoyl-sn-glycero-3-phosphocholine
DOPE	1,2-dioleoyl-sn-glycero-3-phosphoethanolamine
DOPS	1,2-dioleoyl-sn-glycero-3-phospho-L-serine
DTT	Dithiothreitol
E. *coli*	*Escherichia coli*
EDTA	Ethylenediaminetetraacetic acid
TEM	Transmission electron microscopy
HD	Hydrogen deuterium
HEPES	4-(2-hydroxyethyl)-1-piperazineethanesulfonic acid
HSQC	Heteronuclear single quantum coherence
IDP	Intrinsically disordered proteins
IPTG	Isopropyl-1-thio-β-D-galactopyranoside
Kd	Dissociation constant
LB	Luria-Bertani
MES	2-Morpholinoethanesulphonic acid
NAC	Non-Ab component
NAC	Non-amyloid-β component
NDs	Neurodegenerative diseases

NMR	Nuclear Magnetic Resonance
ºC	Celcius degree
OD	Optical density
p300	histone acetyltransferase
PBS	Phosphate buffered saline
PcTS	Phthalocyanine tetrasulfonate
PD	Parkinson's disease
PFA	Paraformaldehyde
PMSF	Phenylmethylsulfonyl fluoride
PTMs	Post-translational modifications
rcf	Relative centrifugal force
RIPA	radioimmunoprecipitation assay
SDS-PAGE	Sodium dodecyl-sulfate polyacrylamide gel electrophoresis
SN	Supernatant
SNCA	Gene encoding for alpha-synuclein
SNARE	Soluble N-ethylmaleimide sensitive factor activating protein receptor
SUV	Small unilamellar vesicles
Synph	Synphilin-1
SynT	C-terminally modified variant of alpha-synuclein
ThT	Thioflavin T fluorescence
TRIS	2-Amino-2-hydroxymethyl-propane-1,3-diol
UV	Ultraviolet
wt	Wild type

Abstract

Neurodegenerative diseases are a heterogeneous group of disorders affecting the lives of millions of people worldwide. A shared pathologic hallmark is the appearance of insoluble aggregates in the brain. The components of these are different, given a wide spectrum of neurodegenerative diseases. The presence of amyloid fibrils of specific proteins in the deposits allowed the identification of proteins involved in the development of the disease, and their study *in vitro*.

Parkinson's disease is considered a neurological disorder where spherical intraneuronal inclusions known as Lewy bodies are found in brain regions. The determination of inherited mutations has aided the research of alpha-synuclein, as one protein involved in the misfolding and deposition into Lewy bodies. Alpha-synuclein is an intrinsically disordered protein, found free or bound to membranes under physiological conditions. However, in pathological conditions adopt β-sheet conformations, resulting in amyloid fibrils.

Many factors are modulating the pathways mentioned before, such as some regions of the protein, point mutations, and post-translational modifications. The physiological conditions could be addressed following the interaction of monomers with membranes, as one model for gaining knowledge in parameters such as membrane affinity, membrane-bound conformations, and even residues involved in the binding. Amyloid fibrils of alpha-synuclein can be generated *in vitro*, and be able to uncover fibril core, specific residues implicated in the aggregation process, stability and structure of fibrils. These tools permit the study of how different factors affect the physiological and pathological condition.

Our study aimed to unravel the aggregation properties of alpha-synuclein through the characterization of conformational assemblies, as well as in terms of binding properties. Key factors in this process have been studied. A combination of kinetics assays, nuclear magnetic resonance, circular dichroism, dynamic light scattering, cell culture, fluorescent probes, electron and atomic force microscopy, was chosen to gain insight into all the features investigated.

Structural changes induced for point mutations or post-translational modifications gave relevance to the implication of residue-specific in the pathological and functional state of the protein. We observed how particular

amino acids can impair the in vitro amyloid assembly and even impact the binding to membranes. These factors are likely modulating structural conformations, that may be attributed then to the variety of alpha-synucleinopathies.

The work presented here is a step forward towards understanding the role of alpha-synuclein in the pathology of Parkinson's disease.

Resumen

Enfermedades neurodegenerativas son un grupo heterogéneo de desórdenes que afectan la vida de millones de personas. Un marcador patológico compartido es la presencia de agregados insolubles en el cerebro. Los componentes de estos son diferentes, dando un gran espectro de enfermedades neurodegenerativas. La presencia de fibras amiloides de específicas proteínas en los depósitos permite la identificación de proteínas involucradas en el desarrollo de la enfermedad, y su estudio *in vitro*.

La enfermedad de Parkinson es considerada un desorden neurológico donde inclusiones intraneuronales esféricas conocida como cuerpos de Lewy son encontrados en regiones del cerebro. La determinación de mutaciones heredadas ha ayudado la investigación de alfa sinucleina como una proteína involucrada en el mal plegamiento y deposición en cuerpos de Lewy. Alfa sinucleina es una proteína intrínsicamente desordenada, se encuentra libre y unida a membranas bajo condiciones fisiológicas. Sin embargo, en condiciones patológicas adopta conformaciones hojas beta, resultando en fibras amiloides.

Muchos factores están modulando las vías mencionadas antes, como algunas regiones de la proteína, mutaciones puntuales, y modificaciones post traslacional. Las condiciones fisiológicas pueden ser estudiadas a través de la interacción de monómeros con membranas *in vitro*, como un modelo para ganar más conocimiento en parámetros como afinidad y conformaciones unidas a membrana, e incluso residuos involucrados en la unión. Fibras amiloides de alfa sinucleina pueden ser generadas in vitro, para poder descubrir el *core* fibrilar, residuos específicos implicados en el proceso de agregación, estabilidad y estructura de fibras. Estas herramientas permiten el estudio de como diferentes factores afectan las condiciones fisiológicas y patológicas.

Nuestro estudio ayudó a discernir los procesos de agregación de alfa sinucleina a través de la caracterización de ensambles conformacionales, como así también en términos de propiedades de unión. Factores claves en este proceso han sido estudiadas. Una combinación de ensayos de cinética, resonancia magnética nuclear, dicroísmo circular, dispersión dinámica de la luz,

cultivo celular, moléculas fluorescentes, y microscopia electrónica y de fuerza atómica, fue elegido para investigar todas estas características.

Cambios estructurales inducidos por mutaciones puntuales o modificaciones post traslacional dio relevancia a la implicación de residuos específicos en el estado patológico y funcional de la proteína. Nosotros observamos como aminoácidos particulares pueden impactar el ensamble amiloide *in vitro* e incluso la unión a membranas. Estos factores están probablemente modulando conformaciones estructurales, que pueden ser atribuidos luego a la variedad de alfa sinucleinopatias.

El trabajo presentado aquí es un paso hacia adelante en el entendimiento del rol de la alfa sinucleina en la patología de la enfermedad de Parkinson.

1. Introduction

1.1. Neurodegenerative diseases and the case of Parkinson's disease

1.1.1. Neurodegenerative diseases

Neurodegenerative diseases (NDs) are characterized by the accumulation of specific proteins within neurons (Figure 1). Neurodegenerative diseases affect millions of people worldwide and occur when cells in the brain or peripheral nervous system die. The likelihood of developing a neurodegenerative disease rises dramatically with age[1].

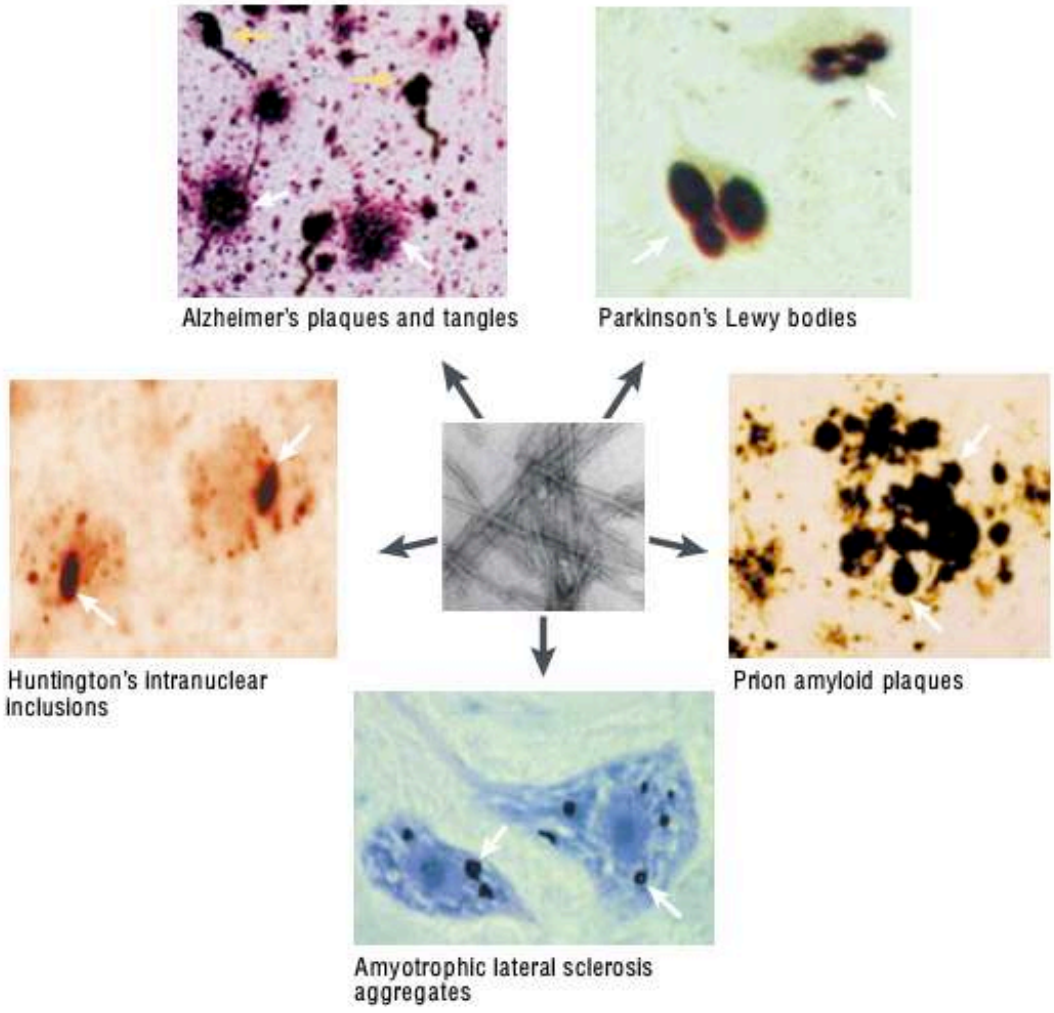

Figure 1: Different aggregates in neurodegenerative diseases. From reference 3.

Many hallmarks defining neurodegenerative diseases are[2] :

- Neuronal cell death
- Inflammation
- DNA and RNA defects
- Aberrant proteostasis
- Synaptic and neuronal network defects
- Cytoskeletal abnormalities
- Altered energy homeostasis
- Pathological protein aggregation

Focusing on the last one, despite the different proteins involved in several NDs, misfolding and aberrant accumulation of specific proteins is a shared feature[3] (Table 1).

Table 1: Overview of several neurodegenerative diseases and their related protein.

Neurodegenerative diseases	**Aggregating protein(s)**
Alzheimer's disease[4]	Amyloid beta peptide; Tau
Parkinson's disease[5]	α-synuclein
Huntington's disease[6]	Huntingtin protein
Amyotrophic lateral sclerosis[7]	Superoxide dismutase 1
Spongiform encephalopathies[8]	Prion proteins

1.1.2. Protein folding and misfolding

The folding of proteins is one of the biological processes in the cell, where a polypeptide chain folds into a specific three-dimensional protein structure that corresponds to the most thermodynamically stable one under physiological conditions[9].

In a cell, the proteins are synthesized in the ribosome from the DNA. Afterwards, in the cytoplasm or some cellular compartments (such as the endoplasmatic reticulum or mitochondria) the protein folds. Molecular chaperones work to achieve their proper structure, stabilization and prevent

misfolding; for example, HSP70, HSP90 and other small heat shock proteins can prevent neurodegeneration by regulating alpha-synuclein (aSyn) misfolding, oligomerization and aggregation[10].

However, what happens when proteins are misfolded? The proteasome is a cellular machinery responsible for protein degradation, as well as autophagy, where protein misfolded is sequestered in autophagosomes and delivered to lysosomes for their degradation. Despite the efforts of the cell for their degradation, when this process is inefficient the misfolded proteins increase their levels significantly and become prone to aggregate. Many neurodegenerative diseases such as Alzheimer's disease[4], Huntington's disease[6], Creutzfeldt-Jakob disease[8] and Parkinson's disease[5] are also named *proteinopathies* for this common hallmark.

1.1.3. Parkinson's disease

It has been more than 200 years since James Parkinson wrote "An Essay on the Shaking Palsy 1817" where he described the symptoms and features of a neurological disorder that would later be named Parkinson's disease in honour of the author[5]. His work was groundbreaking, but it took several decades to fully appreciate the significance of his observations. In the 19's decade, Fritz Lewy described spherical intraneuronal inclusions in the dorsal nucleus of the vagus nerve and in the substantia innominate, which after were recognized as Lewy bodies[11]. It was not until 1997 that Polymeropoulos et al. attributed mutations in the gene encoding for aSyn (SNCA) to dominantly inherited forms of PD[12]. Subsequently, aSyn was demonstrated to be the major constituent of Lewy bodies[13] (Figure 2).

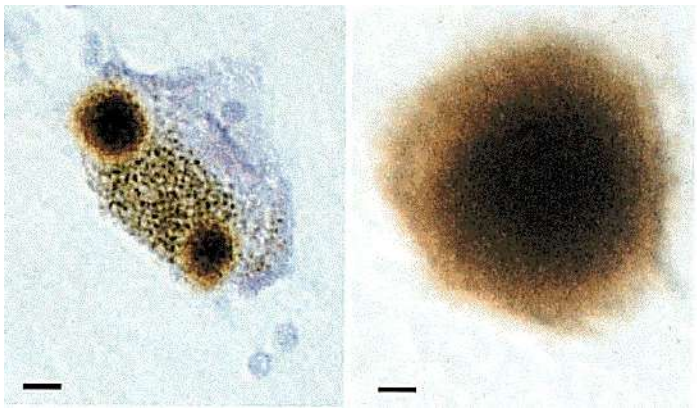

Figure 2: Alpha-synuclein into Lewy bodies. Nerve cell with two alpha-synuclein positive Lewy bodies (left) Scale bar, 20 μm and an extracellular Lewy body (right) Scale bar, 4 μm. From reference 13.

Parkinson's disease is a sporadic and genetic disorder, in which involved autosomal dominant genes (SNCA, LRRK2, and VPS35) and autosomal recessive genes (PRKN, PINK1, and PARK7) are involved. In addition, gene GBA1 and other series of genes reported in small numbers of families are linked with Parkinson's disease[14].

SNCA mutations and gene multiplications led to the identification of the protein aSyn as the hallmark component in Lewy bodies and Lewy neurites, whereas the increase in the level of expression of this protein is sufficient to develop Parkinson's disease.

The identification of mutation on the SNCA gene has allowed the understanding of the molecular mechanism behind the pathology. The neuronal loss and the formation of proteinaceous aggregates in neurons of the substantia nigra are the end phase of the disease. However, with the passing of years, researchers have studied the reverse way to discover the initial steps of the disease.

1.2. Alpha-synuclein and its role in Parkinson's disease

1.2.1. Alpha-synuclein

Intrinsically disordered proteins (IDP) are unable to fold spontaneously into stable, well-defined, globular three-dimensional structures. They are

characterized as being dynamically disordered and fluctuate through a range of conformations.

Alpha-synuclein (aSyn) is considered to be a monomeric intrinsically disordered protein. Under physiological conditions the protein is found in two states: as free monomeric species and as membrane-bound forms, with the population of both states co-existing in equilibrium inside the neuron[15].

Synuclein was discovered by Maroteaux et al. when it was isolated from the electric fish *Torpedo californica* as a protein in the presynaptic nerve terminals[16].

1.2.2. Structural properties of aSyn

The primary structure of human aSyn comprises 140 amino acids distributed in three regions: the amphipathic N-terminus (residues 1-60), implicated in lipid binding[17]; the central region known as NAC (residues 61-95), which is highly hydrophobic and fibrillogenic[18,19]; and the acidic C-terminus (residues 96-140), critical for blocking rapid aSyn filament assembly[20–22] (Figure 3a);

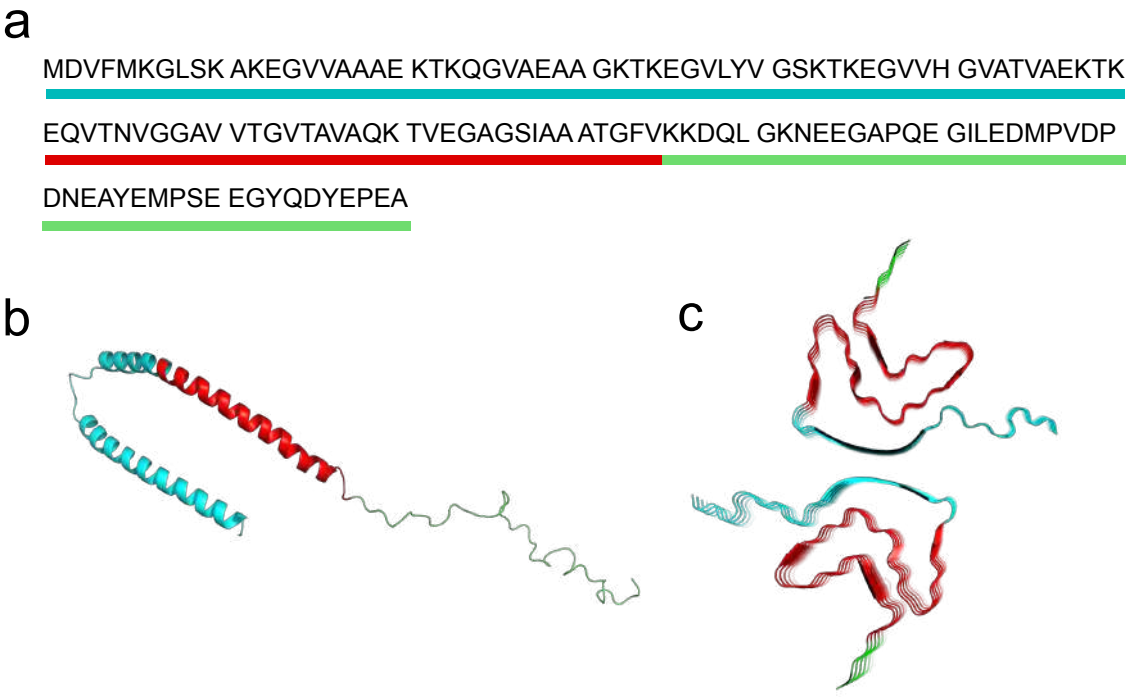

Figure 3: Alpha-synuclein sequence and structures related to function and dysfunction. a) Human aSyn sequence, amphipathic N-terminal region underlined in cyan, NAC region in red

and acidic C-terminus in green. b) Cartoon representation of human micelle-bound aSyn (PDB: 1XQ8[23]) c) Cryo-EM structure of alpha-synuclein fibrils (PDB: 6A6B[24]).

The protein exhibits transient long-range interactions between N- and C-terminal residues which are of electrostatic nature, whereas the C terminus and the NAC regions display hydrophobic interactions[25]. These intramolecular contacts stabilize monomer aggregation-autoinhibited conformations.

1.2.3. The physiological function of aSyn

Alpha-synuclein has been found in presynaptic sites and interacting with membranes; for this reason, it has been attributed to have a role in synaptic functions[26], including neurotransmitter release, endocytosis[27] and plasticity[28].

Native aSyn exists as an unfolded structure but may acquire different structures and functions *in vivo*. Studies showed that it adopts an alpha helix structure where it is in contact with the hydrophobic surface of a lipid or micelle, due to the 11-mer repeat-containing sequences that adopt right-handed coiled coil conformations[17] (Figure 3b). In this way, aSyn could interact with synaptic vesicles and act as an intermediate between the SNARE complex and the plasma membrane[29,30].

Fusco et al. proposed a model that described the interaction of aSyn with membranes (Figure 4), in which there are three distinguished regions: the first 25 residues with a role as “anchoring segment” independent of lipid composition; then the region between residues 26 – 97, that is being considered to act as a “membrane-sensor region”, having a role in the affinity of aSyn for lipid membranes and modulating the free-bound membrane state; and finally the C-terminal domain that has only weak and transient interactions with the lipid surface[31].

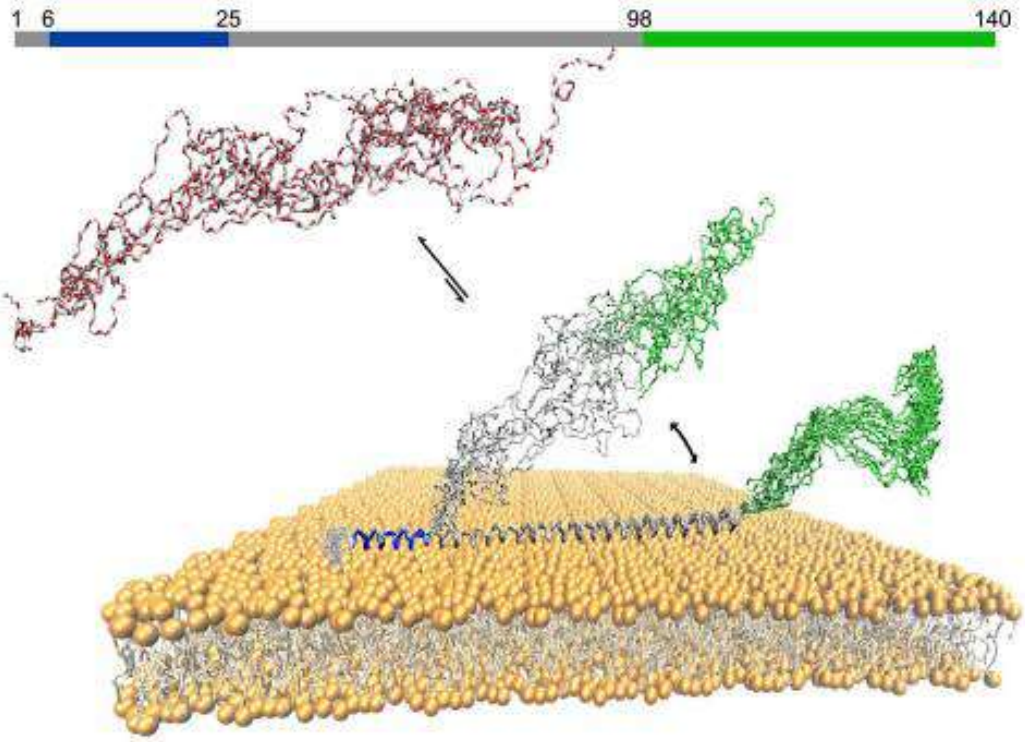

Figure 4: Model of three regions of alpha-synuclein modulating the interaction with membranes. From reference 31.

Alpha-synuclein interacts with a wider variety of cellular membranes, where the lipids composition and curvature are different, and influence the affinity and helical conformations adopted by the protein.

Two helical conformations have been observed for the membrane-bound state of aSyn (Figure 5c); one of them is an extended-helix conformation,[32,33] where the first 100 residues remain bound to lipids, and another is a helix-broken conformation,[34] where two antiparallel helices are separated by a non-helical linker spanning residues 39-45. The different binding modes and their associated structures would be related to different molecular mechanisms in which the protein is involved, where requirements such as size and lipid composition of the vesicles influence the structural features of its membrane-bound state.

A general idea about the interaction is that the helix lies on the surface of the lipids (Figure 5a), and Lys residues are oriented perpendicular to the helical axis (Figure 5b), allowing the interaction with negatively charged phospholipid groups, where hydrophobic residues are lipid-exposed, and negatively charged residues appear located on the outside surface of the helix[33].

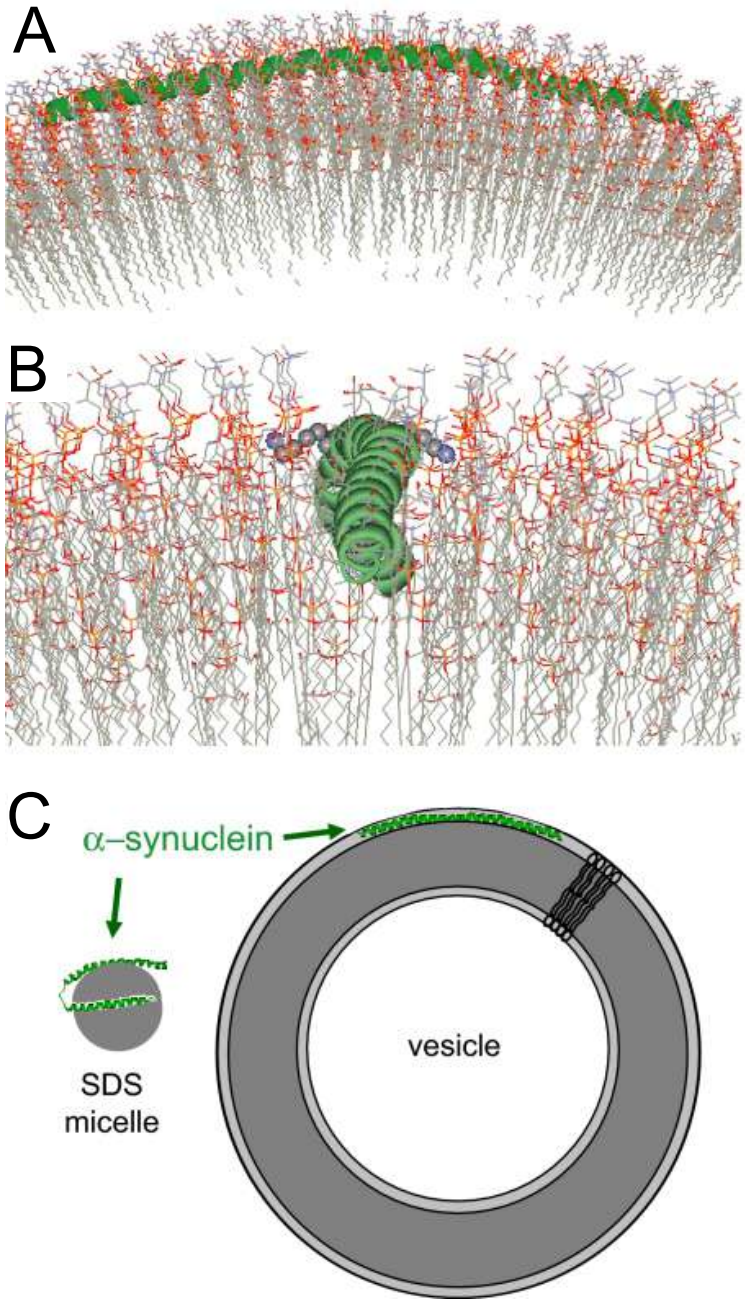

Figure 5: Disposition of alpha-synuclein bound to liposomes. a) Cross-sectional view of the aSyn molecule interacting with the surface of the vesicle. b) The N terminus of the α-helix is in the foreground. Lysine residues at position 58 (oriented to the right of the helix) and 60 (oriented to the left) are shown in space-filling format. The image indicates the proximity of the positively charged lysine side chains to the negatively charged phosphate groups. c) Cartoon representations of the structures of aSyn on micelles and SUVs. Modified from reference 33.

1.2.4. The pathological conformation of aSyn

In the aggregation landscape, aSyn can adopt several conformations rich in β-sheet as amyloid fibrils (Figure 3c) and intermediates (oligomers[35], ring-like oligomers, protofibrils).

In vitro, aSyn fibril formation is monitored by using the fluorescent dye Thioflavin-T[36]. The aggregation kinetics have three phases: the lag phase (is the time to detect a change in the fluorescence), the exponential growth phase (fibrils are growing, and include the $T_{1/2}$, which is the time to reach half of the maximum fluorescence), and saturation or plateau phase (time to reach the maximum fluorescence and include the T_{max}).

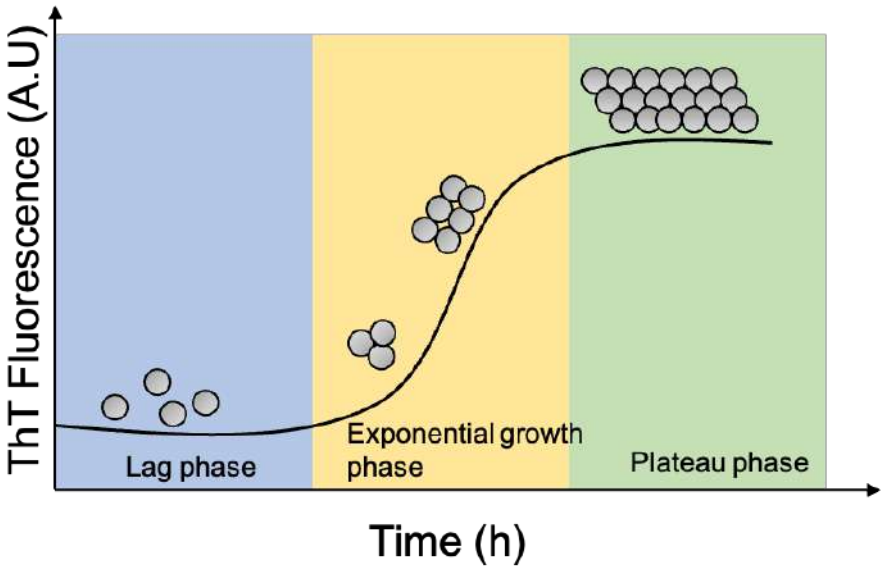

Figure 6: Aggregation kinetics of aSyn. The three phases are highlighted, the lag phase (blue area) where the monomers are in solution, the exponential growth phase (yellow area) where monomers assemble into oligomers and protofibrils, and the plateau phase (green area) where mature fibrils are formed.

Several steps are included in the aggregation process of aSyn: primary nucleation, elongation and secondary nucleation. First, monomers are in solution and start the nucleation, where monomers assemble into oligomers (the association of a few monomeric units); this involves a conformational change of unstructured aSyn into structured intermediates that can aggregate[37]. The second step is elongation, when free monomer binds to the ends of nuclei,

resulting in fibril formation. Secondary nucleation refers to the creation of new aggregates from pre-existing ones (called seeds).

Oligomers are composed of a small number of monomers, are soluble and usually unstable because their structures change rapidly; if they tend to form fibrils are considered on-pathway oligomers, but if cannot form fibrils are called off-pathway oligomers. A research group discovered that the structure of oligomers adopts an antiparallel β-sheet organization, and arrangement different than fibrils which adopt a parallel-sheet structure[38]

The core of aSyn fibrils was studied by Hydrogen-Deuterium Exchange NMR and revealed that the solvent-protected core of aSyn fibrils comprises residues 30-110, where the first 30 residues as the last 30 are not involved in secondary structure[39].

Techniques such as Cryo-EM allowed recently the determination of the fibril structure formed by recombinant full-length aSyn with N-terminal acetylation[24]. The fibril is composed of two protofilaments, including residues 37-99 with a Greek key-like topology, the hydrophobic residues fold inside to form a stable core and the hydrophilic residues at the periphery. The interface is composed of residues 50-57, stabilized by electrostatic interactions between residues K45, H50 and E57.

Equally important, the interaction of aSyn with lipids has been associated with the physiological function of the protein. Interestingly, Lewy bodies are composed as well of a large quantity of lipids. By using correlative light, electron microscopy and tomography to analyze postmortem human brain tissue from Parkinson's disease brain donors, Shahmoradian and colleagues observed the presence of inclusion clusters of membrane fragments, dysmorphic mitochondria, lysosomes, etc[40]. Another research group showed distinct cryo-EM structures of lipidic aSyn fibrils[41] due to the act that protein has been implicated in lipid extraction[42] and a co-aggregation with aSyn fibrils[43]. Further studies in the modulation of lipid-fibril interactions could help resolve new structures of fibrils according to the environment in which they are formed.

Galvagnion et al. showed that the presence of SUVs can enhance the rate of the essential primary nucleation step that initiates amyloid formation by three orders of magnitude or more. They proposed that primary nucleation occurs on the vesicle surfaces on which aSyn is bound[44]. A possible

explanation is that due to the high local concentration of protein molecules at the surface of the vesicle, aSyn might adopt different conformations which could enhance the primary nucleation process[31].

To gain insight into the 3D-structure and orientation of lipid-bound aSyn, a research group performed interface-specific vibrational sum-frequency generation (VSFG) experiments with MD simulations to determine the molecular conformations of aSyn. The study shows that an upright conformation is formed at high concentrations of aSyn, in which the aggregation-prone NAC regions come closer and enhance intermolecular contacts[45] (Figure 7).

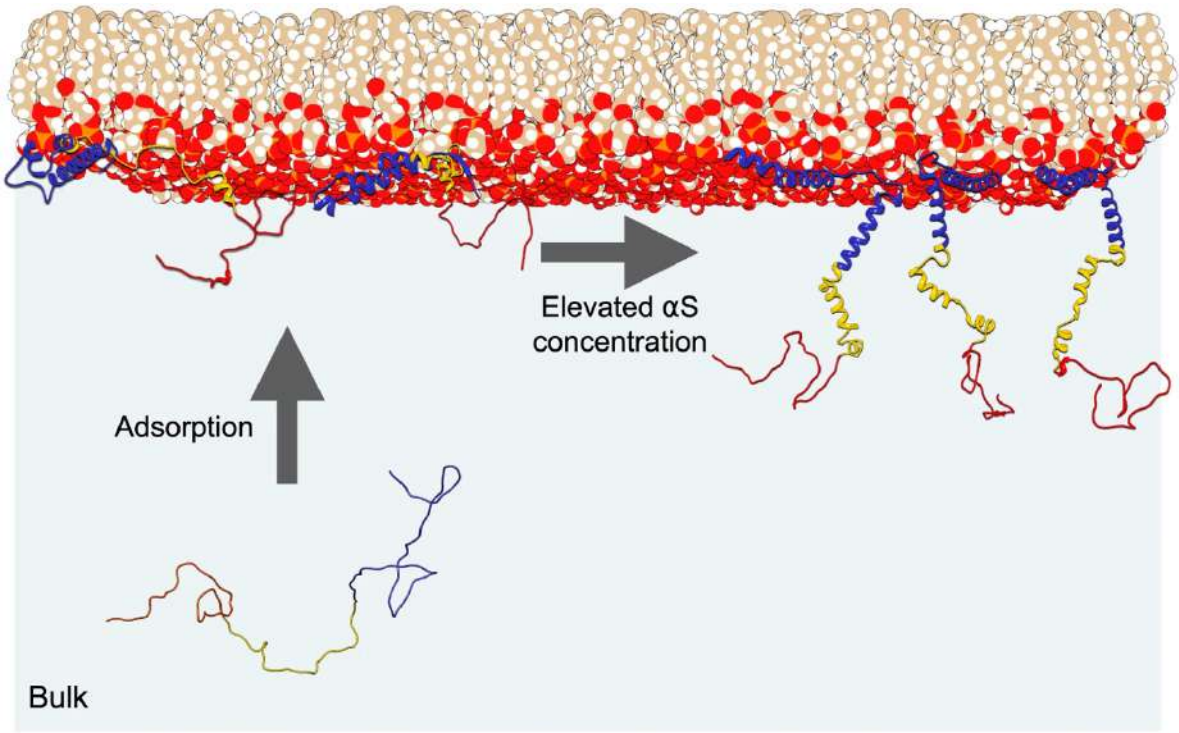

Figure 7: Model of Up-right conformation of aSyn. At low concentrations, aSyn converts from a randomly-coiled structure to an α-helical structure after adsorption to the lipid membrane. The protein adopts an upright orientation at higher concentrations. From reference 44.

1.3. Factors modulating physiological and pathological pathways of aSyn

1.3.1. Hot sites as tools to uncover function and pathogenesis.

The interest in several segments of the protein as new therapeutic approaches has increased in the last few years. These relevant regions are usually known as aggregation “hot spots”, and their studies become critical to identify determinant factors governing protein aggregation and reveal specific interactions that must be disrupted to prevent amyloid assembly. For example, NAC flanking regions have been demonstrated to act as a modulator of aSyn aggregation[46]. This knowledge can be used for therapeutic intervention by targeting the aggregation pathway of these proteins and their associated toxicity[47] .

Studies have shown that the region consisting of residues 36–42 is important in promoting aSyn aggregation. Deletion of this region prevents the formation of amyloid fibrils, by affecting specific interactions with other regions and altering the spacing of the KTKEGV motifs in the N-terminal region [46,48].

The π-stacking of aromatic residues has been suggested to serve as structural and functional elements for the progression of the self-assembly process[49]. Furthermore, a critical role for aromatic–aromatic interactions in aggregation has been also suggested. Indeed, further support for this comes from the evaluation of the molecular mechanisms behind the anti-amyloid effects of chemical compounds[50].

An example of these compounds are phthalocyanines, which exhibit anti-amyloid assembly and inhibition of aSyn, tau, and aβ[51–59]. These molecules are cyclic tetrapyrroles, and their characteristic is the planarity of their aromatic ring system, which contributes to the ability of these molecules to bind strongly and selectively to aromatic amino acids in proteins via π-π interactions.

Further studies directed to understand the role of individual residues in these motifs called “hot spots” need to be performed. In that direction, studies focused on the role of Y39, which lies in the center of the region 36-42, became an active field of research. The mutation Y39A impairs the amyloid fibril

assembly of the protein[60], and aSyn phosphorylated at Y39 is enriched in brain tissues and Lewy bodies in the substantia nigra and striatum of PD patients[61]. In addition, this same region is involved in binding Hsp70 for fibril disassembly[62].

1.3.2. Familial mutations

Parkinson's disease can also be inherited as an autosomal dominant trait due to missense mutations. The SNCA gene has many variants implicated in rare autosomal dominantly inherited forms of PD[12].

To date, several potentially pathogenic variants of aSyn have been associated with familial PD. This includes the well-studied A30P[63], E46K[64], and A53T[12] variants, as well as A30G[65], H50Q[66], G51D[66,67], A53E[68] and A53V[69].

Copy number variations (i.e., duplication[70], triplication[71]) also demonstrated the implicates of SNCA overexpression and their clear dosage effect, according to the number of supernumerary copies of this gene.

The different familial forms of PD have a different impact on the membrane binding properties and aggregate formation and have been deeply studied.

1.3.3. Influence of familial mutants on aSyn lipid-membrane interactions

Since all the identified missense mutations are located in the N-terminal region, and based on the fact that the physiological function of aSyn is related to its binding to lipid membranes, the interaction of the variants with lipids has been deeply studied.

Some mutants such as A30P and G51D, show a weaker binding to lipid membranes compared to the wt aSyn species[72,73]. The effect of the G51D might be attributed to the substitution of glycine for a negatively charged (aspartate) residue, decreasing membrane interactions. Meanwhile, A30P reduced alpha helix propensity[74,75], since Alanine is one of the strong α- helix-forming residues[76].

By contrast, E46K has increased membrane affinity[77,78]. Since the negative glutamate is replaced with a positive lysine, this contributes likely to enhance the electrostatic interactions with negatively charged lipid membranes.

1.3.4. Impact of familial mutation on aSyn aggregation and fibril structures

PD familial mutants such as H50Q, G51D, and A53T/E introduce a change in the interface of fibrils, with the insertion of hydrophilic or charged residues that might contribute to disrupting the dimer interface and promoting the appearance of novel structures. Mutants A53T, H50Q, and E46K have been demonstrated as well to increase the rate of self-aggregation[19,77,79–81].

It has been reported that E46 with K80 form an intra-molecular salt bridge, important for the Greek-key folding. According to this structure, E46K has a new rearrangement[82] possible due to the fact that the mutation breaks the electrostatic interactions. These fibrils are less stable but more efficient in seeding amyloid formation, which might be due to the instability and fragmentation-prone properties leading to an increased ability of propagation.

1.4. The relevance of PTMs in Parkinson's disease

Post-translational modifications (PTMs) are processes that change the chemical properties of the protein, affecting its structures and dynamics. This includes the addition of a modifying group, such as acetyl, phosphoryl, glycosyl and methyl, reversibly or irreversibly, in one or more amino acids of the primary sequence of the protein.

Many factors have been studied on the aggregation and progression of the disease. In that context, during the last years, research groups investigated the impact that PTMs at specific sites may have on aSyn aggregation and clearance[83–91].

One of those studies showed that PTMs on soluble aSyn extracted from brain samples of distinct α-synucleinopathies and normal brains by immunoprecipitation (IP), were mostly found in the N-terminal domain.

Phosphorylation at S129 is one of the most studied main-disease-associated aSyn PTMs. This modification is found in a higher percentage in human brain samples[92], and is one of the reasons why the phospho-serine129 (pS129) is used as a specific marker of synucleopathies. However, it was discovered that the phosphorylation is a late event in the pathology, meaning that firstly the aggregation of non-phosphorylated aSyn occurs, and later phosphorylation at Ser-129 takes place, with pS129 aSyn as a possible inhibitor of the aggregation. Thus, this might be the reason of the higher presence of pS129 aSyn in Lewy bodies[93].

Acetylation in proteins can exist in different ways, the Nα-acetylation is an irreversible modification, but Nε-acetylation and O-acetylation are reversible. Acetylation occurs on many residues, but Lysine is the most reported acetylated residue. It has been demonstrated that acetylation at K21 and K43 residues modulates the amplification of pathological aSyn[94].

Other PTMs have been found that prevent aSyn aggregation as O-GlcNAc sites[88] or arginylation sites[95]. On the other hand, truncation has been implicated in increasing the accumulation of aSyn, for example when the C-terminal is truncated (aSyn 1-120)[96]. Is in this context where many questions arise: Do PTMs occur once the amyloid structure is already formed? Are aberrant PTMs on soluble aSyn the reason for the aggregation of the protein? Could PTMs inhibit aSyn aggregation? Are PTMs the reason for the occurrence of different fibril polymorphs of aSyn?

2. Aims of the study

Structural factors derived from point mutations, specific residues in strategic sequential motifs and PTMs have been recognized as key modulators of function and dysfunction of aSyn

To achieve a better understanding of these molecular events we decided to conduct research focused on the physiological and pathological states of different aSyn mutants, expanding our work to the field of PTMs.

To achieve this, our goals were:

1. to unravel the early steps of aSyn aggregation through the characterization of the conformational and aggregation properties of aSyn in the context of rational-designed mutant species;

2. to characterise a novel pathogenic SNCA variant in terms of the structural properties of its monomeric state and its lipid binding features;

3. to provide insights into the aggregation propensity and membrane binding features of aSyn monomers modified by a specific PTM, extending the characterization to the folding and stability of the formed aSyn fibrils.

3. Material and Methods

Experiments of this thesis were performed in two different labs during the duration of my research, for this reason, some methods have different approaches, depending on the place they were performed.
Every detail about it is described below.

3.1. *Bacterial strains and plasmids*

Cell line:	Competent BL21 (DE3) cells provided by Claudio Fernandez
	H4 cells provided by Claudio Fernandez
Plasmids:	pT7-7 aSyn wt provided by Tiago Outeiro
	pNatB provided by Tiago Outeiro
	pT7-7 aSyn Y39F / Y39L / Y93A were provided by Claudio Fernandez.
	pT7-7 aSyn V15A was performed by Sol Cima (Translational Structural Biology in Dementia, DZNE, Göttingen, Germany)

3.2. *Buffers*

MES buffer:	20 mM MES, 100 mM NaCl, pH 6.5
HEPES buffer:	50 mM HEPES, 100 mM NaCl, pH 7.4, 0,02% NaN_3

3.3. *Protein preparation*

Purification of alpha-synuclein and variants was carried out as previously reported[20] with the exception that chloramphenicol and ampicillin were added to the selection of the doubly transformed *E. coli* colonies. Proteins were purified by a chromatography system and the purity of samples was determined by SDS-PAGE. Sol Cima helped with the preparation of the V15A variant of alpha-synuclein.

3.3.1. Transformation of competent cells

Unlabeled and ^{15}N isotopically enriched N-terminally acetylated aSyn and its Y39F, Y39L, and Y39A variants were obtained by co-transforming E. coli BL21 (DE3) cells with the plasmid pT7-7 encoding for human alpha-synuclein and NatB plasmid that encodes for the components of yeast NatB acetylase complex[97]. Competent *E. coli* cells were taken out of -80ºC and thawed on ice for 20 – 30 minutes and agar plate ampicillin and chloramphenicol resistance were warmed up to room temperature then 500ng of each plasmid was added to the cells and incubated on ice for 45 minutes. Heat shock was done for 45 seconds at 42ºC in a water bath. The tube was put again on ice for 2 minutes and 1 ml of sterilized LB medium was added. The growing of colonies was performed at 37ºC shaking incubator for 45 minutes. 50 µl was plated onto LB agar plates containing the appropriate antibiotics (100µg/ml Ampicillin and 25µg/ml Chloramphenicol) and incubated at 37 ºC overnight. The next day a colony was picked up and grown in LB medium overnight with both antibiotics to make glycerol stock mixing 500µl of culture with 500µl sterile 50% Glycerol in water, gently mixed, and shock frozen in nitrogen liquid, storage at -80ºC.

In the case of the familial variant, ^{15}N isotopically protein-enriched N-terminally acetylated aSyn and its mutant V15A were obtained by co-transforming E. coli BL21 (DE3) cells with the plasmid pT7-7 and NatB. Competent cells were thawed on ice, added 5 – 10 ng of DNA, and mixed by gently tapping. It was incubated for 15 min on ice. Heat shock of cells was made by incubating the vial for 30 seconds in the 42°C water bath. The vial was put again in ice and it was added 250µl of pre-warmed SOC medium and incubated at 37°C for 1 hour at 300 rpm. 25µl of transformation reaction was plated out on LB agar plates containing the appropriate antibiotic for both plasmids (100µg/ml Ampicillin and 34µg/ml Chloramphenicol) and incubated at 37 ºC overnight. The following day, 50 ml of preculture was prepared (100

µg/ml Ampicillin, 34 µg/ml Chloramphenicol) and one colony was incubated there at 37°C, 230 rpm, overnight.

3.3.2. Protein expression

The transformed cell with our interested plasmid was picked up with a spreader from Glycerol stock and mixed with 2 ml sterile water; 100 µl was plated out on LB-agar plates with 200 µg/ml Ampiciline and 25 µg/ml Chloramphenicol, these were incubated at 37 ºC over-night.

Unlabeled protein

Transformed competent cells were collected from plates with 300 ml Terrific medium. It was grown in a 3 L Erlenmeyer at 37 ºC, constant shaking (240 rpm) until increased two units OD_{600} from the initial. Induction was carried out with 1 mM IPTG, at 37 ºC, with constant shaking (240 rpm) for 2 hours.

Table 2: Recipe for Terrific medium.

Terrific medium	**Volume**
MTB 2X	150 ml
$MgSO_4$ 1M	600 µl
Glucose 40%	3.75 ml
$(NH_4)_2SO_4$ 1M	7.5 ml
Ampiciline 500X	600 µl
Chloramphenicol 1000X	300 µl
KH_2PO_4/NA_2HPO_4 0.5 M	30 ml
Sterile water	Up to Vf = 300 ml

Labeled protein

Transformed competent cells were collected from plates with 300 ml LB medium (1% Glucose, 200 µg/ml Ampiciline, and 25 µg/ml Chloramphenicol). It was grown in a 3 L Erlenmeyer at 37 ºC, constant shaking (240 rpm) until reached OD_{600} 0.8. LB culture was transferred to Falcon tubes and centrifugated to 2500g for 5 minutes.

Pellets were resuspended with minimum medium for labeled protein and grown at 37 ºC, 250 rpm until the initial OD_{600} increases by one unit. 1 mM IPTG was added for induction and protein expression at 37 ºC for 2 hours.

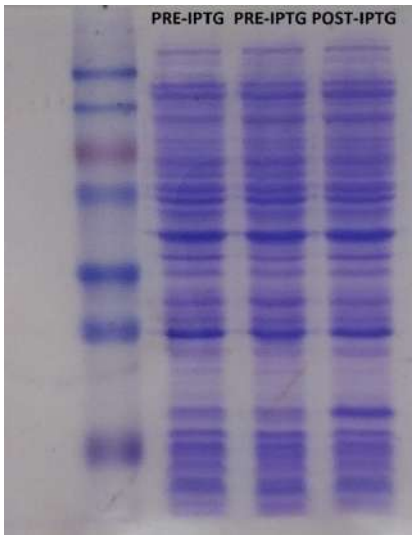

Table 3: Recipe for 250 ml M9 minimum medium

Minimum medium	**Volume**
M9 Salts (10X)	25 ml
MgSO4 1M	1.25 ml
Glucose 40%	6.25 ml
$^{15}NH4Cl$	250 mg
Ampiciline 500X	500 µl
Chloramphenicol 1000X	250 µl
Trace elements	250 µl
CaCl 100mM	500 µl
Sterile water	Up to Vf = 250 ml

M9 salts 10X: 43 g Na_2HPO_4, 15 g KH_2PO_4, 2.5 g NaCl dissolved in 500 ml H_2O

Trace elements: 0.6 $FeSO_4$ x 7 H_2O, 0.115 g $MnCl_2$ x 4 H_2O, 0.08 g $CoCl_2$ x 6H2O, 0.07 $ZnSO_4$ x 7 H_2O, 0.03 $CuCl_2$ x 2 H_2O, 0.002 gH_3BO_3, 0.025 g $(NH_4)_6Mo_7O_{24}$ x 4 H2O, 0.5 g EDTA dissolved in 100 ml H2O (deionized)

The approach for protein expression of V15A aSyn mutant was 10 ml of preculture medium was inoculated in 1 L of minimum medium (100 µg/ml Ampicillin, 34 µg/ml Chloramphenicol, 300 µM $CaCl_2$). The growing of cells was performed in an incubator at 37 ºC, with 110 rpm constant shaking until reached OD_{600} near 0.8, followed by induction at 25 ºC with 1mM IPTG overnight.

3.3.3. Cell harvest

Cells expressing wt and Y39 mutants were harvested by Thermo Scientific Sorvall RC 6 plus Superspeed Centrifuge at 4 ºC, 2500 rpm for 15 minutes. The supernatant was discarded and the cell pellet was frozen at -20 ºC until the next day. The bacteria pellet was resuspended in 20 ml Lysis buffer (10 mM Tris, pH 8, 1mM EDTA, and 1mM PMSF). Cell lysis was carried out by Branson sonifier 250 with 10 cycles 30 sec ON, 2 min OFF. The cell lysate was boiled for 20 min at 95 ºC and centrifugated at 11000 rpm, for 40 min at 4 ºC by Eppendorf Centrifuge 5810R. The supernatant was recovered and incubated at 4 ºC, 50 rpm for 30 minutes with 0.01 g/ml of streptomycin sulfate for DNA precipitation. To separate DNA precipitation from the sample, it was centrifugated at 4 ºC, 1000 rpm for 40 minutes by Eppendorf Centrifuge 5810R. In the end, alpha-synuclein and impurities were precipitated incubating at 4 ºC, 50 rpm for 30 minutes with 0.361 g/ml ammonium sulfate and centrifugated at 11000 rpm, for 40 min at 4 ºC by Eppendorf Centrifuge 5810R. The supernatant was discarded and the pellet was resuspended in 5 ml 25 mM Tris pH 8 and dialyzed overnight in 1 L 25 mM Tris pH 8 at 4 ºC.

Cells expressing V15A were harvested by Beckman Coulter Avanti JXN-26 centrifuge 4 ºC, 3000g for 40 minutes with JLA 8.1000 rotor. The supernatant was discarded and the cell pellet was resuspended in 35 ml Lysis buffer (10 mM Tris, pH 8, 1 mM EDTA, 1 mM PMSF, 0.2 mM $MgCl_2$, Lysozyme, and DNase I). The lysed was performed

by the French press. The lysate was boiled at 95 ºC for 20 min in a water bath followed by centrifugation in Beckman Coulter Avanti JXN-26, at 4°C, 22000rpm for 1 hour with JA-25-50 rotor. The supernatant was incubated at 4°C, with constant shaking, for 15 minutes with 10 mg/ml of streptomycin sulfate for DNA precipitation. To discard the precipitate it was centrifugated at 4 ºC, 15000 rcf for 30 minutes by Eppendorf Centrifuge 5810R. The protein of our interest and impurities were precipitated incubating at 4 ºC, with constant shaking for 15 minutes with 0.36 mg/ml ammonium sulfate and centrifugated at 11000 rpm, for 40 min at 4 ºC by Eppendorf Centrifuge 5810R. Pellet was resuspended with 10ml of 25mM TRIS-HCl pH 7.7 and 0.1 mM PMSF and dialyzed overnight.

3.3.4. Purification by ÄKTA Pure

Dialyzed wt and Y39 protein was centrifugated at 4 ºC, 10000 rpm for 10 minutes by Eppendorf Centrifuge 5810R and filtered. HiTrap Q HP anion exchange chromatography column (GE Healthcare) was used for the purification of alpha-synuclein with a gradient of salt (25 mM TRIS pH 8, 0 – 3 M NaCl). The fractions were collected and SDS-Page was run to check and chose the most purity fractions. Purified protein samples were dialyzed with 1 L 20 mM MES, 100 mM NaCl pH 6.5 overnight. The final protein concentration was determined by Jasco spectrophotometer V-630 at a fixed wavelength (274 nm) using an extinction molar 5960 M^{-1} cm^{-1}, and a cuvette of 100 µl. It was stored at - 80 ºC

Dialyzed V15A protein was centrifugated at 4 ºC, 10000 g for 10 minutes by Eppendorf Centrifuge 5810R and filtered. Mono Q 10/100 GL anion exchange column (GE Healthcare) was used for the purification of alpha-synuclein with a gradient of salt (25 mM TRIS pH 7.7, 0 – 2 M NaCl). The fractions were collected and loaded into a HiLoad 26/600 Superdex 75pg gel filtration column using 50 mM HEPES, 100 mM NaCl, 0.02 % NaN_3, pH 7.4 for separation of

high/low weight impurities from our protein. The chosen fractions were collected, and SDS-Page was run to check and chose the most purity fractions. The final protein concentration was determined by NanoDrop, and stored at - 80 ºC.

3.4. *SUVs preparation*

Different lipids were purchased from Avanti Polar Lipids (Alabaster, AL). 1,2-Dioleoyl-sn-glycero-3-phosphoethanol-amine (DOPE), 1,2-dioleoyl-sn-glycero-3-phospho-L-serine (DOPS), 1,2-dioleoyl-sn-glycero-3-phosphocholine (DOPC) were mixed in a proportion 5:3:2 w/w respectively (called Coagulation Reagent I) or 5:3:12 w/w respectively. Every mixture is dissolved in chloroform and dried under a stream of N_2 gas, lyophilized overnight.

For experimental data used in Y39 mutants, the lipid layer was resuspended in 20 mM MES, 100 mM NaCl, pH 6.5, the sample was sonicated by Branson sonifier 250 with 10 cycles 2 min with 2 min break. The size of the resulting SUVs was determined by dynamic light scattering using a Zetasizer Nano ZS instrument (Malvern Instruments, Worcestershire, U.K) with a diameter of ~100 nm.

For interaction of lipids with V15A and ac-Lys aSyn, the lipid layer was resuspended 50 mM HEPES, 100 mM NaCl, pH 7.4 the sample was sonicated by Ultrasound bath with 10 cycles 1 min with 3 min break. The size of the resulting SUVs was determined by dynamic light scattering using a DynaPro NanoStar instrument (Wyatt Technologies Corporation) with a diameter of ~60 nm.

3.5. *CD Spectroscopy*

The binding of the protein (wt and Y39 mutants) in SUVs and their transition from random coil to alpha helix was followed for the ellipticity

at 222 nm, measured by far-UV Circular Dichroism. These were carried out with 10 μM of monomer and varying concentrations of SUVs, and it was recorded from 200 to 250 nm in a J-1500 CD spectrophotometer (JASCO, Inc) using a 0.1 cm quartz cuvette.

CD data were collected at 25 °C, 1 time-per-point (s) in 1 nm steps. The datasets were averaged from three repeats. All spectra were baseline corrected against buffer in deionized water and smoothened.

The mean residue molar ellipticity at 222 nm ($[\theta]_{MR,222}$) was calculated using Equation 1:

$$[\theta]_{MR,222} = \theta_{222}/(10Cnl)$$

Where θ_{222} is the measured ellipticity (millidegrees) at 222 nm, C is the protein concentration (molar), n = 140 (number of amino acid residues in the protein), and l is the path length of the cuvette in cm (0.1 cm). Lipid titration curves generated by plotting $[\theta]_{MR,222}$ versus the lipid concentration were analyzed by fitting to Equation 2, as previously described[98] [3]:

$$R = R_0 - \left(R_0 - R_f\right)\frac{k_d + C + \frac{L}{N} - \sqrt{\left(k_d + C + \frac{L}{N}\right)^2 - 4CL/N}}{2C}$$

where R is the measured $\theta_{MR,222}$ at a given lipid concentration, R_0 is the $\theta_{MR,222}$ in the absence of lipid, R_f is the $\theta_{MR,222}$ in the presence of saturating lipid, L is the total lipid concentration, C is the total protein concentration, K_d is the apparent macroscopic dissociation equilibrium constant, and N is the binding stoichiometry (lipids/ protein).

Titration of wt, ac-Lys aSyn, and V15A alpha-synuclein-to-liposome ratios was performed at a protein concentration of 10 μM of monomer and varying concentrations of SUVs, and it was recorded from 190 to 250 nm by using a Chirascan-plus qCD spectrometer (Applied Photophysics, Randalls Rd, Leatherhead, UK) using a 0.2 mm pathlength cuvette. CD data were collected at 20 °C, 1 time-per-point (s) in 1 nm steps. The datasets were averaged from three repeats. All

spectra were baseline corrected against buffer in deionized water and smoothened (window size: 5).

3.6. *Aggregation assay*

Aggregation of wt alpha-synuclein and Y39 mutants was performed with 50 μM of monomer in 20 mM MES, 100 mM NaCl, pH 6.5, and a magnetic stirrer inside a 5 mm NMR tube incubated at 37°C. The level of remaining soluble alpha-synuclein monomer was followed by 1D ^{1}H-NMR at different times. The amount of monomer was determined by the integration of the curve in the aliphatic region in the NMR spectra (0.7 – 1.0 ppm). These were acquired and processed by TOPSPIN 7.0 (Bruker Biospin). Endpoint aliquots of aggregation assay were analyzed by the Thioflavin-T fluorescence assay and CD spectroscopy.

Aggregation kinetics for ac-Lys aSyn and V15A familial variant, were performed with 25 μM of protein and 25 μM of Thioflavin T concentration in HEPES buffer (50 mM HEPES, 100 mM NaCl, pH 7.4, 0.02% NaN_3). The kinetic was followed by TECAN Spark 20M reader at 37 °C with cycles consisting of 1 min shaking intervals followed by 10 min rest intervals. Two PFTS beads were added per well. The aggregation assay with liposomes was measured at 25 μM of protein, 5 mM of liposomes, and 25 μM of Thioflavin T concentration in HEPES buffer

3.7. *Thioflavin-T fluorescence*

Thioflavin is a fluorescent dye that its binding to beta-sheet-rich structures. For the endpoints aggregation assay, Thioflavin-T was measured in a quartz cuvette (excitation wavelength: 440 nm, excitation bandwidth: 10 nm, emission wavelength: 482, emission bandwidth: 10 nm) by Varian Cary Eclipse Spectrophotometer. For aggregation kinetics, the fluorescence of Thioflavin-T was measured from the top (excitation wavelength: 440 nm, excitation bandwidth: 10 nm, emission wavelength: 482, emission bandwidth: 10 nm, gain level: 60) by TECAN Spark 20M reader

3.8. *AFM microscopy*

Samples were prepared by spin-coating. A volume of 20 µL of each sample was deposited over Muscovite mica discs grade V1 (Ted Pella) of 10 mm diameter, which was previously cleaved. After promoting interactions with the substrate, mica discs were accelerated up to a constant rotation speed of 2000 rpm to ensure complete drying of the substrate. AFM imaging was performed on a Bruker Multimode 8 SPM (Santa Barbara, CA, USA) and a NanoScope V Controller (Santa Barbara, CA, USA) using a "J" type scanner. The AFM images were acquired in tapping mode using silicon tips NCHV (Bruker) with a spring constant of 40 N m^1 and a resonance frequency of ˜320 kHz. Images analyses were performed using Gwyddion version 2.46 software (Brno, Czech Republic).

3.9. *Negative stain transmission electron microscopy*

Electron microscopy experiments were performed by Leonie Kopecny (Facility for Electron Microscopy, Fassberg Campus Göttingen). Samples after aggregation were adsorbed onto 400 mesh carbon-coated copper grids and the buffer was removed using filter paper. Subsequently, samples were stained by the addition of 1% uranyl acetate solution, which was subsequently dried with filter paper. The grids were imaged using a Talos L120C G2 electron microscope.

3.10. *Cell-based assay*

3.10.1. Cell Culture and transfection

For *in vitro* experiments, H4 neuroglioma cells were defrosted from nitrogen liquid and were maintained in an incubator at 37 °C, 5 % CO_2 environment in Dulbecco's Modified Eagles Medium (DMEM) (Gibco) supplemented with 10 % fetal bovine serum and 1% Penicillin Streptomycin. Cells were seeded 24 h before use and

plated for 80% of confluency in a 12-well plate. Cells were co-transfected with Synphilin-1[52] and a C-terminally modified variant of alpha-synuclein (SynT) wt or its point mutants. The transfection was performed using Fugene, following the manufacturer's instructions. Briefly, every well was treated with 1 µg Synph + 1 µg SynT + 6 µl Fugene, the mix was incubated for 15 minutes at room temperature before being added to the plate. Inclusion formations were evaluated after 48 h transfection.

3.10.2. Immunocytochemistry

Transfected cells were washed 3 times with PBS and fixed with 4 % PFA at room temperature for 20 minutes. Afterward, wells were washed again 3 times with PBS, followed with permeabilization of cells with 0.1 % Triton at room temperature for 20 minutes. The blocking step was carried out with 1,5 % horse serum for one hour. Incubation of the primary antibody was performed with alpha-synuclein (BD Transduction Laboratories, Lot 7069936, Purified mouse) and Rb pAb to V5 tag (Abcam, Lot. GR256657-9, Rabbit), diluted 1:1000, at 4 °C, overnight. The following day, cells were washed 3 times with PBS and incubated with secondary antibody Alexa Fluor 555 Donkey anti-mouse IgG (H+L) (Life Technologies, Lot. 1575605) and Alexa Fluor 488 Donkey anti-rabbit (H+L) (Life Technologies, Lot. 1670152) diluted 1:1000, at room temperature, for 2 hours. Cells were washed with PBS before the incubation with DAPI (Roth) diluted 1:10000, for 5 minutes. In the end, cells were fixed with Mowiol for epifluorescence microscopy. Images were captured using a Nikon C2 plus confocal microscope.

3.10.3. Quantification of alpha-synuclein intracellular inclusions

Quantification was carried out by screening for every condition and scoring according to the number of inclusions present; classifying into cells without inclusions, less than five inclusions, between five to nine inclusions, and equal/more than ten inclusions[99]. For statistical analysis, Graph Prims was used expressing the results as

the percentage of the total number of transfected cells obtained from three independent experiments.

3.10.4. Western blot analysis

Cell lysis and solubilization of proteins were realized by Radioimmunoprecipitation assay buffer (RIPA buffer; 50 mM TRIS pH 8, 0.15 M NaCl, 0.1 % SDS, 1% NP40, 0.5 % Na-deoxycholate) and 2 mM EDTA and supplemented with a Protease Inhibitor Cocktail (Roche Diagnostics, Mannheim, Germany). Sample denaturation was performed for 5 minutes at 100 °C in SDS-PAGE protein sample buffer. The 12 % SDS-polyacrylamide gels were loaded with 40 µg of protein determining the concentration by Bradford assay (BioRad Laboratories, Hercules, CA, USA). The transfer was carried out into nitrocellulose membrane (Amersham™ Hybond®, GE Healthcare Life Sciences) using Tris-Glycine transfer buffer, for 90 min with constant 0.3 A at 4 °C. The fixing and blocking steps were performed with 8 % paraformaldehyde and 5 % (w/v) skim milk in 1x TBS-Tween (50 mM Tris, 150 mM NaCl, 0.05 % Tween, pH 7.5) respectively for 60 min at room temperature. Primary antibodies as mouse anti-alpha-synuclein (1:1000, 2B2D1 BD Biosciences, San Jose, CA, USA) and mouse anti-αtubulin (1:1000, T6199, Sigma-Aldrich) were incubated overnight at 4 °C. The following day, membranes were washed three times in TBS-Tween for 5 minutes, and incubated with secondary antibodies, anti-mouse IgG (1:10000, A4416, Sigma-Aldrich). A chemiluminescence kit (Bio-Lumina; Kalium Technologies, Argentina) was used to detection of bands on the membrane using a Licor C-Digit Blot Scanner (LI-COR Biosciences).

3.11. *NMR Spectroscopy*

3.11.1. Free state

Experiments related with Y39 mutants were recorded on a Bruker 600 MHz HD Advance III spectrometer with a cryogenically cooled

triple resonance 1H (13C/15N) TCI probe. Samples of alpha-synuclein unlabeled 100 µM dissolved in 20 mM MES buffer supplemented with 100 mM NaCl at pH 6.5, 10 % D_2O were recorded at 15 °C in one-dimensional 1D ^{1}H NMR spectra, and samples of alpha-synuclein ^{15}N labeled 50 µM dissolved in 20 mM MES buffer supplemented with 100 mM NaCl at pH 6.5, 10 % D_2O were recorded at 15 °C in two-dimensional 2D ^{1}H-^{15}N heteronuclear single quantum correlation (HSQC) with pulsed-field gradient enhanced pulse sequences[100]. Chemical shift perturbation was calculated according to $(((\delta_H)^2+ (\delta_N/10)^2)/2)^{1/2}$. TOPSPIN 7.0 (Bruker Biospin) was used for the acquisition and processing of NMR spectra. Analysis and visualization of NMR spectra were performed by CCPN.

NMR spectra of ac-Lys aSyn and V15A variant, were obtained on a Bruker 700 MHz spectrometer equipped with a 5 mm triple-resonance and pulsed-field z-gradient cryoprobe. Monomer characterization was performed using $^{1}H–^{13}C$ HSQC (heteronuclear single quantum coherence), at 15°C. Samples were prepared with 100 µM ^{15}N-labeled monomers of alpha-synuclein (natural abundance) and its variant, in 50 mM HEPES buffer supplemented with 100 mM NaCl at pH 7.4, 10 % D_2O. TopSpin 3.6.1 (Bruker) was used for the adquisition and processing of data and Sparky 3.13 (T. D. Goddard and D. G. Kneller, SPARKY 3, University of California, San Francisco) for the corresponding analysis. Chemical shift perturbation was calculated according to $(((\delta_H)^2+ (\delta_N/10)^2)/2)^{1/2}$.

3.11.2. Binding/Interaction state

Nuclear magnetic resonance (NMR) spectra were obtained using a Bruker 600 MHz HD Advance III spectrometer with a cryogenically cooled triple resonance 1H (13C/15N) TCI probe in the case of Y39 mutants. Two-dimensional (2D) $^{1}H–^{15}N$ HSQC experiments were conducted at 15°C using standard pulse sequences from the Topspin suite (Bruker) library. Sequence-specific assignments for

the backbone of the intrinsically unfolded aSyn were obtained from previous studies. Binding experiments of Y39 mutants, were carried out by 2D $^{1}H–^{15}N$ HSQC, with 100 μM ^{15}N-labeled monomers of alpha-synuclein and its variants, in 20 mM MES buffer supplemented with 100 mM NaCl at pH 6.5, 10 % D_2O, were incubated in the absence and presence of 2.5 mM SUVs (60 % DOPC, 25 % DOPE, and 15 % DOPS). As previously described[101], for experiments on lipid-protein binding, every residue peak was monitored to follow the interactions with SUVs, comparing their intensities in the presence (I) and the absence of SUVs (I_0). The protein-lipid interaction profiles were plotted as I/I_0 ratios of non-overlapping cross-peaks in the Y axis and the protein sequence in the X axis. The total bound population was determined by the mean attenuation of residues 3-9[98,102] (Table 4). The hidden population was determined by the mean attenuation of residues 66-80[98,102] (fractional population of the protein in the associated state), giving information about the conformation of the hydrophobic domain NAC at the membrane surface (Table 4). The exposed population was determined by subtracting the hidden population from the total bound population (Table 4). For experiments ligand-protein, intensities (I) of the ^{1}H-^{15}N HSQC amide cross-peaks affected during titrations were compared with the same cross-peaks in the data set of free protein (I_0). Intensity profiles were plotted in the same manner as lipid-protein experiments. TOPSPIN 7.0 (Bruker Biospin) was used for the acquisition and processing of NMR spectra. Analysis and visualization of 2D spectra were performed by CCPN.

NMR spectra of ac-Lys aSyn and V15A variant were obtained on a Bruker 700 MHz spectrometer equipped with a 5 mm triple-resonance and pulsed-field z-gradient cryoprobe. Liposome titration was recorded using 2D $^{1}H–^{15}N$ HSQC Liposome titration experiment was performed using 40 μM of protein, incubating it in the absence and presence of SUVs (5:3:2 w/w; DOPE:DOPS:DOPC; Avanti

Polar Lipids). Processing of spectra was done with TopSpin 3.6.1 (Bruker) and analyzed with Sparky 3.13.

3.11.3. HD backbone exchange

HD exchange coupled to NMR was recorded according to a previously established protocol[51]. The forward HD exchange of amide protons in aSyn fibrils was done in 0.1 % formic acid (pD 4.0) in 99.9 % D_2O at 37 °C for 1.5 days, fibrils were collected by ultracentrifugation at 165.000 g for 2 hours, room temperature. Back-exchange of aSyn fibrils was performed using dissociation buffer (4M GdSCN, 0.4 % formic acid, pH 2.5, in 60 % D_2O) followed by 120 2D $^{1}H,^{15}N$ heteronuclear single quantum coherence (HSQC) recorded over a time of ~ 16 h at 3 °C. NMR experiments were measured on a Bruker 800 MHz spectrometer equipped with a 5 mm triple-resonance, pulsed-field z-gradient cryoprobe. Spectra were processed with TopSpin 3.6.1 (Bruker) and analyzed using Poky (Woonghee Lee, University of Colorado Denver).

3.11.4. Analysis of HD back-exchange

The relative intensity (height) data for 120 HSQC-separated aSyn residues were extracted from 2D ^{1}H-^{15}N HSQC spectra using the centered peak position of the final fully exchanged HSQC spectrum of the series normalized to a value of 1.0. For each aSyn residue, the back-exchange curves were fitted to a single exponential decay using Prism (GraphPad). Knowing the exact dead time and HSQC experiment duration the relative t_0 intensity level was back-calculated and the scale was transformed into absolute protonation levels by referencing the average maximum intensity value of the five residues with the highest signal intensity.

3.12. *C. elegans study (Performed by Nicola Boeffinger)*

3.12.1. Strains

All types of strains were cultivated on Agar plates that had OP50 bacteria at a temperature of 20 °C, following a previously described method[103]. Transgenic organisms that had an additional chromosomal array expressing human aSyn with mCherry attached to its C-terminus were created by injecting wild-type Bristol N2 worms with plasmids expressing various forms of human alpha-synuclein. Mutations in alpha-synuclein (Y39F, Y39L, and Y39A) were introduced by mutagenesis PCR and validated by sequencing. The neuronal cell of *C. elegans* expressing alpha-synuclein by the control of pan-neuronal rab-2 promoter (*rab-3p:alpha-synuclein-mCherry*) using the expression vector pD115.64 as a backbone. The transgenic lines were generated by injecting with a plasmid mix containing 50 ng/µl of a co-injection marker (*myo-2p::mTFP*), and 45 ng/µl pBluescript KSII (Stratagene) into the gonads of young adult N2 worms, to reach a final DNA concentration of 100 ng/µl, as described previously[104].

3.12.2. Fluorescent imaging and analysis

Immobilization of young adult *C. elegans* was carried out with 50 mM sodium azide in M9 buffer (17.2 mM KH_2PO_4, 42.3 mM Na_2HPO_4, 85.6 mM NaCl, 1 mM $MgSO_4$), mounting worms onto a 2 % agarose pad. Z-stacks images of the neuronal cell bodies were acquired by Zeiss LSM 780 confocal microscope with a 63x/1.40 NA oil immersion objective. Projections of the stacks and statistical analysis were carried out with ImageJ 2.1.0 and Prism Version 5.03.

3.12.3. Western Blotting

Worms expressing alpha-synuclein were washed twice in ice cold PBS with phosphatase and protease inhibitor (PhosphoStop Phosphatase Inhibitor Cocktail Tablets (Roche), complete EDTA-free Protease Inhibitor Cocktail Tablets (Roche)). There were lysed *in 60* µl lysis buffer (150 mM NaCl, 1 mM EDTA, 25 mM Tris pH 7.5, 10% (v/v) glycerol, 1% (v/v) Triton X, and freshly added 100 mM

DTT, 4 mM Pefabloc SC-Protease Inhibitor (A 154.1, Roth), phosphatase and protease inhibitor, prior to shock-freezing in liquid nitrogen. Samples were stored at -80 °C. For protein extraction, samples were thawed, and added SDS-PAGE protein sample buffer before sonicated step. Sonication was performed on ice for 3 minutes (20 sec ON, 10 sec OFF, 70 % amplitude) with a SonoPlus mini20 sonicator (3.665, Bandelin, Sonotrode Type MS2.5). Afterwards, samples were boiled at 100 °C for 10 minutes, and centrifugated at 17000g for 10 min. Next, 30 µl of lysate was used to run into 12 % SDS-polyacrylamide gels and transferred to PVDF membrane (10,600,023, Amersham Hybond) for 90 min at 220 mM under cooling conditions. The blocking step was performed with 1 % semi-skimmed milk in 1 % TBS-T buffer (20 mM Tris, 150 mM NaCl, 0.1% (v/v) Tween 20, pH 7.6) for 1 hour. Membranes were incubated with primary antibodies: mouse anti-alpha-synuclein (1:1000, 610,787 BD Transduction Laboratories), mouse anti-alpha-tubulin (1:2000, T6199, Sigma-Aldrich) dissolved in blocking solution, with agitation at 4 °C, overnight. The following step was washing, 3 times in TBS-T buffer for 7 minutes, and next, were incubated with secondary antibodies: (goat) anti-mouse HRP-conjugated (1:5000, 1,721,011, Bio-RAD Laboratories, Inc.). ECL Kit Prime Western Blotting Detection Reagents (RPN2232, Amersham) were used for the detection of bands and an IntasChemoCam Imagen was used according to the manufacturer's instructions.

3.13. *Acetylation of alpha-synuclein*

450 µM of alpha-synuclein and labeled 15N alpha-synuclein, were incubated at 30 °C for 48 h in an Eppendorf thermomixer with 350 rpm shaking in the presence of 0.028 mg/mL CBP (BML-SE452, Enzo), 0.028 mg/mL p300 (BML-SE451, Enzo), and 4 mM acetyl-coA (Sigma-Aldrich), 1 mM PMSF, 1 mM EGTA. The sample was then boiled at 98 °C for 20 min to precipitate the acetyltransferases, followed by centrifugation at 20,000 × g in an Eppendorf centrifuge 5424 for 30 min. Next, the pellet was discarded, and the supernatant containing

acetylated alpha-synuclein was dialyzed against the aggregation assay buffer or NMR buffer (50 mM HEPES, 100 mM NaCl, pH 7.4, 0.02% NaN_3). Samples of monomers were analyzed by mass spectrometry to confirm the acetylation of lysines (Appendix 8.2).

3.14. *Pronase digestion*

Fifty microliters of fibril solution at 100 µM was mixed with 0.4 mg/mL and 0.2 mg/mL of pronase from Streptomuces griseus (53702, Merck-Millipore) and incubated in HEPES buffer for 15 min at 37 °C using a thermomixer (Eppendorf). The reaction was stopped by Protease inhibitor 1X. The pronase-resistant fibril core was pelleted down by centrifugation at 160.000 g for 30 minutes at 4 °C using a Beckman Coulter Optima MAX-XP ultracentrifuge. Supernatant was discarded and the pellet was dissolved in 10 µL of HEPES buffer with loading buffer, and then it was loaded onto a 15 % SDS PAGE gel. The gel was incubated with Comassie Blue overnight.

3.14.1. In-gel digestion and extraction of peptides for mass spectrometry

The respective bands from the SDS-PAGE gels were carefully cut and kept in an Eppendorf tube. To wash the gel pieces, 150 µL of water was added and incubated for 5 min at 26 °C with 1050 rpm shaking in a thermomixer. The gel pieces were spun down and the liquid was removed using thin tips (the same washing protocol was used in all subsequent steps with different solvents). The gel pieces were washed again with 150 µL acetonitrile. After washing, the gel pieces were dried for 5 min using a SpeedVacc vacuum centrifuge. To reduce disulfide bridges, 100 µL of 10 mM DTT was added to the gel pieces and incubated for 50 min at 56 °C fol- lowed by centrifugation and removal of liquid. The gel pieces were washed again with 150 µL of acetonitrile. To alkylate reduced cysteine residues, 100 µL of 55 mM iodoacetamide were added and incubated for 20 min at 26 °C with 1050 rpm shaking followed by centrifugation and removal of liquid. Subsequently, the gel pieces were washed with 150 µL of 100 mM NH_4HCO_3, and then twice with 150 µL of acetonitrile and dried for 10 min in a vacuum centrifuge.

The gel pieces were rehydrated at 4 °C for 45 min by addition of small amounts (2–5 µL) of digestion buffer 1 (12.5 µg/mL trypsin, 42 mM NH_4HCO_3, 4 mM CaCl). The samples were checked after every 15 min and buffer was added in case the liquid was completely absorbed by the gel pieces. Twenty µL of digestion buffer 2 (42 mM NH_4HCO_3, 4 mM $CaCl_2$) were added to cover the gel pieces and incubated overnight at 37°C.

To extract the peptides, 15 µL water was added to the digest and incubated for 15 min at 37 °C with 1050 rpm shaking followed by spinning down the gel pieces. Fifty µL acetonitrile was added to the entire mixture and incubated for 15 min at 37 °C with 1050 rpm shaking. The gel pieces were spun down and the supernatant (SN1) containing the extracted peptides was collected. Thirty µL of 5% (v/v) formic acid was added to the gel pieces and incubated for 15 min at 37 °C with 1050 rpm shaking followed by spinning down. Again 50 µL acetonitrile were added to the entire mixture and incubated for 15 min at 37 °C with 1050 rpm shaking. The gel pieces were spun down and the supernatant (SN2) containing the extracted peptides was collected. Both supernatants (SN1 & SN2) containing the extracted peptides were pooled together and evaporated in the SpeedVacc vacuum centrifuge. The dried peptides were resuspended in 5% acetonitrile and 0.1% formic acid and analyzed using an Orbitrap Fusion Tribrid (Thermo Fischer Scientific) instrument.

3.15. *Proteinase K digestion*

Digestion of 50 µM of fibrils was performed with 3.8 µg/mL of Proteinase K for different times at 37 °C. The reaction was stopped by loading buffer and boiled at 95 °C for 5 minutes, followed by loading onto a 15 % SDS PAGE gel. The gel was incubated with Comassie Blue overnight.

3.16. *Fluorescent dye binding*

Curcumin stock solution of 5 mM in DMSO was stored at 20 °C in the dark. Working solutions of 50 µM dye in HEPES buffer was freshly prepared and 100 µL was mixed thoroughly with 30 µL of aSyn fibrils at

25 µM. Samples were transferred to a 96-well microplate (PS, F-bottom (Chimney well), µCLEAR, black, non-binding from Greiner) and measurements were performed on a TECAN Spark 20M reader at 37 °C, intensity average over 30 flashes, 2 nm steps. Curcumin: ex.: 440 nm, gain: 80, ex. bandwidth: 20 nm, em. bandwidth: 20 nm, 485–800 nm. All spectra were baseline subtracted by dye buffer blank measurements and smoothed (windows size: 8).

3.17. *Sarkosyl treatment*

Incubation of 50 µM of fibrils was performed with 1% sarkosyl in PBS for 30 min at room temperature. Soluble supernatant and insoluble pellet fractions were isolated upon centrifugation. Samples were loaded to a 15 % SDS PAGE, followed by Coomassie Blue staining.

4. Results

4.1. Role of Y39 in structural and aggregation properties, and bound to membranes.

As already mentioned in the introduction, protein aggregation is a process in which proteins misfold and accumulate in abnormal clumps or aggregates within cells. One of the major unanswered questions of protein aggregation is the propensity of specific primary sequences to aggregate[3,105].

Several studies suggest that the N-terminus of aSyn is involved in the initiation of aggregation[46,106]. In the last years, research has focused on specific residues in the N-terminal that can control aSyn aggregation and function of the protein. During the assembly process, aSyn was shown to form transient inter-molecular interactions involving the stretch of residues centered at position 40 at the N-terminus and 40 a segment of residues in the negatively charged C-terminal region of wt aSyn[46]. In that direction, the implication of Tyr residues (at position 39 and the cluster located at the C-terminus) on the aggregation of the amyloid protein aSyn, has been explored by mutagenesis-based approaches[60,85,107–109]. In that context, the systematic analysis of the role of distinct sequential motifs and specific residues of aSyn primary sequence on its physiological and pathological states remains an important open avenue of investigation. Studies focused on aSyn mutations, post-translational modifications, and molecular interactions are emerging as of central importance to the normal function of the protein, as well as to its pathogenic role in Parkinson's disease[46,48,85,86,89,102,110–116]. Recently, a segment of 12 residues at the amino-terminus as well as a region surrounding Tyr-39 were identified as canonical chaperone interaction motifs of aSyn in mammalian cells, through which molecular chaperones might prevent the transformation of aSyn towards pathological states[110,112]

The protein contains three Tyr residues in the C-terminal region (Tyr-125, Tyr-133, Tyr-136) and one in the N-terminus (Tyr-39). Cysteine substitution in the latter but not in Tyr-125, Tyr-133, and Tyr-136 positions preferentially enhanced dimer and oligomer formation under oxidative conditions, suggesting a dimerization pathway mediated by this region[107]. On the other hand, the

substitution of Tyr-39 and Tyr-133 by Ala resulted in substantial inhibition of fibrillation, suggesting that Tyr-39 and the C-terminal Tyr residues might form an aromatic cluster that stabilizes the native state of aSyn[60].

On the other hand, the small molecule phthalocyanine tetrasulfonate (PcTS) (Appendix 8.3) was demonstrated to be an efficient inhibitor of aSyn assembly, reducing strongly the inclusion formation of the protein and its associated cytotoxicity in a cell-based model[53]. In parallel, biophysical studies demonstrated that the structural basis for the inhibitory effect of PcTS is mediated by interactions between the aromatic side chain of the Tyr residue at position 39 and its polyaromatic ring system[50,51]. These interactions might cause a loss of function of aromatic side chains involved in aSyn-filament-assembly mechanism, compromising intra- and intermolecular interactions necessary for amyloid structure transition, impairing the formation of amyloidogenic core.

Our specific aims are:

- To uncover the role of aromaticity at position 39 in aSyn aggregation (dysfunction) and lipid binding (function) features by replacing Tyr-39 with the following residues:

  Phe, which keeps aromaticity and removes a hydrophilic group such as OH;

  Leu, which is similar to Phe in size and hydrophobicity but it is not aromatic;

  Ala, which is hydrophobic as Phe and Leu but it is smaller in size.
- To analyze the impact of these mutations on monomeric aSyn structural properties by NMR
- To determine the role of these residues in directing the binding of the anti-amyloid compound PcTS to the N-terminus.
- To validate other amyloid assembly data obtained in vitro in both cell and anima-based l models of aSyn aggregation
- To investigate the effect of mutations at Y39 on the binding features of aSyn to lipid vesicles.

4.1.1 Monomeric aSyn remains disordered after Y39 mutation.

Biophysical description of the new mutants was made by circular dichroism, and NMR spectroscopy (1D ^{1}H spectra and HSQC spectra) to elucidate any possible changes with the insertion of new residues in position 39 of aSyn sequence.

The structural features of the monomeric wild-type (wt), Y39F, Y39L, and Y39A aSyn species were investigated by circular dichroism (CD), a tool to investigate secondary structure involving circularly polarized light; wt and all the variants have a negative minimum at ~199 nm in the far-UV CD spectra (Figure 8), indicative of random coil structure. As we know, aSyn is an intrinsically disordered protein, and these structural features are kept after the substitution of Tyr at position 39 for the new residues.

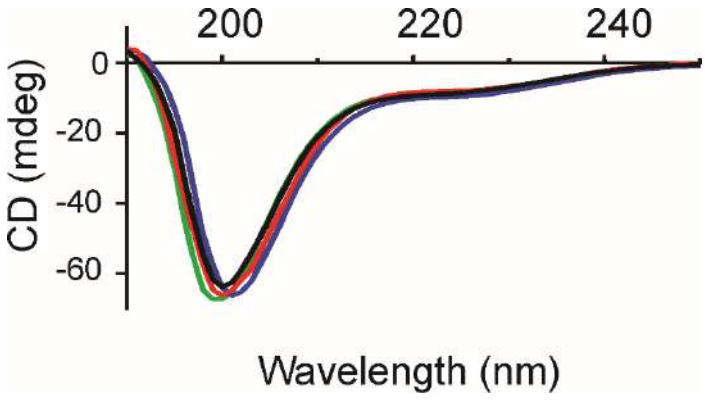

Figure 8: The far-UV circular dichroism (CD) spectra of aSyn in solution. wt (black), Y39F (blue), Y39A (red), and Y39L (green) aSyn monomers show spectral features that are characteristic of random coil conformations.

The 1D ^{1}H NMR spectra of non-labelled wt aSyn showed well-resolved clusters of resonances in the 6.0–8.0 ppm range, comprising the side chains of different aromatic residues: His (residue 50), Phe (residue 4 and 94), and Tyr (residue 39, 125, 133, and 136) (Figure 9). The replacement of tyrosine at position 39 by phenylalanine, leucine, and alanine residues in the 1D ^{1}H NMR spectra of the mutant species was confirmed by the lack of signals

corresponding to the Tyr-39 residue (marked by asterisks) and the detection of new signals corresponding to the presence of an additional phenylalanine residue in the Y39F variant (marked by circles).

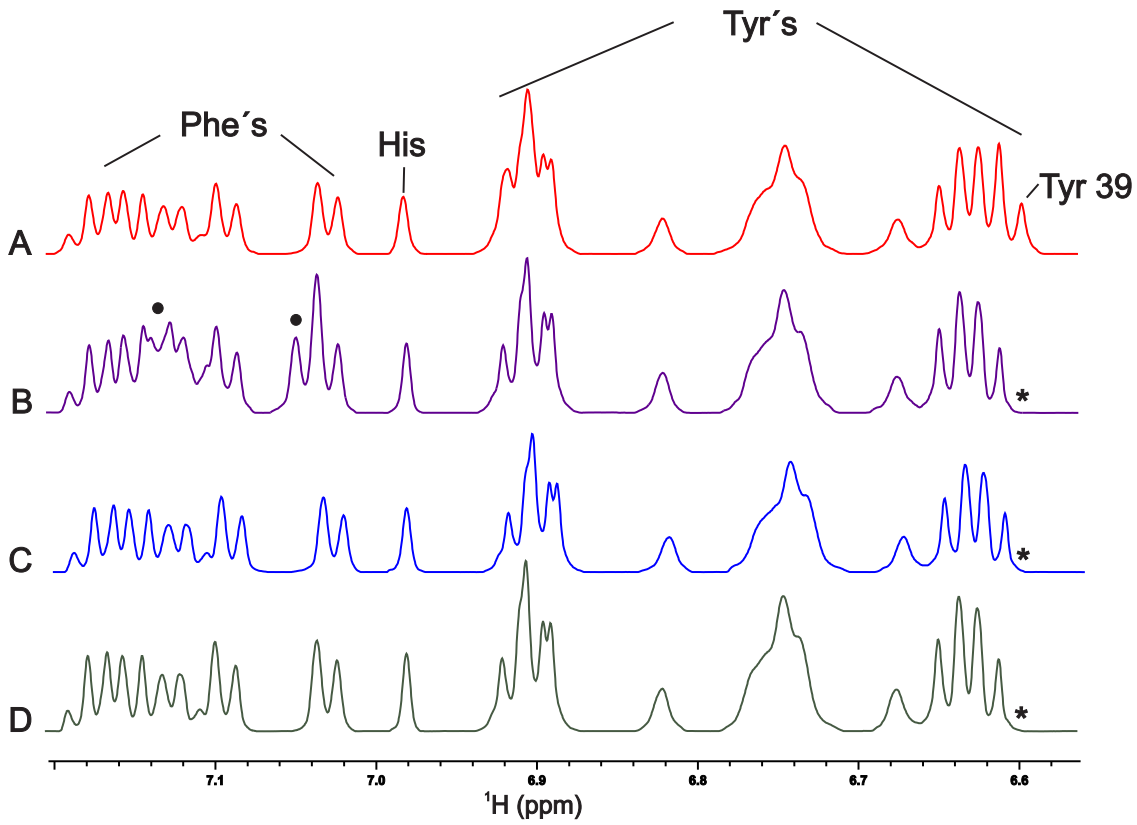

Figure 9: ^{1}H NMR of aromatic side chains at position-39 of aSyn variants. Spectra were registered at 15 ℃ on samples containing 100 µM wt (a), Y39F (b), Y39A (c), and Y39L aSyn (d). Asterisks indicate the lack of peaks corresponding to the Tyr-39 residue. Circles indicate the detection of new signals assigned to the Phe residue in position 39.

The ^{1}H-^{15}N HSQC NMR spectra of ^{15}N-labeled wt aSyn and their mutants show peaks well resolved and sharp, with a poor dispersion of chemical shifts, again reflecting the disordered nature of the backbone (Figure 10). The overlaid spectra of wt (black) and Y39L (green) (Figure 10a) as well as differences in the mean weighted chemical shifts show that structural perturbations were only local and restricted to the immediate vicinity of the Tyr residue (Figure 10b). The absence of noticeable changes in the structural properties indicated that the monomeric state of the protein variants remained disordered upon the replacement of Tyr-39 by Phe, Leu, and Ala.

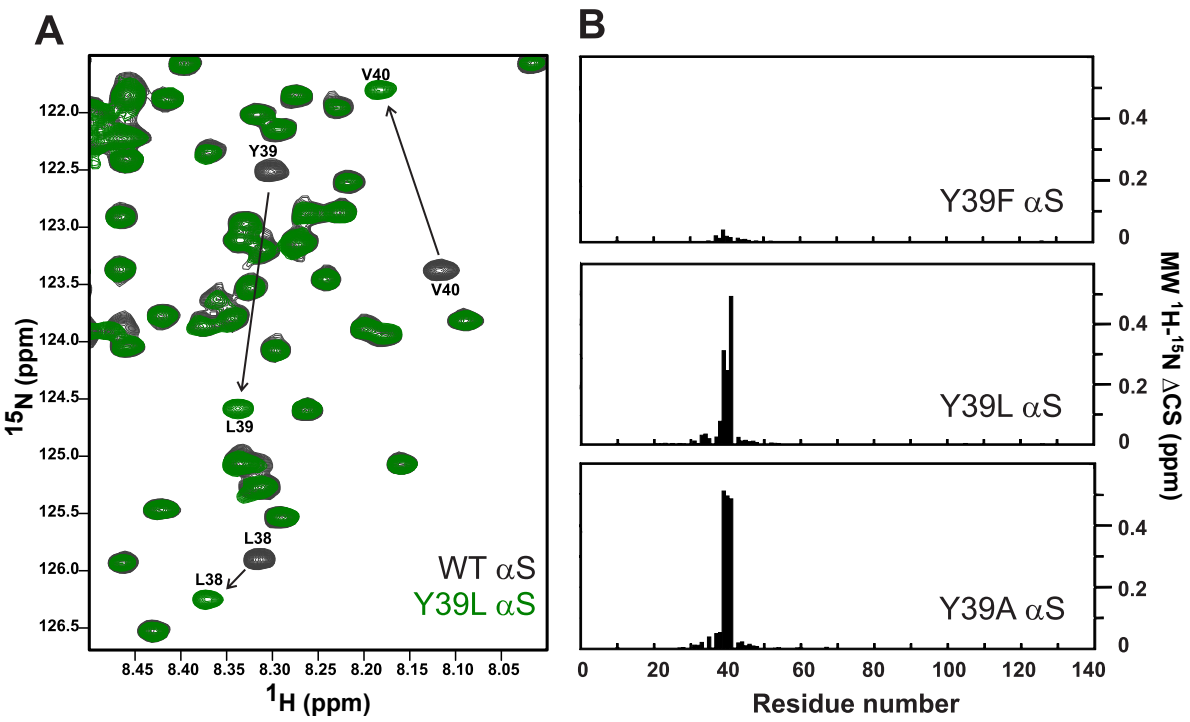

Figure 10: Changes induced by the mutations are only local and restricted to the immediate vicinity of the position-39 residue. a) Overlaid contour plots of ^{1}H-^{15}N heteronuclear single quantum correlation (HSQC) spectra of 50 µM wt (black) and Y39L aSyn (red). Most affected residues located in the vicinity of the mutated site are labeled. b) Differences in the mean weighted chemical shifts (MW ^{1}H-^{15}N ΔCS) displacements between wt and Y39F, Y39A, and Y39L aSyn mutants.

4.1.2. Local structural propensities of the Y39 aSyn variants

Conformational properties were analyzed by $^{3}J_{HN\text{-}H\alpha}$ couplings in NMR to uncover any differences among the aSyn variants studied

$^{3}J_{HN\text{-}H\alpha}$ couplings are reliable quantitative reporters of the time-averaged distribution of the backbone torsion angles φ and are frequently used to probe the propensity of intrinsically disordered proteins (IDP) to sample different regions of conformational space[117]. Therefore, we measured residue-specific $^{3}J_{HN\text{-}H\alpha}$ couplings in all of these proteins, values between 6 – 8 are typically for random coil, over 8 is beta-sheet, and under 6 alpha-helix. As shown in Figure 11, the values measured for the wt and Y39F, Y39L, and Y39A aSyn proteins

were typical of random-coil conformations and essentially indistinguishable from the mutant species studied.

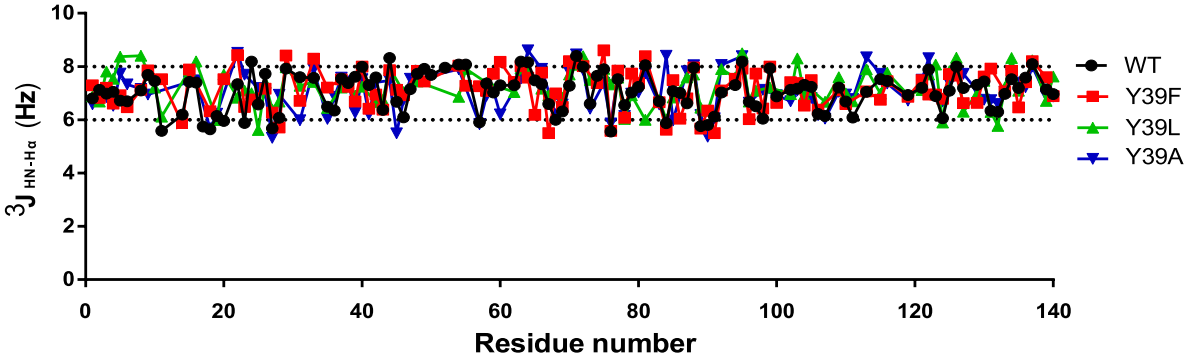

Figure 11: $^3J_{HN-H\alpha}$ profiles measured for the wt and Y39F, Y39A, and Y39L aSyn proteins.

4.1.3. Aromaticity at position 39 and its impact on aSyn-PcTS interaction

The binding of the compound is characterized at a residues specific level by monitoring the changes in the intensities of cross-peaks in 2D NMR spectra

As previously shown, complete loss of PcTS binding to the 35–41 region was observed when the Tyr residue in position 39 was replaced by Ala[51]. We then studied the mutants Y39F, Y39L, and Y39A of aSyn, aiming to determine the role of these residues in directing the binding of the anti-amyloid compound PcTS to the N-terminus (Figure 12). We measured I/I_0 profiles of backbone amide groups based on the severe broadening observed for the most affected signals, a behaviour that is typical of a system undergoing intermediate exchange on the NMR timescale.

In Figure 12 we observe low I/I_0 ratios for residues near Phe4, that are conserved even after mutation at position 39, indicating that both sites are non-interacting, independent binding sites. On the other hand, the interaction of PcTS with Tyr 39 is kept for wt and Y39F but replacing the aromatic side-chain with leucine and alanine was sufficient to impair PcTS binding at the motif centered at position 39.

Altogether, these results demonstrate unequivocally that aromaticity at position 39 also has a critical role in PcTS binding to the N-terminus of aSyn and confirm that specific aromatic interactions with the Y39 residue provided a central mechanistic basis for the inhibitory process of PcTS on aSyn fibrillation.

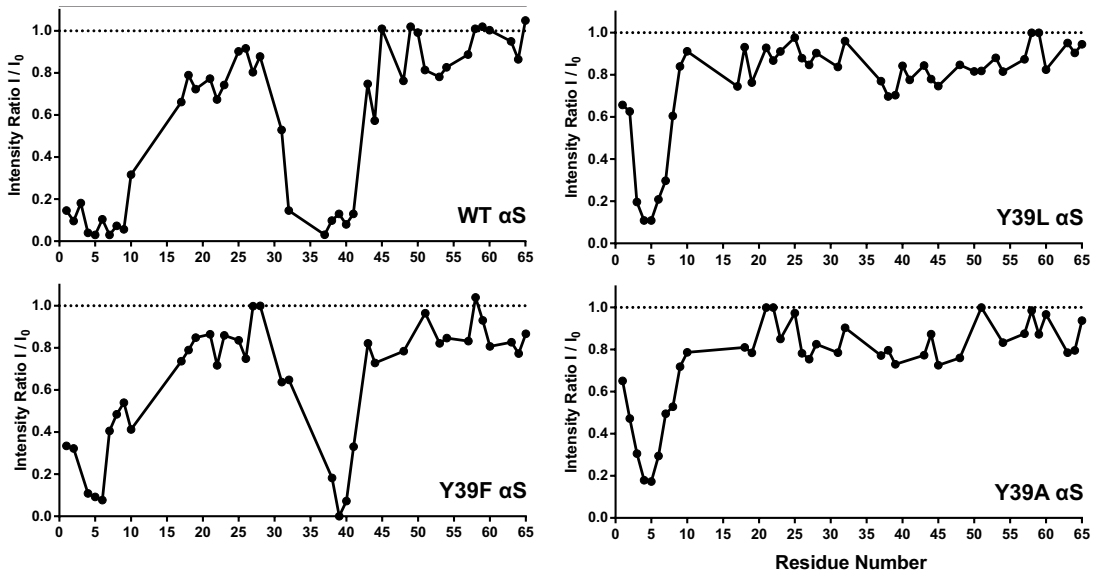

Figure 12: Structural characterization of the interaction between phthalocyanine tetrasulfonate and the Y39 aSyn mutants monitored by NMR spectroscopy. I/I_0 profiles of 50 μM wt, Y39F, Y39L, and Y39A aSyn proteins in the presence of 50 μM phthalocyanine tetrasulfonate (PcTS).

4.1.4. Removal of aromaticity at position 39 impairs the in vitro amyloid fibril assembly of aSyn

Monomers consumption measurements by NMR, and TEM-AFM images, were combined to assess the characterization of aSyn amyloid assembly.

The time course of aggregation of wt aSyn was monitored as monomer consumption by 1D ^{1}H NMR spectroscopy, where the amount of monomer remaining soluble was determined by the integration of the curve in the aliphatic region in the NMR spectra (0.7 – 1.0 ppm); whereas wt was comparable to that measured for the Y39F mutant, those species containing the Y39L and Y39A mutation showed a significant reduction in the rate and amount of aggregated protein (Figure 13a).

The morphology of the aggregation products of the aSyn variants after 120h incubation was then characterized by transmission electron microscopy (TEM). Ultrastructural visualization of the protein deposits obtained for the Y39F species revealed the presence of abundant amounts of typical amyloid fibrils that were morphologically indistinguishable from those formed for the wt protein. In contrast, the TEM images corresponding to the Y39L and Y39A species showed predominantly nonfibrillar protein structures, with a minuscule amount of isolated fibrillar components detectable only for the Y39L variant (Figure 13b).

To further characterize the structures observed in electron micrographs, atomic force microscopy (AFM) was performed. As shown in Figure 13c, samples of wt and Y39F aggregates are comprised of typical amyloid fibrils. In contrast, AFM images of the final products of aggregation of Y39L and Y39A resulted mostly in the formation of nonfibrillar, spheroid-like aggregates.

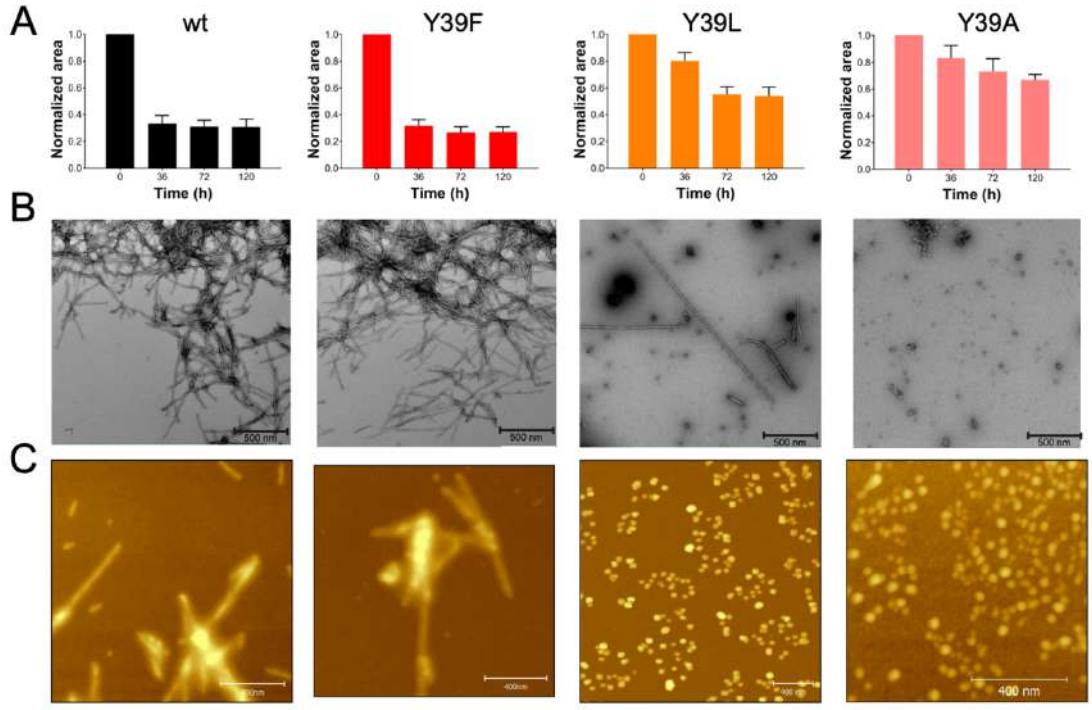

Figure 13: Effects of Y39 mutations on aSyn fibril formation. a) Level of remaining soluble aSyn monomers determined by 1D ^{1}H-NMR as a function of aggregation time. b) Representative negative-stain electron microscopy images of aSyn aggregates (50 µM samples) taken at 120 hr. Scale bars, 500 nm. c) AFM of aSyn aggregates (50 µM samples) after 120 h incubation. Scale bars, 400 nm

Results consistent with those reported by NMR were independently obtained when circular dichroism (CD) and the amyloid-sensitive Thioflavin T (ThT) fluorescence assay were used to determine the change in secondary structure content of aSyn species during fibril assembly (Figure 14). The final product of aggregation after 120 h was studied by CD spectroscopy (Figure 14a). Supernatants (red) showed a typical curve for random coil structure for all the species, whereas pellets (green) of wt and Y39F variants were the only ones showing the typical beta-sheet profile. Black curves correspond to CD spectra of the monomeric states (t=0h). More information was obtained with the ThT fluorescence intensities (Figure 14b), which upon binding to amyloid fibrils ThT gives strong fluorescence. At the final stage (t=120h) the intensity of fluorescence is high for wt and Y39F, being lower for the Y39L and Y39A species due to the absence of amyloid fibrils formation. Altogether, these results demonstrate that mutations Y39L and Y39A impair the in vitro amyloid fibril assembly of aSyn.

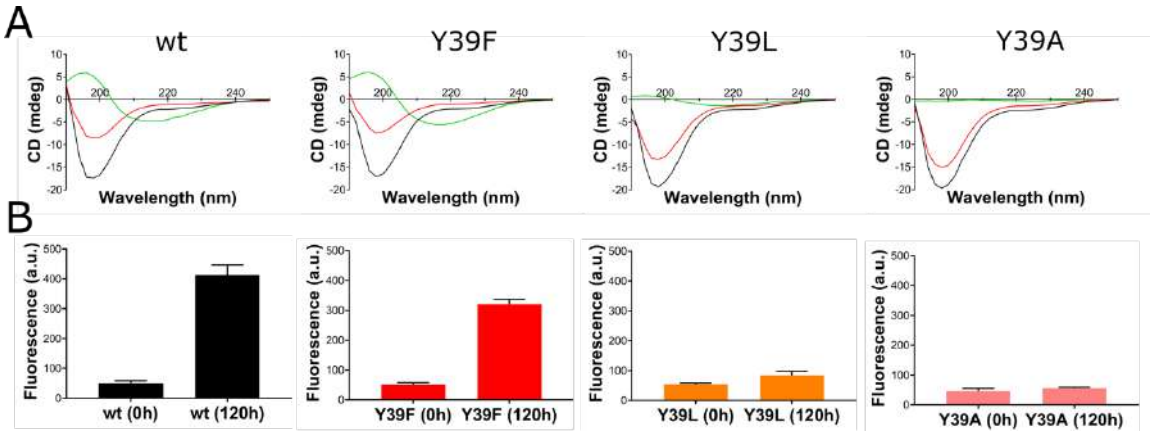

Figure 14: Change of the secondary structure in the Initial and end points of the aggregation. a) FAR-UV CD spectra corresponding to the supernatant (red) and pellet (green) obtained from the final product of aggregation(t=120h) of the studied aSyn species. Black curves correspond to the CD spectra of the monomeric states (t=0h). b) ThT fluorescence intensities corresponding to the final state of aggregation of the studied aSyn species (t=120h) and their monomeric states (t=0h).

4.1.5. The aggregation propensity of aSyn in biological models is affected by the aromaticity at position 39

Cellular and animal-based assays were performed to corroborate the in vitro behaviour of the mutant proteins, and if it is possible to observe intracellular inclusions formation when the protein has aggregation propensity.

The co-expression with specific proteins facilitates the formation of more mature aggregates that can be used as models for studies of the pathogenic mechanism of aSyn aggregation in Lewy bodies.

Co-expression of synphilin-1, an aSyn interacting protein, and SynT (a partially truncated aSyn-EGFP, non-fluorescent carboxy-terminally modified protein[118]) can induce the formation of inclusions in H4 cells. When cells were treated with aSyn wt and their mutants, aSyn wt promoted a significant number of transfected cells displaying aSyn inclusions (Figure 15a), while analysis of protein inclusion formation in the Y39F transfected cells showed a pattern comparable to that of wt aSyn (Figure 15b). In contrast, for the Y39L and Y39A variants, we observed a significant decrease in the percentage of cells with inclusions (Figure 15a-b); To investigate whether these effects might be explained by differences in the levels of aSyn being expressed, we performed immunoblot analysis. There was no correlation between the expressed levels of the studied proteins and inclusion formation, indicating that the results were intimately correlated with the effects of the mutations on aggregation (Figure 15c).

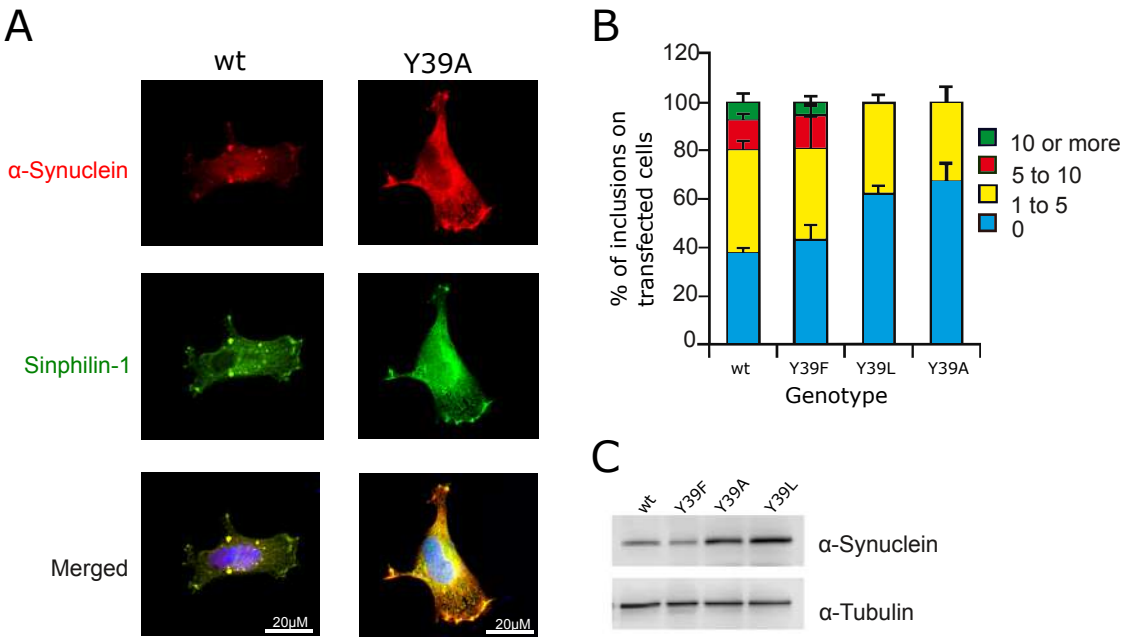

Figure 15: Modulation of aSyn inclusion formation in cultured cells. a) Representative images of intracellular wt and Y39A aSyn inclusion formation in human cultured cells. Scale bars, 20 μm. b) Quantification of aSyn inclusions. Transfected cells were classified in different groups: 1 to 4, 5 to 9, and equal to/more than 10 inclusions. Results were expressed as the percentage of the total number of transfected cells obtained from three independent experiments. At least 50 cells were scored per experiment (n = 3). c) Immunoblot analysis of the expression levels of the aSyn variants studied in H4 cells

Next, to validate the results in postmitotic neurons, we used the nematode C. elegans as a multicellular model system to study the aggregation of aSyn variants at position. These experiments were carried out by Nicola Böffinger (Department of Structural Cell Biology, Institute for Cell Biology and Neuroscience, Goethe University Frankfurt, Frankfurt, Germany). When expressed in motoneurons as a C-terminal fusion with mCherry, wt or Y39F aSyn mutant formed numerous large aggregates (Figure 16a-b). By contrast, the number and size of these aggregates were reduced when Y39L or Y39A mutant forms of aSyn were expressed (Figure 16a-b). Like in the cell model, the observed differences in aggregation were not due to differences in expression levels of aSyn as quantified by Western blot experiments (Figure 16c).

Overall, the results obtained in culture cells and C. elegans neurons demonstrate that intracellular inclusions of aSyn are significantly reduced when

Y39L and Y39A aSyn variants were expressed as compared to wt or Y39F aSyn variants.

This strongly suggests that like biophysical studies, the aggregation propensity of aSyn is also affected by the aromaticity at position 39.

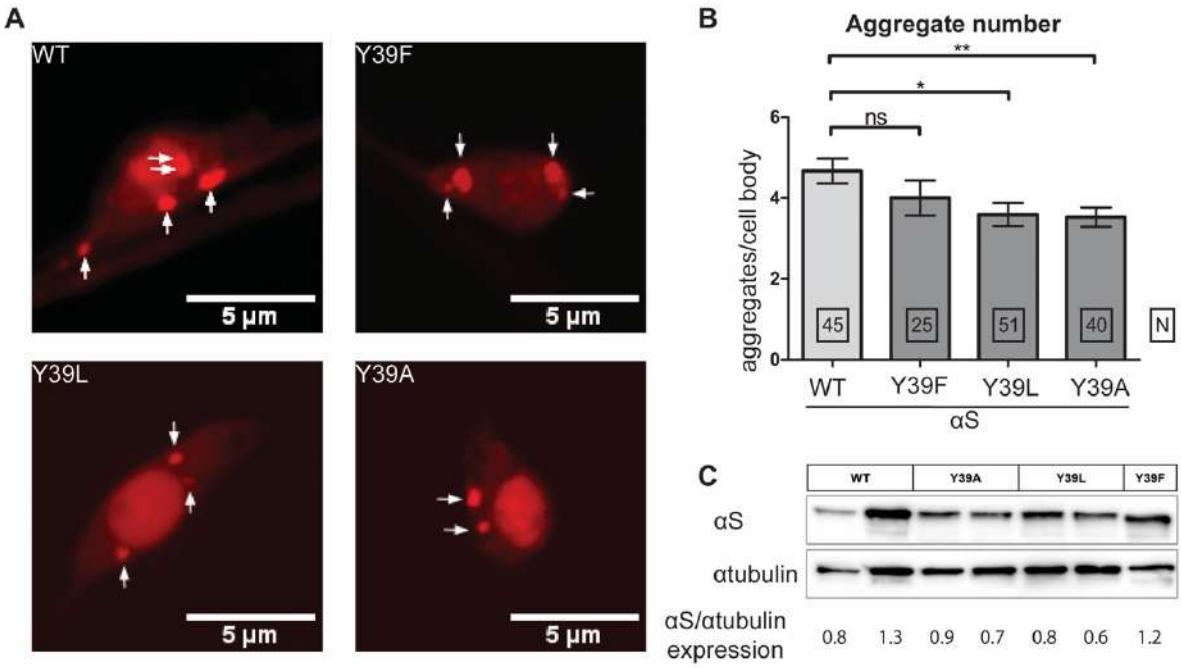

Figure 16: Aggregation of aSyn in C. elegans motoneurons is affected by the aromaticity at position 39. a) Confocal images of one-day adult motoneurons showing the formation of intracellular aSyn-mCherry aggregates. Scale bars, 5 µm. b) Quantification of intracellular aSyn aggregates. The values shown represent the mean ± SEM; for comparison an unpaired, two-tailed t-test was used; * and ** denote $p < 0.05$ and 0.01, respectively. c) Total aSyn expression levels were quantified by Western blot experiments relative to αTubulin loading control.

4.1.6. Aromaticity at position 39 is a determinant of the membrane-bound conformation of aSyn

Conformational changes in aSyn associated with membrane binding were monitored by far-UV CD and NMR spectroscopy.

Since the association of aSyn with cellular membranes and changes in those interactions might have functional and pathological implications, we also investigated the effect of mutations at Y39 on the binding features of aSyn to lipid-vesicles (small unilamellar vesicles: SUVs).

Changes in aSyn structure associated with membrane binding were monitored by far-UV CD, which reports on the increase in aSyn α-helicity upon interaction with phospholipids[102]. The far-UV CD spectra of aSyn is characterized by a minimum at 198 nm in the absence of SUVs, whereas a maximum at 192 nm and minima at 208 nm and 222 nm are typical of its membrane-bound state.

CD spectra for the wt and Y39A aSyn species in the presence of varying concentrations of SUVs are shown in Figure 17a-b, showing the typical transition from random coil to alpha-helix in both cases. To compare the binding affinities of aSyn and its Y39F, Y39L, and Y39A variants to SUVs, the mean residue molar ellipticity at 222 nm ($[\theta]_{MR,222}$) for all species was plotted as a function of lipid concentration (Figure 17c). In all cases, analysis of the titration data yielded Kd values in the 0.1–0.2 μM range.

To explore the structural features behind the binding, we used NMR spectroscopy. The ^{15}N-labeled aSyn mutants were analyzed by 2D ^{1}H–^{15}N HSQC spectra recorded in the absence or presence of SUVs. This assay provides a residue-by-residue readout of lipid binding that is useful to evaluate which residues on the protein are in greatest contact with the vesicle[101].

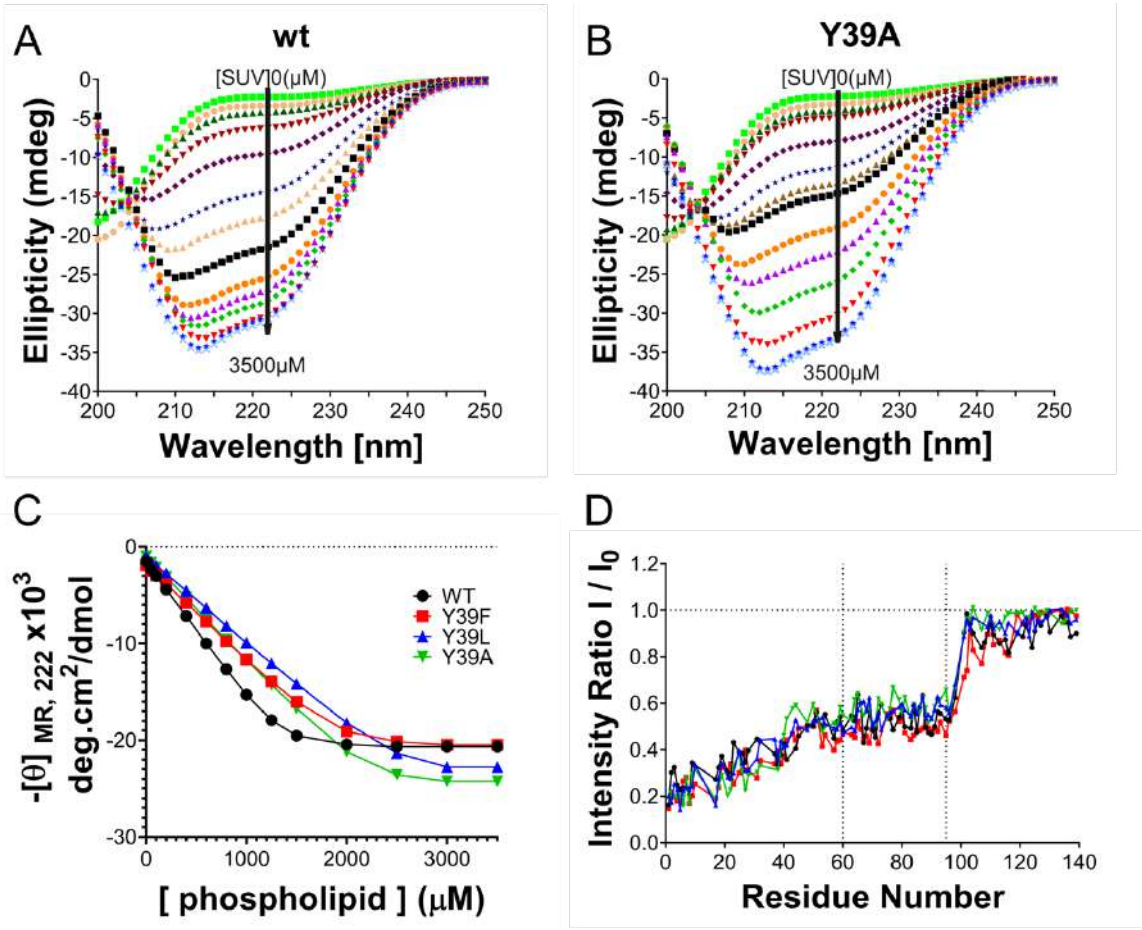

Figure 17: Effect of Y39 mutations on the membrane binding features of aSyn. a-b) cd spectra of wt (a) and Y39A aSyn (b) species with increasing concentrations of SUVs (0 to 3.5 mM). c) Data from $\theta_{MR,222}$ in wt aSyn and its Y39F, Y39L, and Y39A variants as a function of lipid concentration were fit to Equation 2 to calculate K_d values. d) Graphs of I/I_0 (where I and I_0 are the peak intensities observed in the presence and absence of SUVs, respectively) plotted against residue number for wt aSyn and its Y39F, Y39L, and Y39A variants.

NMR experiments correlate the normalized signal attenuation of resonances from specific residues, obtained in the presence of SUV, to the binding of these residues to the membrane. For each residue of aSyn, I/I_0 is the proportion of molecules in an aSyn/ SUV mixture in which the residue remains mobile and in solution (Figure 17d), and the fractional attenuation ($1 - I/I_0$) is the proportion of molecules in which the residue is tightly associated with the membrane[101]. We used this approach to characterize the aSyn–membrane interaction; in particular, to determine the fractional population of molecules bound to the membrane ("total bound population") and whether the central

hydrophobic (aggregation-prone) region was either dissociated or associated in the case of conformers referred as “exposed” or “hidden,” respectively[102].

The fractional population of molecules bound to the membrane in either mode was determined from the mean attenuation of residues 3–9, based on the fact that the N-terminal segment of aSyn has the higher membrane affinity compared to other regions in the first interacting 100 amino acids[119] and is lipid-bound in the case of both exposed and hidden conformers[101]. Regarding the conformation of the hydrophobic domain NAC at the membrane, which is described to have an important role in the regulation of biological properties of aSyn and its oligomerization[53,120], the fractional population of protein in the hidden state was determined by measuring the mean attenuation of residues 66–80[102], a segment that plays a key role in aSyn self- assembly[19]. On the other hand, the fractional population of protein with residues 66–80 in the exposed state was determined by subtracting the hidden population from the total bound population (residues 3-9)[102].

As shown in Table 4, the aSyn mutants exhibited nearly the same total populations for their membrane-bound states. However, clear structural differences were observed among the vesicle-bound forms of the aSyn variants at the level of the hydrophobic NAC domain. Our results indicate that the percentage of total bound molecules with the hydrophobic NAC in a membrane-dissociated state was increased by a factor of 1.7 and 2.0 in the cases of the Y39L and Y39A variants compared to wt and Y39F. This means that aromaticity at position 39 regulates lipid membrane interactions involving the central hydrophobic NAC domain.

Table 4: Lipid-binding affinities of aSyn variants titrated with SUVs and fractional populations of membrane-bound aSyn conformers determined by NMR.

Variant	Total bound[a,b]	Hidden[a,c]	Exposed[a,d]	K_d (μM)[e]
wt	0.72	0.57	0.15	0.17 ± 0.02
Y39F	0.71	0.56	0.15	0.17 ± 0.03
Y39L	0.74	0.49	0.25	0.12 ± 0.02
Y39A	0.70	0.40	0.30	0.13 ± 0.05

[a] Values were determined from 2D ^{1}H-^{15}N-HSQC data in Figure 4 and are expressed as a fraction of the total protein; each sample consisted of a mixture of aSyn and phospholipids at concentrations of 100μM and 2.5 mM respectively.

[b] Determined from the mean attenuation of residues 3-9 (i.e total bound = 1 - $\{I/I_0\}_{mean,3-9}$)[98,102]

[c] Determined from the mean attenuation of residues 66-80 (i.e total bound = 1 - $\{I/I_0\}_{mean,66-80}$)[98,102]

[d] Calculated as the difference between the total bound population and the hidden population[98,102]

[e] Estimated from the fitting of CD titration data to Eq. 2

4.2. V15A mutation in aSyn facilitates aggregation by reducing membrane affinity

In 2019 was reported a patient with familial PD harboring V15A, whose age at onset (AAO) was 59 years old[121], and a family history of disease: two of his three siblings also developed PD and dementia and another older sibling was an unaffected carrier.

In 2020, the variant V15A was identified in four siblings belonging to an Italian family[122]. A 56-year-old woman experienced PD at the AAO of 47, characterized by rapid progression. Two other siblings, a 53-year-old male, and a 57-year-old female, also developed PD at the age of 50. The fourth sibling, aged 61, did not exhibit motor signs of PD but displayed psychiatric disturbances such as depression and anxiety around the age of 54. Notably, the parents of these individuals were not reported to have Parkinson's disease. Through next-generation sequencing (NGS) analysis of a panel of PD-related genes, a novel heterozygous missense variant (p.V15A) in the SNCA gene was identified, and this variant was found to be shared by all four siblings.

Subsequently, in 2022 a genetic screening identified the missense variant in three affected individuals from two independent Japanese PD families with typical parkinsonism[123], suggesting a potential pathogenic role of the V15A aSyn variant.

Initial biochemical and aggregation experiments pointed to a reduced affinity for phospholipids and increased fibril elongation activity for V15A aSyn when compared to the wild-type (wt) protein[123].

Our specific aims are:

- To elucidate the impact of the V15A mutation on the conformational ensemble of monomeric aSyn.
- To characterize the amyloid assembly of the V15A variant.
- To evaluate the effect of the V15A mutation on aSyn lipid interaction

4.2.1. The change of Valine for Alanine at position 15 does not change the structural properties of aSyn monomers

Biophysical characterization of V15A variant was performed by circular dichroism and NMR spectroscopies

First, we examined by 2D ^{1}H-^{15}N NMR spectroscopy the structural changes between the wt (black) and V15A variant (orange) in aqueous. The network of cross-peaks in both spectra displayed similar chemical shift profiles (Figure 18a), except those located in the vicinity of the mutation (Figure 18b). This is consistent with the results from CD, where both spectra show a minimum at 198 nm (characteristic of random coil structure) (Figure 18c). Consistent with these findings, a residue-specific analysis of the secondary structure propensity of V15A aSyn by C^{α} secondary chemical shifts measurements revealed the presence of small perturbations close to the mutation site (Figure 18d).

Overall, the data allow us to conclude that the V15A mutation does not strongly perturb the conformational ensemble of monomeric aSyn in solution.

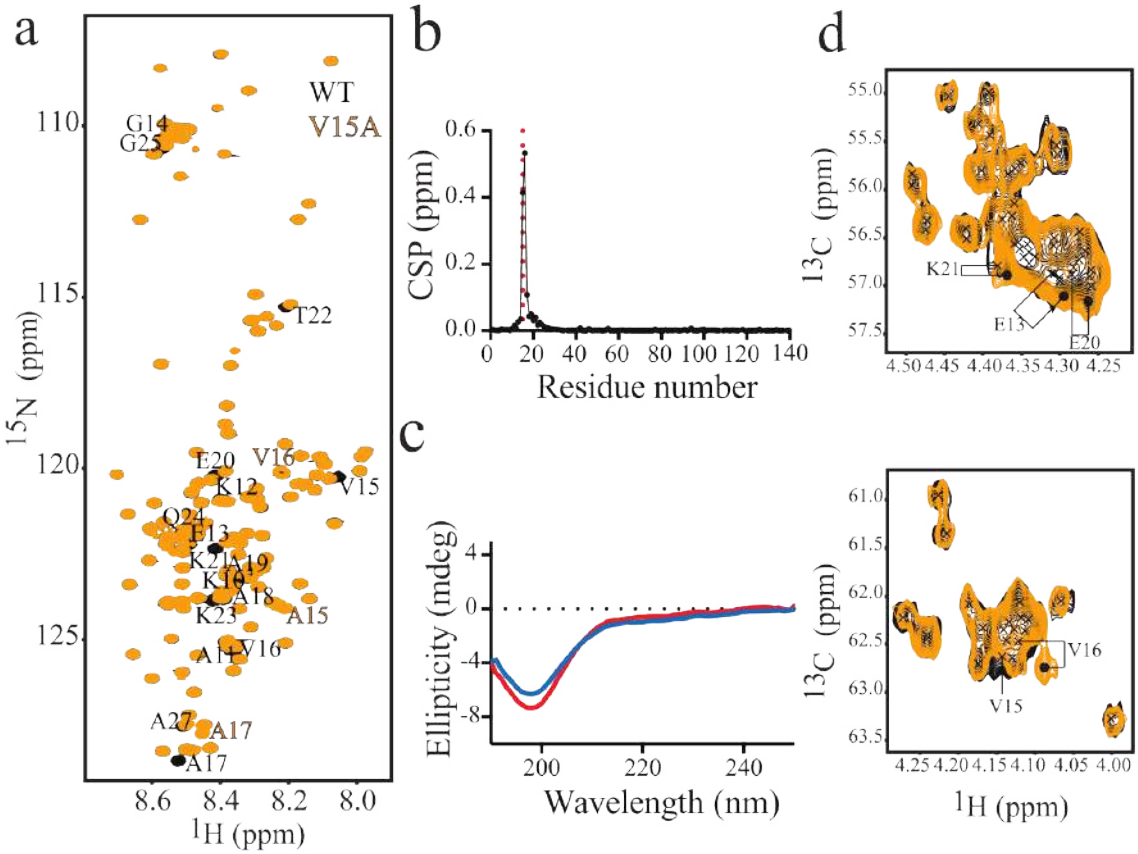

Figure 18: Structural analysis of the monomeric state in the V15A aSyn variant. a) HSQC spectra for wt (black) and V15A mutant (orange), residues with some shifts are labelled. b) Chemical shift perturbation is only near to the mutated residue, red dot at position 15. c) Spectra of random coil for wt (blue) and V15A mutant (red) by CD. d) Secondary chemical shift in C^{α} for wt (black) and V15A mutant (orange)

4.2.2. V15A mutation attenuates aSyn membrane binding

Liposomes that mimetic synaptic vesicles were used to analyze the binding features of the V15A variant by NMR spectroscopy

We investigated the effect of the V15A mutation on aSyn lipid interaction by preparing liposomes from a mixture of DOPE:DOPS:DOPC (5:3:2 w/w). Dynamic light scattering showed that the size of the liposomes remained largely unaffected in the presence of aSyn (Figure 19).

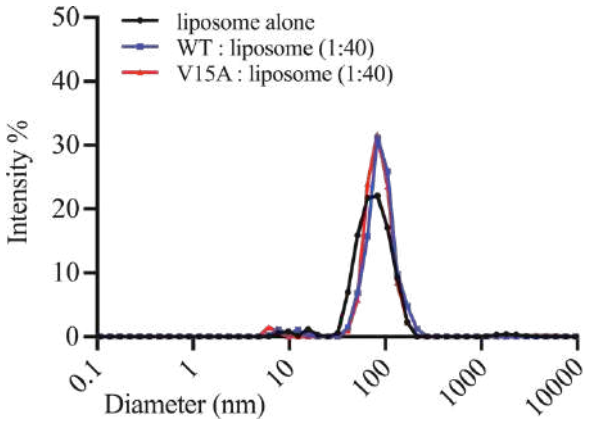

Figure 19. Interaction of aSyn with liposomes by DLS. Dynamic light scattering experiments of liposomes alone (black) and liposomes in the presence of wt (blue) and V15A (red) aSyn at 1:40 lipid-protein ratio.

NMR spectroscopy was then used to examine the effect of the mutation on aSyn's membrane binding ability with a residue-specific level of resolution. To this purpose, we monitored the changes in cross-peaks of amide groups in the presence of increasing liposome concentrations (Figure 20). The intensity profiles of overlapping spectra of wt (blue) and V15A (orange) aSyn variants in

the absence (black, both samples) and the presence of liposomes are indicative of a weaker binding of V15A compared to wt.

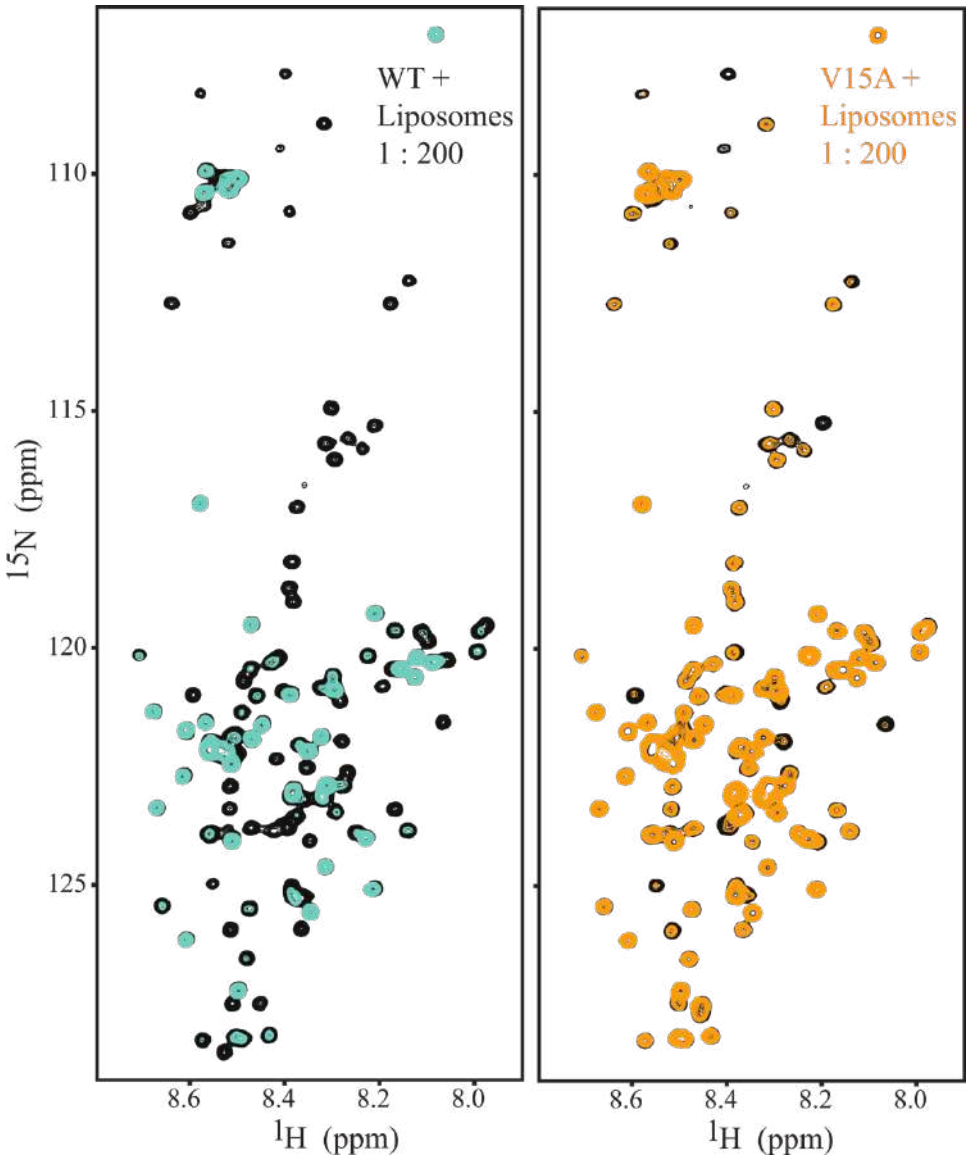

Figure 20. Interaction of aSyn with liposomes by NMR. ^{1}H-^{15}N-HSQC of wild-type (wt, left) and V15A mutant (right) aSyn without (black) and with liposomes (molar ratio 1:200).

Figure 21a reveals that both proteins have a similar binding profile, with the 100 N-terminal residues experiencing intensity reduction upon binding. However, the decrease in intensity was considerably less for the mutant when is exposed to increased concentrations of liposomes. Added to that, we observed that the region most affected by lipid-binding comprises the stretch of residues in the segment 1 to 25 (Figure 21a), which was shown to act as a membrane anchoring moiety in aSyn[31,124].

As it was shown in previous chapters, aSyn adopts α-helical conformation upon interaction with membranes. We therefore also used CD to follow the transition from random coil (minimum at 198 nm) to alpha helix (two minimum at 222 nm and 208 nm) and to compare the ability of both proteins to form α-helical structure in the presence of increasing levels of liposomes. The CD-based binding studies showed that the V15A aSyn variant displays a lower propensity to fold into α-helical structure in the presence of the liposomes (Figure 21b).

All together, our results indicate that the V15A aSyn variant has a lower membrane affinity compared to the wild-type protein.

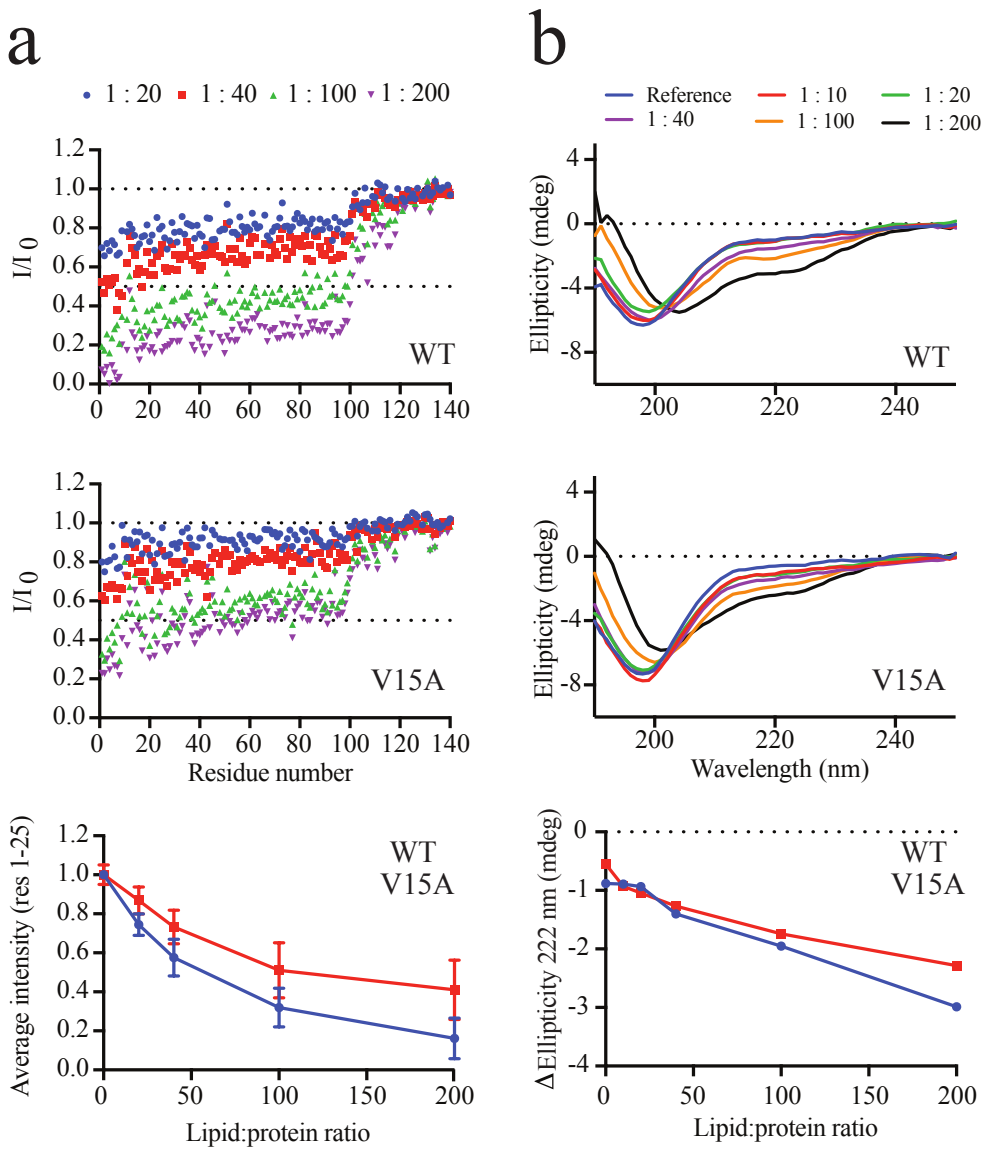

Figure 21: Binding properties of V15A followed by NMR and CD. a) Residue-specific 2D $^{1}H/^{-5}N$-HSQC peak intensity ratios for wt (top) and V15A (bottom) aSyn at increasing liposome

concentrations (molar protein:lipid ratios are indicated in different colors). In the lower panel, changes in the average intensity of the cross-peak signals of residues 1-25 in wt (blue) and V15A (red) species are shown for increasing liposome concentration. Errors bars represent std. b) Circular dichroism-based analysis of wt and V15A aSyn membrane binding at different protein:lipid ratios. The lower panel displays changes in the ellipticity ratio at 222 nm upon increasing concentrations of lipid for wt (blue) and V15A (red) aSyn.

4.2.3. Addressing the role of specific residues in aSyn anchoring to membrane.

AlphaFold2 (Structure Prediction Software) was used to observe the localization of particular residues and assess possible loss/gain of intramolecular interactions with the mutation.

In the AlphaFold2-predicted α-helix, the three hydrophobic residues F4, V15, and V26 are located on the same side of the helix, with their side chains pointing in a similar direction. A decrease in membrane affinity by the V15A mutation is consistent with the location of Valine 15 in the helical structure of aSyn predicted by AlphaFold2 (Figure 22, left).

When aSyn is bound to a membrane, these side chains are likely to insert into the hydrophobic environment of the lipid bilayer and thus anchor aSyn to the membrane. Consistent with this hypothesis, the artificial F4A mutation attenuates aSyn membrane binding[113], whereas from continuous-wave EPR measurements, it becomes evident that all the lipid-exposed residues are generally hydrophobic[33]. When Valine 15 is replaced by Alanine, one of the three membrane anchors is lost. In addition, fewer intramolecular interactions might be formed (Figure 22, right). Thus, after mutation this position becomes less hydrophobic and less stable, which could contribute further to the decreased membrane binding of the V15A aSyn variant.

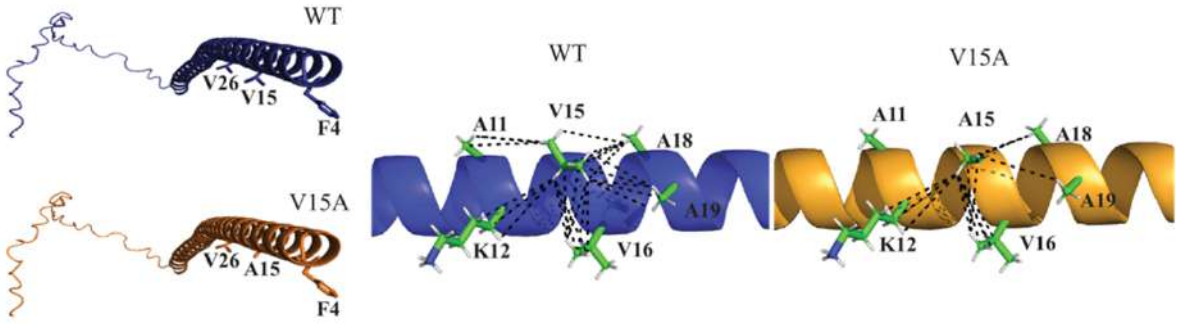

Figure 22: α-helical structure predicted by AlphaFold2 (AlphaFold database id AF-P37840-F1) for wt (top) and V15A (bottom) aSyn variants. Interactions between side chains from some residues (right) of wt and V15A aSyn are shown with a cutoff of 5 Å.

4.2.4. V15A mutation facilitates aSyn aggregation in the presence of liposomes

Aggregation kinetics of wt and V15A aSyn variants in their free and membrane-bound state were monitored by the ThT fluorescence assay, in the free state and in the presence of liposomes.

From the analysis of the aggregation features of the studied aSyn variants in solution, it becomes evident that (Figure 23a, left) the kinetic parameters of fibrillization were very similar for both wt and V15A aSyn variants. In both cases, aggregation started after 25 h of incubation, reaching similar values of fluorescence intensity, with potentially a slight delay in aggregation of V15A aSyn (Figure 23b).

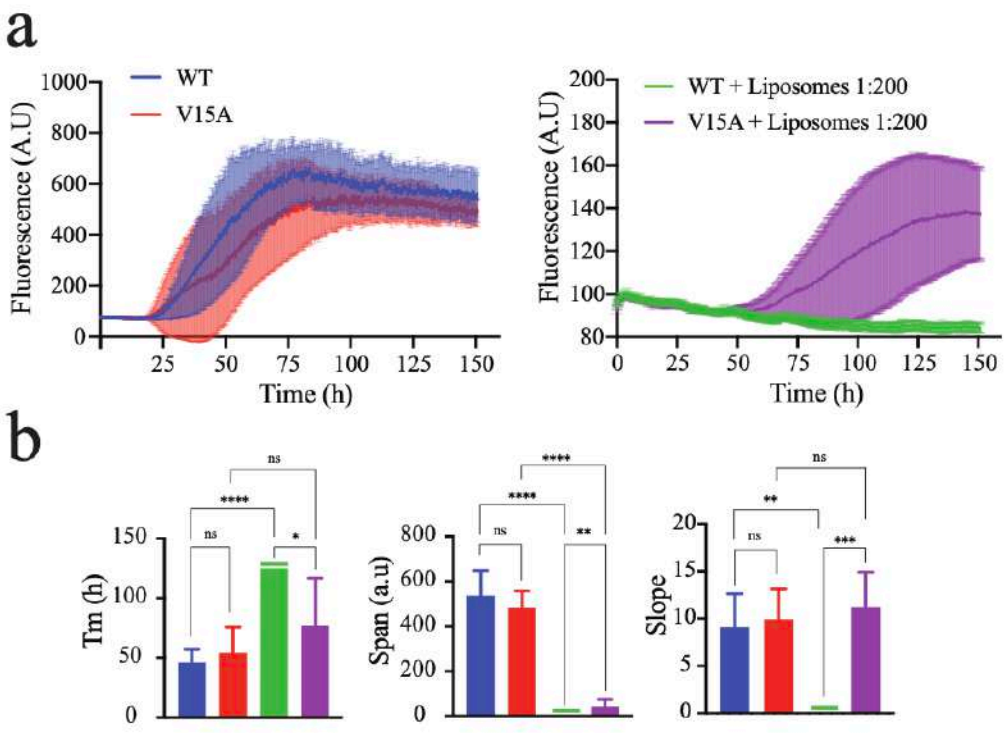

Figure 23. V15A mutation facilitates aSyn aggregation in the presence of liposomes. a) Fibrillization kinetics of aSyn wt (blue) and V15A (red) in solution (left), and in the presence of liposomes (right; wt/green and V15A/purple) measured by ThT fluorescence. Each curve represents the average of the group, error bars indicate std. b) Parameters describing the kinetics of aSyn aggregation in the absence (blue/wt, red/V15A) or presence of liposomes (green/wt, purple/V15A). T_m is the half-time of aggregation, span is the difference in fluorescence intensity at the start (bottom) and end of aggregation (top). Statistical analysis was conducted using t student test: ($p < 0.05$) and non-significant (ns), significant (*, 0.0109), (**, 0.005), (***, 0.0009), (****, <0,0001).

We next asked whether the decreased membrane affinity of V15A aSyn might trigger aSyn aggregation in the presence of membranes, i.e. in a condition that mimics the pre-synaptic localization of aSyn. In comparison, the ThT intensity of aggregated V15A aSyn in the presence of liposomes was significantly smaller than in the absence of liposomes. Interestingly, while the intensity of the ThT signal in the V15A samples increased after ~50 h, samples containing wt aSyn did not show any changes in the ThT levels even at incubation times as long as 150 h. (Figure 23a, right).

4.2.5. Linking the weaker binding of V15A to liposomes with its fibril state in aggregation-inducing conditions

Aggregation assays in plate reader were performed combined with TEM imaging and CD spectroscopy to observe final structures.

Electron microscopy demonstrated the formation of ß-structure containing amyloid fibrils for wt (blue) and V15A aSyn (red) in the absence of liposomes (Figure 24). However, the situation drastically changed when we incubated the proteins in the presence of liposomes (protein:lipid molar ratio 1:200). Electron microscopy confirmed the presence of fibril-like structures together with liposomes in samples containing the V15A aSyn variant (purple). In contrast, no fibrillary structures were found in wt aSyn samples (green) (Figure 24). This observation is consistent with the results derived from aSyn aggregations performed in presence of liposomes.

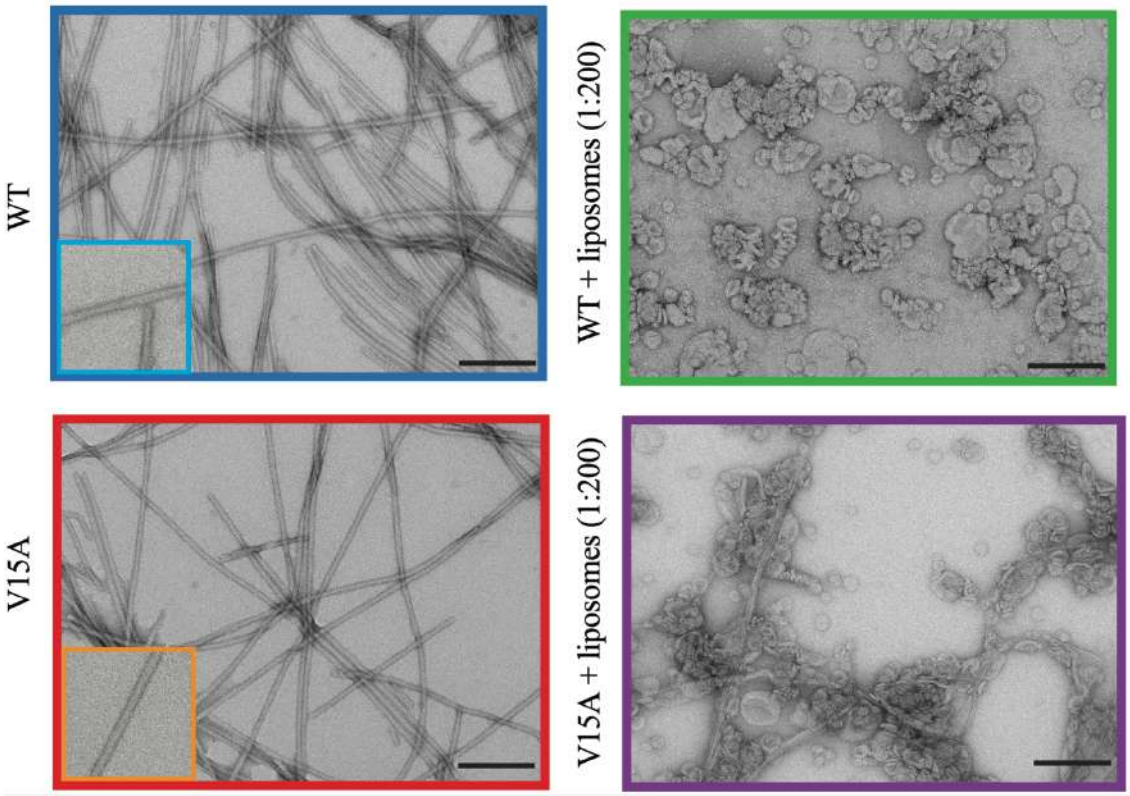

Figure 24: Electron micrographs of wt and V15A aSyn after aggregation, in the absence (left) or presence of liposomes (right). Scale bar, 200 nm. Insets show zoomed fibril views.

To gain further insights, CD spectra were registered for the free and bound-states of the aSyn variants in aggregated conditions (Figure 25, left). Analysis of samples containing wt and V15A aSyn in solution revealed the typical random coil profile. On the other hand, in the presence of liposomes, the wt species shows the characteristic alpha-helix band at 222 nm, whereas this is not observed for the V15A aSyn variant (purple curve). Consistent with this finding, the quantitative analysis of the CD spectrum of aggregated V15A aSyn in the presence of liposomes indicates ~70 % ß-structure and ~30 % α-helical content, suggesting that a large population of V15A aSyn was converted into amyloid fibrils (Figure 25, right).

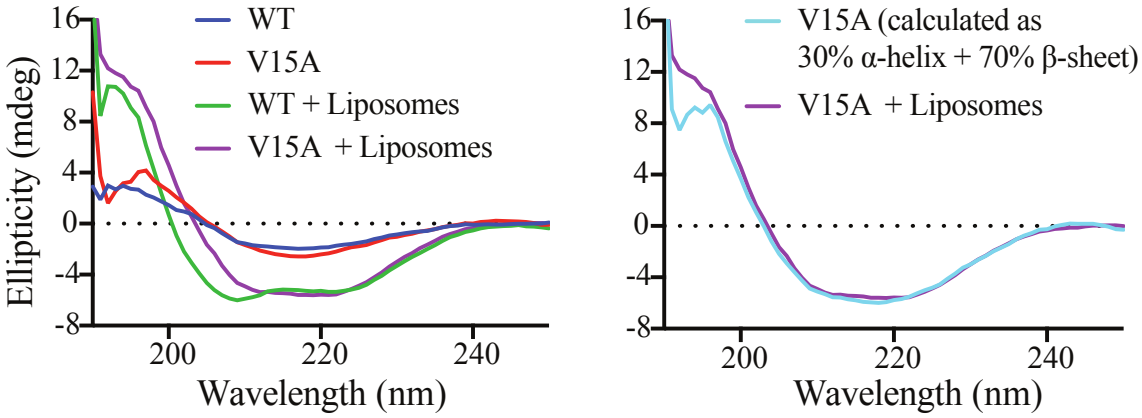

Figure 25: Secondary structure of V15A free and binding to liposomes. CD spectra (left) of samples taken from the aggregation assay in Figure 23 at the end of incubation. On the right CD spectrum of V15A aSyn in the presence of liposomes (purple) compared to a calculated curve (light blue).

4.3. Acetylation of lysines in aSyn modulates fibril assembly and impairs binding to membranes.

Several PTMs have been implicated in the pathogenesis of neurodegenerative diseases[125]. In particular, changes in acetylation are believed to play a role in disrupting the proper functioning of protein clearance processes[126,127]

In that direction, while several studies have been reported about the acetylation of the N-terminus[128–132] of alpha-synuclein and its impact on protein function and dysfunction, only a few were focused on the acetylation of lysines at the N-terminal region of the protein and its potential effects[133]. However, the high abundance of this residue in the protein sequence of aSyn together with the accessibility of the Acetyl COA to these residues in such a disordered protein are factors that make this modification more frequent than previously thought.

Added biological relevance to this structural modification, the strategic location of lysines in the helical conformations adopted by aSyn in the presence of lipid membranes makes these residues and their charges a key factor in the modulation of the interaction process. On the other hand, Lysines are believed to be perpendicular to the helical axis and the alignment of the alpha helix structure allows the Lysines to interact with the head of the lipids, and the modification of the charge on this residue could impact the ability to bind lipid membranes.

Our specific aims are:

- To evaluate the structural effects of Lysine acetylation on alpha-synuclein
- To assess the aggregation properties of acetylated alpha-synuclein
- To evaluate the impact that Lysine acetylation might have on the affinity features of aSyn by lipid membranes.

4.3.1. Acetylation of lysines in alpha-synuclein impacts strongly on its aggregation profile

Mass spectrometry experiments of modified protein were performed to uncover the degree of acetylation of aSyn followed by the evaluation of its amyloid assembly process and the analysis of the morphology of its final product of aggregation.

Analysis of soluble aSyn purified from Parkinson's disease and other alpha synucleinopathies by using liquid chromatography with tandem mass spectrometry (LC-MS/MS)[94] allowed the identification of many aSyn post-translational modifications (PTMs). Interestingly, one of the most abundant modifications resulted in be acetylation of lysines in about 10 to 15 sites of the primary sequence of the protein. (Figure 26 a).

To determine unambiguously the sites of lysine acetylation in alpha-synuclein with a single-residue resolution, and quantify their degree of acetylation, we first performed in vitro acetylation reaction in samples containing monomeric aSyn in the presence of p300 and CBP. Mass spectrometric analysis of the treated aSyn samples revealed that almost all lysine residues had been acetylated (Figure 26c), with the highest levels of modification in lysines located at positions 43, 45, 58 and 60. (Figure 26b).

Next, we determined the impact of these modifications on the aggregation properties of aSyn. As shown in Figure 26d, the lysine-acetylated variant of aSyn shows a lag time of approximately 10h followed by an unusual aggregation profile characterized by the presence of two exponential growth phases and two plateaus. On the other hand, the untreated aSyn samples showed the typical sigmoidal aggregation profile with a lag phase of ~20h, that's is followed by an exponential growth phase ending in a plateau after 45 h of aggregation reactions.

When the treated aSyn samples were visualized by TEM (Figure 26e), the product of aggregation at the first plateau revealed the presence of abundant amounts of oligomeric species (orange box 1), whereas the second plateau confirmed the presence of twisted fibrillary structures and oligomeric

species (orange box 2). In contrast, unmodified aSyn samples showed typical amyloid fibrils and the absence of oligomeric structures (green box).

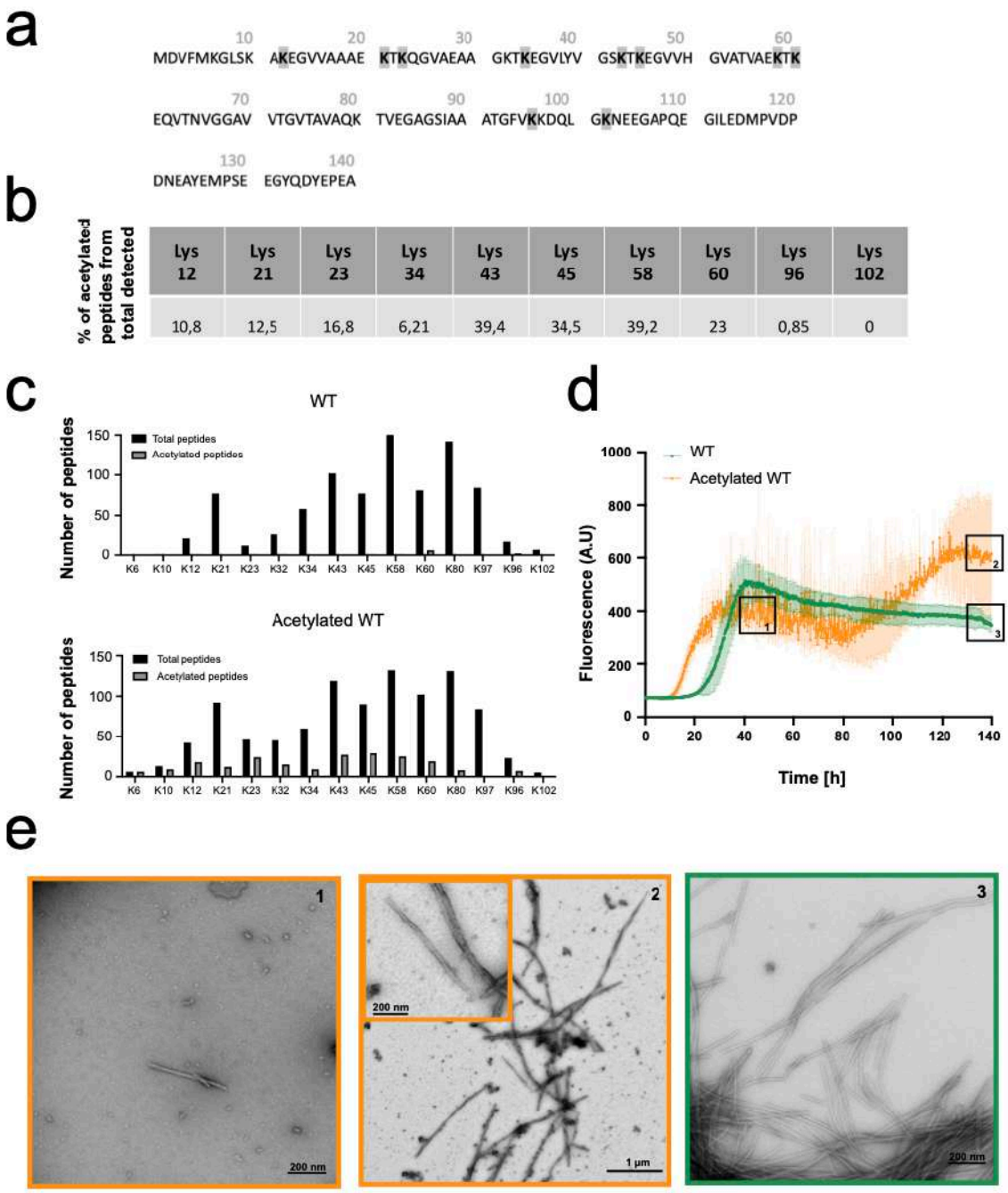

Figure 26: Linking acetylation of lysines in aSyn with its aggregation properties. a) Primary sequence of aSyn. Lysine residues found acetylated in human brain extracts are shaded in grey. b) Percentage of acetylated peptides from the total amount detected by mass spectrometry. c) Number of acetylated peptides in comparison to total peptides detected by mass spectrometry. d) Fibrillization kinetics of unmodified wt (green) and acetylated aSyn samples (orange). e) Negative-stain electron micrographs of unmodified wt (green) and acetylated aSyn samples (orange).

4.3.2. Different conformation strains and stability between unmodified and acetylated fibrils

Differences in structure and stability were addressed by using amyloid-binding dye curcumin, digestion with pronase and proteinase, and sarkosyl treatment.

To investigate the presence of conformational differences, between aSyn fibrils derived from untreated and treated samples we used different approaches. First, we used the fluorescent dye curcumin which binds to specific amyloid conformations and displays two local maxima at ~520 and ~590 nm. Figure 27a shows two fluorescence spectra, corresponding to curcumin bound to aSyn fibrils (green) and modified aSyn fibrils (orange). The clear difference between the intensity ratios of the curcumin fluorescence at ~520 and ~590 in both fibril samples is indicative of their structural differences.

Next, we investigated the propensities of both groups of aSyn fibril to be hydrolyzed by proteases. In that direction, fibrils were incubated with pronase (Figure 27b), and then the pronase-resistant cores were pelleted and followed by mass spectrometry analysis (Figure 27c). Interestingly, although the extension of the rigid core seems to be similar in both types of fibrils, the distribution pattern of peptides along the primary sequence of the proteins reveals clear differences.

In the second stage, the conformational stability of both groups of fibrils was assessed by incubating 50 μM of untreated and modified aSyn fibrils with Proteinase K (3.8 μg/ml) at different times. And the protein products were visualized by SDS-PAGE and staining. As shown in Figure 27d, the banding pattern of PK-resistant aSyn fibril species formed in each case was different. Finally, solubilization of both types of fibrils with Sarkosyl 1% followed by centrifugation reveals the presence of a significant amount of species in the supernatant of modified-aSyn compared with the untreated aSyn samples (Figure 27e). We attribute these differences to the presence of soluble oligomeric species in the modified-aSyn samples. On the other hand, the pellet of both aSyn fibril samples showed the presence of insoluble fibrillar aggregates.

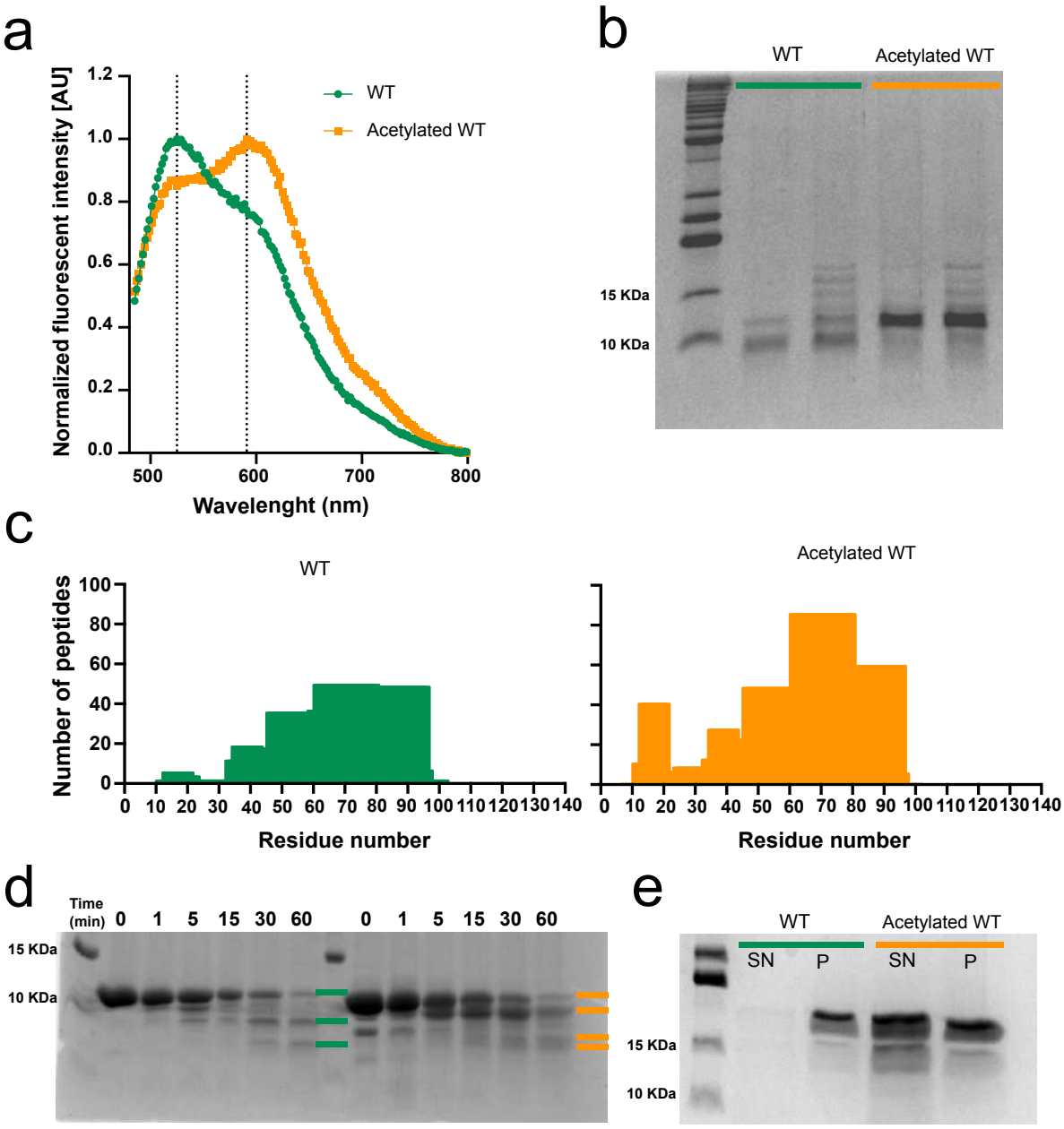

Figure 27: Stability and dye binding of unmodified and modified fibrils. a) Normalized fluorescence spectra of curcumin. b) Pronase digestion of unmodified fibrils (lane 1: 0.4 mg/mL, and lane 2: 0.2 mg/mL) and modified fibrils (lane 3: 0.4 mg/mL and lane 4: 0.2 mg/mL). c) Number of peptides detected by mass spectrometry after pronase digestion. d) Proteinase K digestion of unmodified fibrils (left) and acetylated fibrils (right). Band pattern at 60 min is highlighted in green and orange, respectively. e) Sarkosyl treatment of unmodified and acetylated fibrils. Soluble supernatant (SN) and insoluble pellet (P) fractions were isolated upon centrifugation.

4.3.3. Residue-specific HD exchange profiles for different strains

Hydrogen-deuterium exchange coupled to NMR combined with methods of rapid fibrils dissociation is used to gain insight into the structural basis determining the different conformational stability of the studied aSyn fibrils.

Previous studies from our labs[134], demonstrated conclusively that the NMR measurement of HD exchange profiles of aSyn samples is a key tool to identify the presence of different polymorphs. In that direction, we used this strategy to gain insight into the conformational basis of the distinction observed between unmodified and acetylated fibrils.

As previously described, aSyn fibrils were pelleted and resuspended in forward exchange buffer, 0.1 % formic acid (pD 4.0) in 99.9% D_20 (pH 4.7), and incubated for 36 h at 37 □C, to discriminate better among different amide proton exchange rates (Figure 28a). After that, the sample was pelleted and back exchange measurements were performed using dissociation buffer, 4M GdSCN, 0.4 % formic acid, pH 2.5 in 60% D_20, followed by the recording of 120 2D ^{1}H-^{15}N HSQC over a total time of ~ 16 h at 3 □C. We observed that the fastest solvent exchange occurs in residues located in the segment of residues 1-38 aa and 100-140 aa located at the N-terminal and C-terminal regions, respectively. On the other hand, residues L38-V96 retained a large fraction of their amide protons after exchange in D_2O, indicating that this region is part of the core of fibrils and these amide protons participate in hydrogen bonds. Interestingly, the HD exchange profile of acetylated fibrils shows higher protonation levels in the segment encompassing 17 - 21, indicative of a lower degree of solvent exchange and increased hydrogen bond strength. In contrast, the protonation level was lower in the range 42-45, likely due to the lack of hydrogen-bonded structure (Figure 28b).

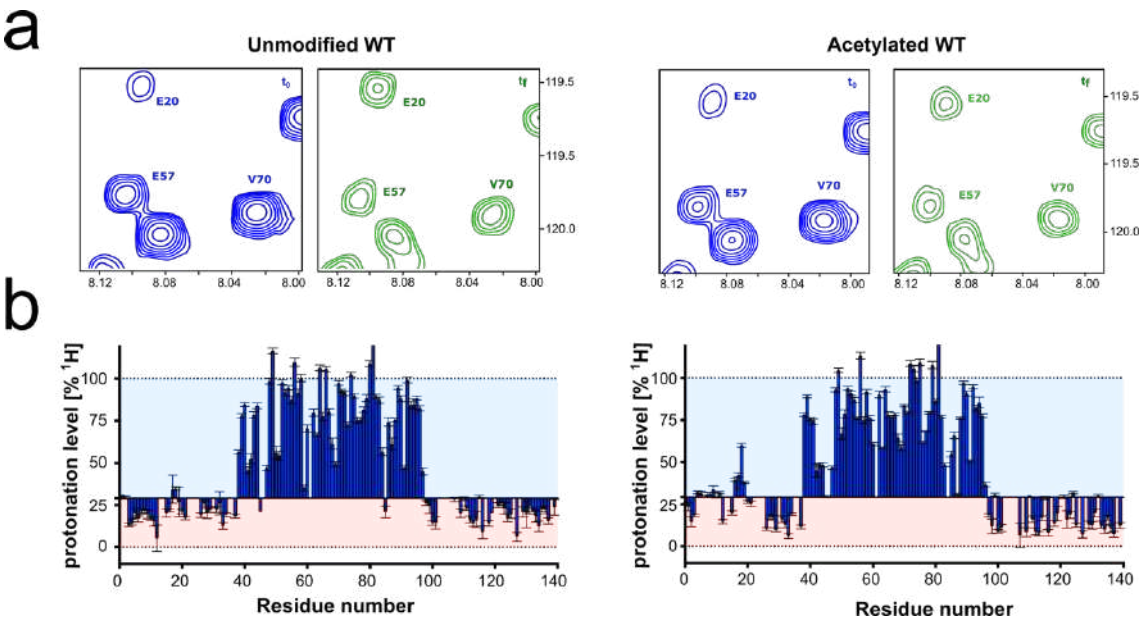

Figure 28: HD exchange profiles of unmodified and ac-Lys alpha-synuclein. a) selected region from 2D ^{1}H – ^{15}N HSQC spectra recorded after fibril dissociation at the beginning (left) and end (right) of the back-exchange period for unmodified and acetylated fibrils. b) HD-exchange profiles of unmodified and acetylated fibrils.

4.3.4. Acetylation of lysines in monomeric alpha-synuclein interferes with the binding to liposomes

Lipid binding properties were followed by CD spectroscopy and visualization of TEM images

To assess the lipid-binding proteins of modified aSyn monomers we incubated protein samples with DOPE:DOPS:DOPC (5:3:2 w/w) liposomes made of (~ 50 nm in diameter). Figure 29a shows that liposomes remained unaffected upon the addition of aSyn samples. Interestingly, when the concentration of liposomes was increased, acetylated monomers of aSyn showed a lower shift from random coil to alpha helix compared to unmodified protein samples (Figure 29b-c). To gain more insight into the weakest binding features observed for acetylated aSyn, we then incubated protein samples in the presence of liposomes under aggregation-inducing conditions and negative stain TEM was performed to analyze the final product of aSyn aggregation in

untreated and modified aSyn samples (Figure 29d). In comparison, when the final product of aggregation of acetylated aSyn samples was analyzed by TEM, the images revealed the presence of fibrillar structures, which were absent in the images obtained for unmodified samples. Overall, we attribute these differences to the weakest lipid binding observed for acetylated-aSyn, a factor that contributes to the increase in the population of free aSyn monomers available to aggregate.

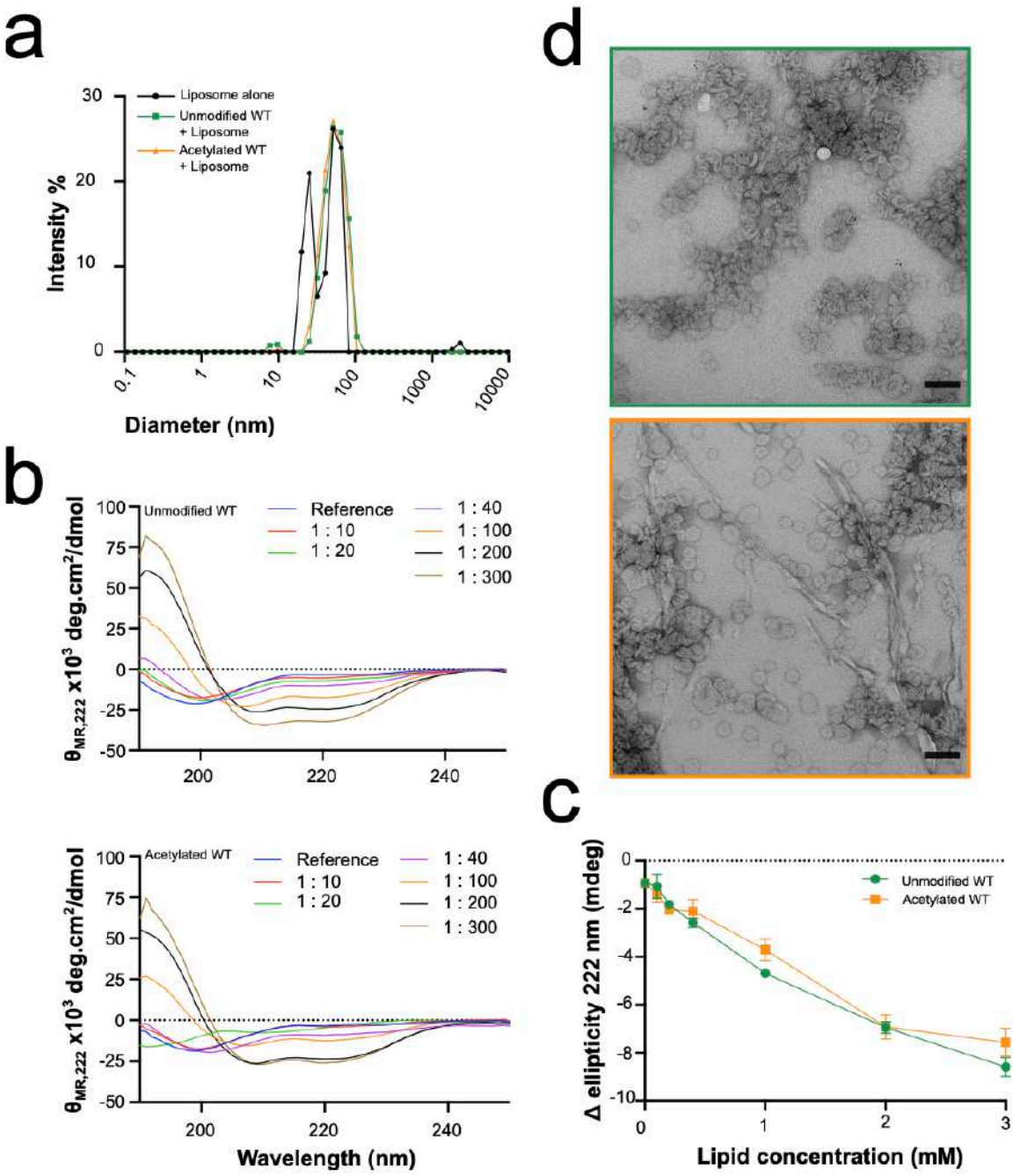

Figure 29: Binding properties of both species of aSyn monomers. a) Dynamic light scattering of liposomes in the absence (black) and presence of unmodified monomers (green)

and acetylated monomers (orange). b) Circular dichroism spectra of unmodified and acetylated aSyn monomers in the presence of increasing levels of liposomes. c) Changes in ellipticity at 222 nm upon increasing concentrations of lipids for unmodified (green) and acetylated protein samples (orange). d) Negative stain electron micrographs of unmodified (green) and acetylated aSyn(orange) after aggregation in the presence of liposomes. Scale bar, 200 nm.

5. Discussion

Alpha-synuclein plays an important role in the pathogenesis of several neurodegenerative diseases, named synucleopathies. We focus our efforts on the evaluation of the impact of chemical properties of specific residues such as aromaticity, hydrophobicity, and those derived from post-translational modifications on the aggregation kinetics, lipid binding to membranes, fibril structure and stability, etc. Here, we will discuss our investigations, and how our new findings might contribute to a better understanding of key aspects related to the function and dysfunction of this protein.

5.1. Aromaticity of specific residues and its roles in early steps of aggregation.

It was recently shown that the segments residues 36–42 and residues 45–57 in the aSyn primary sequence play a key role in the modulation of aggregation and function of this protein. For these reasons, these sequences were called master-controller sequence motifs[46]. On this concern, certain questions remained unanswered, such as what is the significance of individual residues in a sequential motif in modulating the aggregation of aSyn? Our findings point to the significance of aromaticity at position 39 in the ^{36}GVLYVGS^{42} motif as a key factor determining the amyloid fibril assembly of aSyn.

Moreover, the region encompassing residues 34–45 of aSyn has been identified as a ganglioside-binding domain[135], which is specific to outer plasma membrane leaflets and is related to the cellular uptake of aSyn monomers[136], and its pathological aggregates[74,137]. In that domain, Tyr-39 was shown to be the most critical residue for the interaction.

The results presented here demonstrate that aromaticity at position 39 of aSyn might play a crucial role in molecular events that might represent functional or dysfunctional states of aSyn. In fact, the pre-NAC segment ^{36}GVLYVGS^{42} was suggested to be a critical requirement for aSyn aggregation in vivo, whereas removal of this motif prevented aSyn aggregation and also suppressed the aggregation-induced toxicity in vivo[46,48]. Indeed, synergic

effects on early stages of aggregation were shown between these regions and the NAC and C-terminal regions [106]. Furthermore, computational studies also support the conclusion that the N-terminal domain plays a role in the dimer formation of aSyn[138,139].

In secondary nucleation events, when monomers are added to the fibril surface, transient electrostatic interactions were shown to be a prerequisite for protein aggregation, whereas π-π interactions between the N and C termini also seem to play a role. Indeed, Kumari P. et al. showed that if Phe4 and Tyr39 are replaced by Ala residues the transient binding of aSyn monomers to fibrils in secondary nucleation events is strongly affected, indicating that in addition to electrostatics interactions, aromatic π-π interactions might contribute critically to this process[140].

The substantial change of aggregation rate in the Y39A and the Y39L variants observed in this work, compared with the wt species might be attributable to a loss of function of the aromatic side chain in the early steps of the self-assembly process and/or to a conformational stabilization of the native state. The importance of residue 39 was also confirmed by Yun Zhou et al. who showed strong π-π interactions of naphthoquinone-dopamine hybrids with Y39/F94, which led to the disruption of preformed aSyn fibrils[141].

5.2. Impact of mutations at the N-terminal region on the lipid-binding features of aSyn

In this work, we studied two different punctual mutations: V15A, located in the first 25 residues, which is considered a critical segment for the anchoring of the protein to lipid membranes, and distinct Y39 variants, a residue that, in the context of this section, is part of the sequence motif known as “broken-helix” in one of the conformations adopted by aSyn upon membrane binding. Chemically, both amino acids are non-polar, and hydrophobic in nature, highlighting the relevance of this type of interaction in the binding of the protein to lipid membranes.

Interestingly, all presently identified disease-linked mutations of aSyn appear located in its membrane binding domain, underscoring the critical

involvement that aSyn/membrane interactions might play in α-synucleinopathies. Nevertheless, the degree to which each disease-associated mutation impacts aSyn-membrane binding is different as mentioned in the introduction.

In the case of the V15A aSyn variant, which has been identified in four PD-affected families[121–123], we observed decreased membrane binding affinity, despite the higher helix propensity of alanine as compared to valine. With this in mind, addressing whether hydrophobicity or helical propensity are more or less determinants in aSyn-lipid interactions is an issue open to question and the focus of further investigations.

In neurons, a delicate balance exists between populations of membrane-bound and free forms of aSyn, with the distribution of the protein between the two states being finely tuned[142]. In that concern, our analysis reveals that the V15A mutation of aSyn might alter this balance in vitro. Indeed, our studies indicated that a shift in that balance or equilibrium might impact significantly on aSyn aggregation due to the strong dependence of the assembly process, both in the absence or presence of lipid membranes, on protein concentration (free monomers) in solution.

A recent work proposed that the N-terminal region of aSyn significantly influences the permeability of mitochondrial membranes[143]. There is a strong possibility that this involvement contributes to the neurodegeneration associated with Parkinson's disease. Added to that, Diaw et al. showed by a Drosophila model that expression of the human p.V15A aSyn variant impairs the flying ability and survival of flies, as well as the mitochondrial network tested in cell lines[144].

Related to the membrane binding features of aSyn, our findings on the aSyn mutants at position 39 revealed that the aromatic character at that position of aSyn sequence favours a NAC membrane-anchored state for the lipid-bound conformation of aSyn, supporting further a role for Tyr-39 as a factor aiding in the folding of the amphiphilic region and promoting helix propagation[113]. Interestingly, it was proposed recently that the equilibrium between membrane-bound and unbound states of the region 65–97, which overlaps with the NAC region, might play a role in the regulation of biological properties of aSyn[120]. Indeed, the transition toward partly helical membrane-

bound states of aSyn has been associated with the control of vesicle docking and/or protein–protein interactions mediated by aSyn via a double-anchor mechanism[120]. In line with this hypothesis, phosphorylation of aSyn at Tyr-39 was shown to promote partly helical membrane-bound states[86]. Accordingly, it was suggested that in the cellular context, the alternation of aSyn between its two membrane-bound states might be driven by phosphorylation at Tyr-39, which would play then a role as a conformational switch[86].

5.3. Acetylation of lysines in aSyn and its influence on lipid-binding properties

In this work, we demonstrated that acetylation of lysine residues at specific locations correlates with a weaker binding to liposomes of the modified protein compared to the wt species. Added to that, we detected the presence of fibrils of modified aSyn when this variant was exposed to liposomes under aggregation-inducing conditions. Further supporting evidence comes from studies using continuous-wave EPR[33], which indicate that when aSyn adopts helical structures extended parallel to the lipid surface in a bilayer environment, this arrangement promotes or facilitates that most Lys residues interact with the zwitterionic headgroups (oriented approximately perpendicular to the helical axis).

Guided by this evidence, in combination with our findings, we envision that the lack of charge in lysines due to the acetylation reaction might be the factor determining the weaker interaction with the phospholipids; moreover, considering that lysines are ~10 % aa of the overall protein and that due to its amphipathicity might alter the hydrophobic face of the helix, affecting its penetration and stabilizing the lipid-protein interaction[145].

5.4. Different fibril strains as a consequence of post-translational modifications

It has been suggested that PTMs might modulate protein misfolding and its associated aggregation. In our studies, the aggregation profile of acetylated aSyn monomers reveals the accumulation of metastable intermediates

(oligomeric species) in the first plateau, which is followed by a second plateau characterized by the deposition of more stable aggregates (mature fibrils). We attribute this behaviour to the fact that lysine acetylation might affect concomitantly the network of transient long-range interactions in aSyn monomers and facilitate intermolecular interactions leading to structural assemblies that are less amyloid competent, interfering in that way with its evolution towards the formation of mature fibrils.

The β-sheet structural arrangement in oligomeric species is predominantly antiparallel, whereas the observed accumulation might be a consequence of an extremely slow rate of assembly and reorganization of amyloid-like β-sheet structures[146]. Thus, the early stage of the self-assembly process in the acetylated protein might be key for the generation of oligomeric species with kinetic stability in time.

It has been reported that soluble oligomeric species were found after Sarkosyl treatment from MSA and PD patient samples[147]. In our work, treatment of acetylated fibrils with Sarkosyl gives rise to the presence of protein in the supernatant, a behaviour that is not observed with unmodified fibrils. As shown by TEM images, oligomeric species bound to the fibril surfaces were found in acetylated samples (Figure 30), which can elongate to further serve as templates for secondary nucleation[148,149].

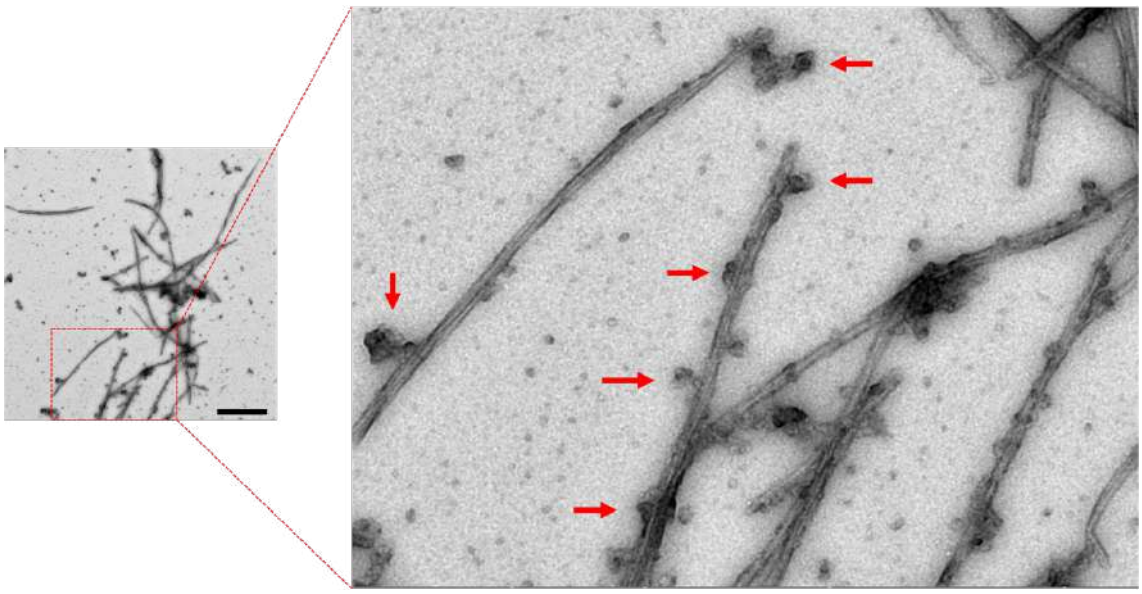

Figure 30: TEM image of acetylated fibrils of aSyn. Oligomers bound to fibril surfaces are clearly observed (red arrows). The background shows also the presence of oligomeric species. Scale bar, 1 µm.

Scientific literature suggests that the formation of highly ordered amyloid fibrils or less ordered oligomer structures could be an outcome of the competition between hydrogen bonding and hydrophobic interactions[150]. In theory, introducing an acetyl moiety to a lysine residue removes a charge and hence can increase the surface hydrophobicity of the protein, and the salt bridge involving lysine residues is also affected.

Chakraborty et al. discovered that the acetylation of tau discriminates its isoform-specific aggregation[151]. Thus, one might consider that acetylation of lysines in aSyn might modulate its aggregation pathway, guiding the assembly of monomers with different PTMs towards the formation of specific fibrillar structures in distinct synucleopathies

A combination of data from dye binding, pronase profiles, and fibril stability experiments allowed us to conclude that acetylated fibrils might have a different conformation and more extended rigid core, involving a higher number of peptides for residues in the segment 10-20. Moreover, Lewy fold (structure resolved by extracted filaments from patients with PD, PDD, and DLB, PDB: 8A9L[152]) has an island possibly made of peptides and has been postulated that residues between 14-23 fit into the island (Figure 31).

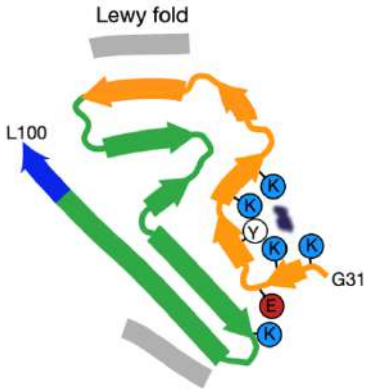

Figure 31: Schematic of secondary structure elements in the Lewy fold. The N-terminal region of aSyn is in orange, the NAC region is in green and the C-terminal region is in blue; thick connecting lines with arrowheads indicate βstrands. Island density in grey. Modified from reference 151

Another highlight observation is that modifications such as lysine acetylation occur in the vicinity of amyloidogenic sequences. It has been argued[153] that lysine acetylation in tau in the proximity of these sequences

becomes sufficient to mediate rapid tau fibrillization. Interestingly, in aSyn, the acetylated Lys43 and Lys45 are flanked by the amyloidogenic sequences described before.

Moreover, the amyloid structure of full-length aSyn with a Greek key-like topology as determined by CryoEM[24] (PDB: 6A6B) showed the occurrence of electrostatic interactions involving E57, H50 and K47 at the edge of the steric zipper core, which block access to the hydrophobic zipper interface and further stabilize dimeric contacts (Figure 32).

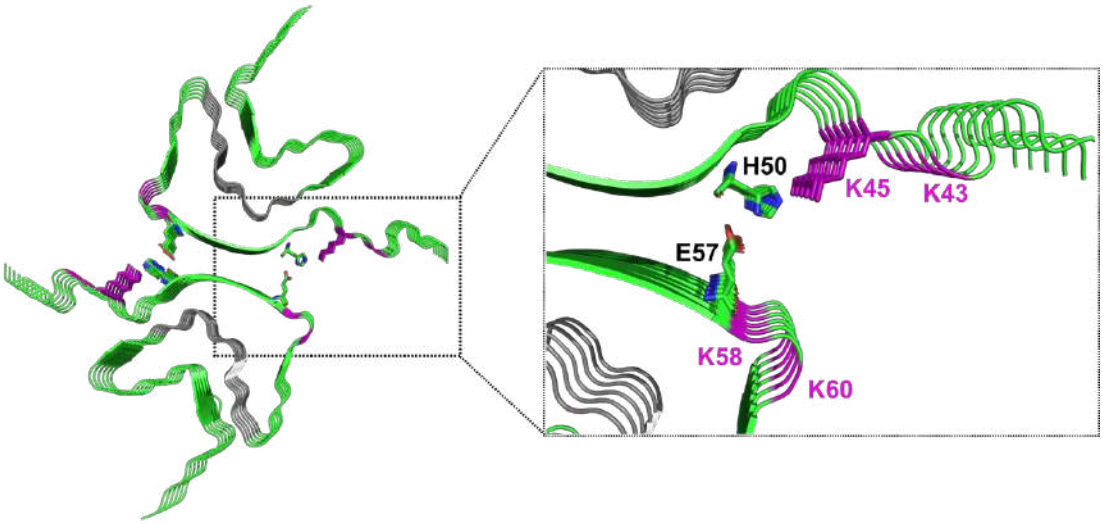

Figure 32: Model of Greek key-like topology of aSyn fibrils. The NACore region (G68-A78) in grey. Lysines 43, 45, 58 and 60 are labeled in pink. H50 and E57 at the edge of the interface, together with K45 interacts electrostatically (PDB: 6A6B)

In that structural arrangement, the hydrophobic residues fold (Figure 33, labelled in grey) and form a stable core. Considering the fact that one of the residues involved in stabilizing the structure is affected by acetylation (K47), one can argue that this modification might contribute to destabilizing the correct structure. Added to that, residue K58, located next to E57 in the aSyn sequence, might play also a relevant role.

When comparing the unmodified and acetylated fibrils by using the HD exchange experiment by NMR spectroscopy, we focus on two regions: the interface region and the NaCore region. Interestingly, those lysines showing the higher degree of acetylation (i.e., K43, K45, K58 and K60) (Figure 33, red lines) are flanking the residues involved in the interface region (Figure 33, green shadow). In this context the only differences observed in the protonation level

correspond to residues K43 and K45, being more exposed to solvent in acetylated fibrils. Regarding the NACore region (Figure 33, grey shadow) a quite similar profile is observed for both groups of aSyn fibrils, while the extremes show less degree of protonation in the acetylated protein and then being more solvent exposed. Despite our work and analysis, it is clear that further research is necessary to get more insights into the structural properties of acetylated fibrils. In that direction, such as CryoEM-based studies are more suitable to explore aspects such as fibril conformation, type and number of residues involved in the interface region, number of protofilaments, etc.

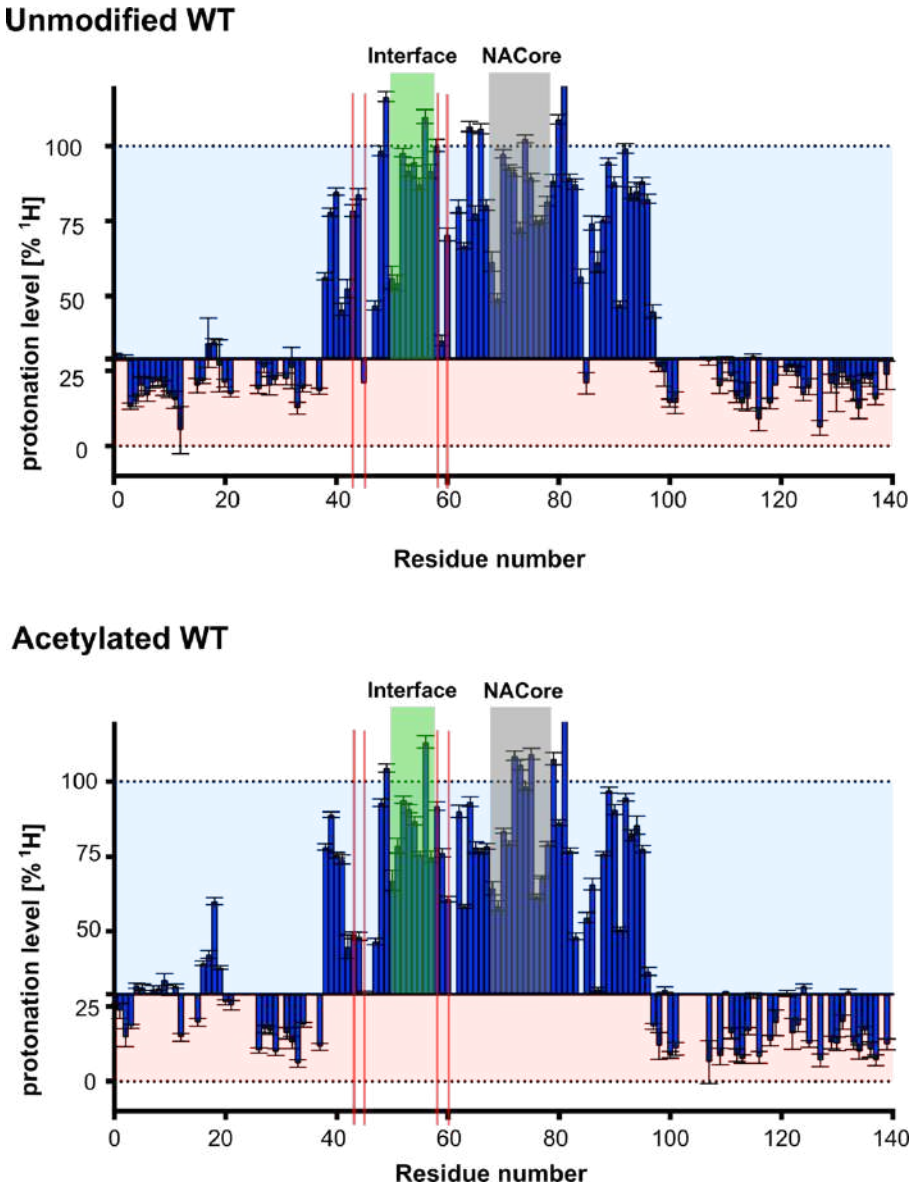

Figure 33: HD exchange profiles by NMR. Protonation levels of every residue at time 0h are shown; Lys43, Lys45, Lys58 and Lys60 are marked with red lines, the interface of the fibrils (residue 50-57) is in the green shadow, and NACore (residue 68-78) in the grey shadow.

Finally, by using CryoEM it was reported that alpha-synuclein filaments from human brains with the MSA fold have a density in front of K32, K34, Y39, K43, and K45 (Figure 34). However, it is not clear yet the factor(s) behind this observation[152]. We hypothesized some post-translational modifications (e.g., Acetylation) could help to understand the basis behind these densities and why there are different folds from human brains and from aggregation in vitro.

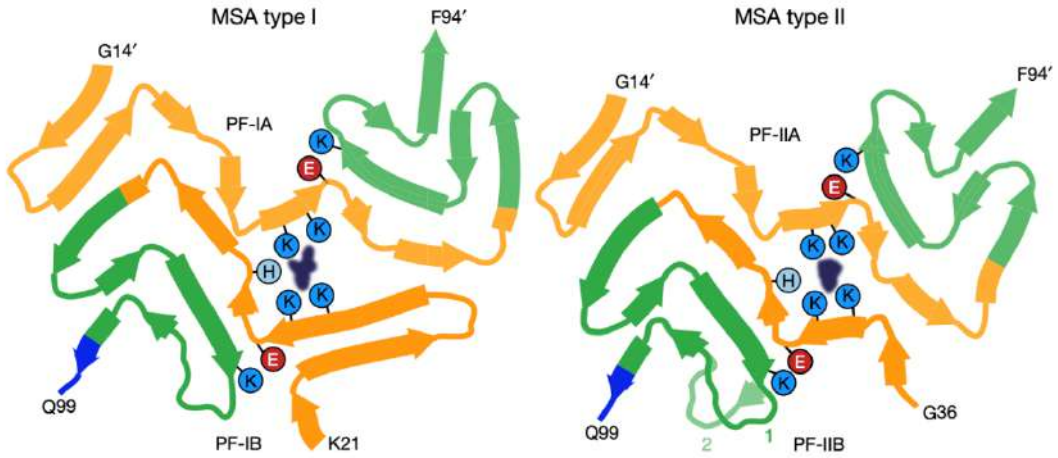

Figure 34: Schematic of secondary structure elements in the MSA fold. The N-terminal region of aSyn is in orange, the NAC region is in green and the C-terminal region is in blue; thick connecting lines with arrowheads indicate βstrands. The extra densities in all structures are depicted in dark blue. Modified from reference 151

We envision that although acetylation or mutations may not control the final folding, these modifications might promote interactions between amyloid motifs and/or play a role in remodelling aSyn fibrils into pathological conformations.

6. Conclusions and future perspectives

This study explores how residue-specific modifications by punctual mutations and PTMs in aSyn may impact on functional and dysfunctional properties of the protein, such as interaction with lipid-membranes and amyloid fibril assembly.

The structural changes induced by the Y39 mutations turned out to be only local, with the monomeric state of aSyn remaining disordered upon replacement of Tyr-39 by Phe, Leu, and Ala. Moreover, the four aSyn species showed no propensities for specific elements of secondary structure, adopting in all cases typical random-coil conformations.

Instead, aromaticity at position 39 resulted in a critical structural determinant for PcTS binding to the N-terminus of aSyn, an event that mediates the inhibition of this molecule on aSyn fibril assembly. These molecular interactions are influenced strongly by the highly aromatic character of the cyclic tetrapyrrole ring system, which contributes importantly to the ability of these molecules to bind strongly and selectively to a protein via π-π interactions with aromatic residues. The implication of this result is certainly relevant for the importance of particular targets of inhibition, as well as the role of specific residues in the formation of pathological states of the protein.

These new findings give further support to a role for Tyr-39 in essential inter and intramolecular contacts that might have important repercussions for the function and the dysfunction of aSyn. The removal of aromatic residue at position 39 impairs the in vitro amyloid fibril assembly, the aggregation propensity, and the formation of inclusion in a cell and animal model. The membrane-bound conformation is also modulated by aromaticity at position 39, altering lipid interaction involving the central hydrophobic NAC domain.

On the other hand, information about a new V15A familial aSyn mutant emerged recently, encouraging us to conduct further research focusing on its aggregation properties and its interaction with lipid-membranes.

Our studies show that the V15A variant remains unstructured after mutation, whereas the mutant showed weaker binding in the presence of liposomes compared to the wt species. Structural modelling using AlphaFold2 suggested that the hydrophobic side chain of V15, together with the

hydrophobic side chains of F4 and V26, are key for anchoring the α-helix of aSyn to the membrane surface. The replacement of V15 with alanine therefore results in a decrease in membrane binding.

The impaired ability of wt aSyn to form fibrils in the presence of liposomes might be explained by the population of aSyn monomers in is free state, i.e. not bound to liposomes, which would be too low to trigger fibrillization during the incubation period. In the case of the V15A aSyn variant, the decreased membrane affinity might contribute to an increase in the population of free aSyn monomers to a concentration level exceeding the critical concentration for fibrillization.

The novel variant highlights the importance of alpha-synuclein binding to membranes, and how not only the biological function of the protein is affected but also explains the relevance of the N-terminal for aggregation and binding conditions. Even if rare missenses represent a lower percentage of cases with Parkinson's disease, it helps to understand the mechanism behind the disease. Further studies are then needed to reveal the factor(s) determining toxicity, spreading, inclusion formation, pathogenicity in other models, etc.

Despite the study of mutations in aSyn sequence is an important research field, PTMs have been implicated in diverse roles in regulating aSyn membrane binding, amyloid aggregation kinetics and fibril structure. Indeed, every year more investigations are reported in this area aimed to shed light on the relation cause/consequence of PTMs in aSyn.

It was suggested that changes in lysine acetylation and deacetylation of many proteins, including histones and nonhistone proteins, might be tightly associated with neurodegenerative diseases[154]. In our work, we found that lysine acetylation in aSyn impacts both the aggregation kinetics and fibril conformation. For acetylated protein, we got a short nucleation event, but with a formation of a huge quantity of oligomers, retarding the assembly of amyloid fibrils.

To gain insight into the conformation of amyloid fibrils and their stability, we recorded curcumin spectra for modified and unmodified fibrils. Similar binding profiles were observed for lysine-acetylated fibrils, and fibrils that were amplified from brain extracts of MSA and PD patients[134], whereas a distinct profile was detected for unmodified aSyn.

Pronase profiles identified by mass spectrometry and digestion by proteinase K report different conformations for the amyloid fibrils in acetylated and non-acetylated aSyn samples. Another aspect that might be relevant is the high number of peptides concentrated in the region spanning residues 10-20 after pronase digestion of acetylated aSyn samples. Added to that, treatment with sarkosyl of these aggregates exhibits different profiles.

To investigate conformational differences and evaluate the properties of the rigid core of aSyn fibrils, we carried out HD exchange profiles by NMR spectroscopy. We identified specific regions with a higher degree of solvent exposure (residue 42-44) and more protected (residue 16-19), in acetylated aSyn fibrils. Lysine residues located at positions 43 and 45 showed a higher degree of chemical acetylation but another important observation is that lysine 45 is located near the protofilament interfaces, supporting the fact that its modification may alter both folding and structure of fibrils.

On the other hand, our studies reveal that binding to liposomes is also affected when the lysines are acetylated, impairing the ability of the monomers to bind to membranes. In consequence, acetylated monomers show the capability to form fibrils in the presence of liposomes under aggregation-inducing conditions. Further research into the effect of multiple PTMs could provide more information about the impact of each PTM on aSyn aggregation and toxicity. Amplification, seeding and/or fibril formation studies with combined cell and animal models, and samples from patients are required.

Our work contributes to understanding the relationship between post-translational modification and/or mutations in aSyn with its aggregation landscape. Future efforts must be focused on Cryo-EM studies at different time points during the aggregation process, which combined with NMR-based studies may provide further insights into the molecular mechanisms of amyloid fibril formation in aSyn.

7. Bibliography

1. Niccoli T, Partridge L (2012) Ageing as a Risk Factor for Disease. Current Biology 22:R741–R752.

2. Wilson DM, Cookson MR, Van Den Bosch L, Zetterberg H, Holtzman DM, Dewachter I (2023) Hallmarks of neurodegenerative diseases. Cell 186:693–714.

3. Soto C (2003) Unfolding the role of protein misfolding in neurodegenerative diseases. Nat Rev Neurosci 4:49–60.

4. Stelzmann RA, Norman Schnitzlein H, Reed Murtagh F (1995) An english translation of alzheimer's 1907 paper, "über eine eigenartige erkankung der hirnrinde." Clinical Anatomy 8:429–431.

5. Parkinson J (2002) An Essay on the Shaking Palsy. JNP 14:223–236.

6. Huntington G (2003) On Chorea. JNP 15:109–112.

7. Rowland LP (2001) How Amyotrophic Lateral Sclerosis Got Its Name: The Clinical-Pathologic Genius of Jean-Martin Charcot. Arch Neurol [Internet] 58. Available from: http://archneur.jamanetwork.com/article.aspx?doi=10.1001/archneur.58.3.512

8. Katscher F (1998) It's Jakob's disease, not Creutzfeldt's. Nature 393:11–11.

9. Dobson CM, Šali A, Karplus M (1998) Protein Folding: A Perspective from Theory and Experiment. Angewandte Chemie International Edition 37:868–893.

10. Hu S, Tan J, Qin L, Lv L, Yan W, Zhang H, Tang B, Wang C (2021) Molecular chaperones and Parkinson's disease. Neurobiology of Disease 160:105527.

11. Tretiakoff K. (1919) Contribution a l'etude de l'anatomie pathologique du locus niger de Soemmering avec quelques deductions relatives a la pathogenie des troubles du tonus musculaire et de la maladie de Parkinson.

12. Polymeropoulos MH, Lavedan C, Leroy E, Ide SE, Dehejia A, Dutra A, Pike B, Root H, Rubenstein J, Boyer R, et al. (1997) Mutation in the α-Synuclein Gene Identified in Families with Parkinson's Disease. Science 276:2045–2047.

13. Spillantini MG, Schmidt ML, Lee VM-Y, Trojanowski JQ, Jakes R, Goedert M (1997) α-Synuclein in Lewy bodies. Nature 388:839–840.

14. Gegg ME, Menozzi E, Schapira AHV (2022) Glucocerebrosidase-associated Parkinson disease: Pathogenic mechanisms and potential drug treatments. Neurobiology of Disease 166:105663.

15. Eliezer D, Kutluay E, Bussell R, Browne G (2001) Conformational properties of α-synuclein in its free and lipid-associated states 1 1Edited by P. E. Wright. Journal of Molecular Biology 307:1061–1073.

16. Maroteaux L, Campanelli J, Scheller R (1988) Synuclein: a neuron-specific protein localized to the nucleus and presynaptic nerve terminal. J. Neurosci. 8:2804–2815.

17. Bussell R, Eliezer D (2003) A Structural and Functional Role for 11-mer Repeats in α-Synuclein and Other Exchangeable Lipid Binding Proteins. Journal of Molecular Biology 329:763–778.

18. Du H-N, Tang L, Luo X-Y, Li H-T, Hu J, Zhou J-W, Hu H-Y (2003) A Peptide Motif Consisting of Glycine, Alanine, and Valine Is Required for the Fibrillization and Cytotoxicity of Human α-Synuclein. Biochemistry 42:8870–8878.

19. Giasson BI, Murray IVJ, Trojanowski JQ, Lee VM-Y (2001) A Hydrophobic Stretch of 12 Amino Acid Residues in the Middle of α-Synuclein Is Essential for Filament Assembly. Journal of Biological Chemistry 276:2380–2386.

20. Hoyer W, Cherny D, Subramaniam V, Jovin TM (2004) Impact of the Acidic C-Terminal Region Comprising Amino Acids 109−140 on α-Synuclein Aggregation in Vitro. Biochemistry 43:16233–16242.

21. Kim TD, Paik SR, Yang C-H (2002) Structural and Functional Implications of C-Terminal Regions of α-Synuclein. Biochemistry 41:13782–13790.

22. Park SM, Jung HY, Kim TD, Park JH, Yang C-H, Kim J (2002) Distinct Roles of the N-terminal-binding Domain and the C-terminal-solubilizing Domain of α-Synuclein, a Molecular Chaperone. Journal of Biological Chemistry 277:28512–28520.

23. Ulmer TS, Bax A, Cole NB, Nussbaum RL (2005) Structure and Dynamics of Micelle-bound Human α-Synuclein. Journal of Biological Chemistry 280:9595–9603.

24. Li Y, Zhao C, Luo F, Liu Z, Gui X, Luo Z, Zhang X, Li D, Liu C, Li X (2018) Amyloid fibril structure of α-synuclein determined by cryo-electron microscopy. Cell Res 28:897–903.

25. Bertoncini CW, Jung Y-S, Fernandez CO, Hoyer W, Griesinger C, Jovin TM, Zweckstetter M (2005) Release of long-range tertiary interactions potentiates aggregation of natively unstructured α-synuclein. Proc. Natl. Acad. Sci. U.S.A. 102:1430–1435.

26. Fonseca-Ornelas L, Viennet T, Rovere M, Jiang H, Liu L, Nuber S, Ericsson M, Arthanari H, Selkoe DJ (2021) Altered conformation of α-synuclein drives dysfunction of synaptic vesicles in a synaptosomal model of Parkinson's disease. Cell Reports 36:109333.

27. Vargas KJ, Makani S, Davis T, Westphal CH, Castillo PE, Chandra SS (2014) Synucleins Regulate the Kinetics of Synaptic Vesicle Endocytosis. Journal of Neuroscience 34:9364–9376.

28. Cheng F, Vivacqua G, Yu S (2011) The role of alpha-synuclein in neurotransmission and synaptic plasticity. Journal of Chemical Neuroanatomy 42:242–248.

29. Burré J, Sharma M, Tsetsenis T, Buchman V, Etherton MR, Südhof TC (2010) α-Synuclein Promotes SNARE-Complex Assembly in Vivo and in Vitro. Science 329:1663–1667.

30. Burré J, Sharma M, Südhof TC (2014) α-Synuclein assembles into higher-order multimers upon membrane binding to promote SNARE complex formation. Proc. Natl. Acad. Sci. U.S.A. [Internet] 111. Available from: https://pnas.org/doi/full/10.1073/pnas.1416598111

31. Fusco G, De Simone A, Gopinath T, Vostrikov V, Vendruscolo M, Dobson CM, Veglia G (2014) Direct observation of the three regions in α-synuclein that determine its membrane-bound behaviour. Nat Commun 5:3827.

32. Georgieva ER, Ramlall TF, Borbat PP, Freed JH, Eliezer D (2008) Membrane-Bound α-Synuclein Forms an Extended Helix: Long-Distance Pulsed ESR Measurements Using Vesicles, Bicelles, and Rodlike Micelles. J. Am. Chem. Soc. 130:12856–12857.

33. Jao CC, Hegde BG, Chen J, Haworth IS, Langen R (2008) Structure of membrane-bound α-synuclein from site-directed spin labeling and computational refinement. Proc. Natl. Acad. Sci. U.S.A. 105:19666–19671.

34. Chandra S, Chen X, Rizo J, Jahn R, Südhof TC (2003) A Broken α-Helix in Folded α-Synuclein. Journal of Biological Chemistry 278:15313–15318.

35. Horvath I, Weise CF, Andersson EK, Chorell E, Sellstedt M, Bengtsson C, Olofsson A, Hultgren SJ, Chapman M, Wolf-Watz M, et al. (2012) Mechanisms of Protein Oligomerization: Inhibitor of Functional Amyloids Templates α-Synuclein Fibrillation. J. Am. Chem. Soc. 134:3439–3444.

36. Khurana R, Coleman C, Ionescu-Zanetti C, Carter SA, Krishna V, Grover RK, Roy R, Singh S (2005) Mechanism of thioflavin T binding to amyloid fibrils. Journal of Structural Biology 151:229–238.

37. Uversky VN, Li J, Fink AL (2001) Evidence for a Partially Folded Intermediate in α-Synuclein Fibril Formation. Journal of Biological Chemistry 276:10737–10744.

38. Celej MS, Sarroukh R, Goormaghtigh E, Fidelio GD, Ruysschaert J-M, Raussens V (2012) Toxic prefibrillar α-synuclein amyloid oligomers adopt a distinctive antiparallel β-sheet structure. Biochemical Journal 443:719–726.

39. Vilar M, Chou H-T, Lührs T, Maji SK, Riek-Loher D, Verel R, Manning G, Stahlberg H, Riek R (2008) The fold of α-synuclein fibrils. Proc. Natl. Acad. Sci. U.S.A. 105:8637–8642.

40. Shahmoradian SH, Lewis AJ, Genoud C, Hench J, Moors TE, Navarro PP, Castaño-Díez D, Schweighauser G, Graff-Meyer A, Goldie KN, et al. (2019)

Lewy pathology in Parkinson's disease consists of crowded organelles and lipid membranes. Nat Neurosci 22:1099–1109.

41. Frieg B, Antonschmidt L, Dienemann C, Geraets JA, Najbauer EE, Matthes D, De Groot BL, Andreas LB, Becker S, Griesinger C, et al. (2022) The 3D structure of lipidic fibrils of α-synuclein. Nat Commun 13:6810.

42. Reynolds NP, Soragni A, Rabe M, Verdes D, Liverani E, Handschin S, Riek R, Seeger S (2011) Mechanism of Membrane Interaction and Disruption by α-Synuclein. J. Am. Chem. Soc. 133:19366–19375.

43. Hellstrand E, Nowacka A, Topgaard D, Linse S, Sparr E (2013) Membrane Lipid Co-Aggregation with α-Synuclein Fibrils Van Der Wel P, editor. PLoS ONE 8:e77235.

44. Galvagnion C, Buell AK, Meisl G, Michaels TCT, Vendruscolo M, Knowles TPJ, Dobson CM (2015) Lipid vesicles trigger α-synuclein aggregation by stimulating primary nucleation. Nat Chem Biol 11:229–234.

45. Roeters SJ, Strunge K, Pedersen KB, Golbek TW, Bregnhøj M, Zhang Y, Wang Y, Dong M, Nielsen J, Otzen DE, et al. (2023) Elevated concentrations cause upright alpha-synuclein conformation at lipid interfaces. Nat Commun 14:5731.

46. Doherty CPA, Ulamec SM, Maya-Martinez R, Good SC, Makepeace J, Khan GN, Van Oosten-Hawle P, Radford SE, Brockwell DJ (2020) A short motif in the N-terminal region of α-synuclein is critical for both aggregation and function. Nat Struct Mol Biol 27:249–259.

47. Liu T, Bitan G (2012) Modulating Self-Assembly of Amyloidogenic Proteins as a Therapeutic Approach for Neurodegenerative Diseases: Strategies and Mechanisms. ChemMedChem 7:359–374.

48. Tripathi T (2020) A Master Regulator of α-Synuclein Aggregation. ACS Chem. Neurosci. 11:1376–1378.

49. Gazit E (2002) A possible role for π-stacking in the self-assembly of amyloid fibrils. FASEB j. 16:77–83.

50. Valiente-Gabioud AA, Miotto MC, Chesta ME, Lombardo V, Binolfi A, Fernández CO (2016) Phthalocyanines as Molecular Scaffolds to Block Disease-Associated Protein Aggregation. Acc. Chem. Res. 49:801–808.

51. Lamberto GR, Binolfi A, Orcellet ML, Bertoncini CW, Zweckstetter M, Griesinger C, Fernández CO (2009) Structural and mechanistic basis behind the inhibitory interaction of PcTS on α-synuclein amyloid fibril formation. Proc. Natl. Acad. Sci. U.S.A. 106:21057–21062.

52. Lamberto GR, Torres-Monserrat V, Bertoncini CW, Salvatella X, Zweckstetter M, Griesinger C, Fernández CO (2011) Toward the Discovery of Effective Polycyclic Inhibitors of α-Synuclein Amyloid Assembly. Journal of Biological Chemistry 286:32036–32044.

53. Fonseca-Ornelas L, Eisbach SE, Paulat M, Giller K, Fernández CO, Outeiro TF, Becker S, Zweckstetter M (2014) Small molecule-mediated stabilization of vesicle-associated helical α-synuclein inhibits pathogenic misfolding and aggregation. Nat Commun 5:5857.

54. Priola SA, Raines A, Caughey WS (2000) Porphyrin and Phthalocyanine Antiscrapie Compounds. Science 287:1503–1506.

55. Park J, Ahn JS, Lee J, Bhak G, Jung S, Paik SR (2008) Amyloid Fibrillar Meshwork Formation of Iron-Induced Oligomeric Species of Aβ40 with Phthalocyanine Tetrasulfonate and Its Toxic Consequences. ChemBioChem 9:2602–2605.

56. Lee E-N, Cho H-J, Lee C-H, Lee D, Chung KC, Paik SR (2004) Phthalocyanine Tetrasulfonates Affect the Amyloid Formation and Cytotoxicity of α-Synuclein. Biochemistry 43:3704–3715.

57. Taniguchi S, Suzuki N, Masuda M, Hisanaga S, Iwatsubo T, Goedert M, Hasegawa M (2005) Inhibition of Heparin-induced Tau Filament Formation by Phenothiazines, Polyphenols, and Porphyrins. Journal of Biological Chemistry 280:7614–7623.

58. Akoury E, Gajda M, Pickhardt M, Biernat J, Soraya P, Griesinger C, Mandelkow E, Zweckstetter M (2013) Inhibition of Tau Filament Formation by Conformational Modulation. J. Am. Chem. Soc. 135:2853–2862.

59. Tabassum S, Sheikh AM, Yano S, Ikeue T, Handa M, Nagai A (2015) A carboxylated Zn-phthalocyanine inhibits fibril formation of Alzheimer's amyloid β peptide. The FEBS Journal 282:463–476.

60. Ulrih NP, Barry CH, Fink AL (2008) Impact of Tyr to Ala mutations on α-synuclein fibrillation and structural properties. Biochimica et Biophysica Acta (BBA) - Molecular Basis of Disease 1782:581–585.

61. Brahmachari S, Ge P, Lee SH, Kim D, Karuppagounder SS, Kumar M, Mao X, Shin JH, Lee Y, Pletnikova O, et al. (2016) Activation of tyrosine kinase c-Abl contributes to α-synuclein–induced neurodegeneration. Journal of Clinical Investigation 126:2970–2988.

62. Wentink AS, Nillegoda NB, Feufel J, Ubartaitė G, Schneider CP, De Los Rios P, Hennig J, Barducci A, Bukau B (2020) Molecular dissection of amyloid disaggregation by human HSP70. Nature 587:483–488.

63. Krüger R, Kuhn W, Müller T, Woitalla D, Graeber M, Kösel S, Przuntek H, Epplen JT, Schols L, Riess O (1998) AlaSOPro mutation in the gene encoding α-synuclein in Parkinson's disease. Nat Genet 18:106–108.

64. Zarranz JJ, Alegre J, Gómez-Esteban JC, Lezcano E, Ros R, Ampuero I, Vidal L, Hoenicka J, Rodriguez O, Atarés B, et al. (2004) The new mutation, E46K, of α-synuclein causes parkinson and Lewy body dementia: New α-Synuclein Gene Mutation. Ann Neurol. 55:164–173.

65. Liu H, Koros C, Strohäker T, Schulte C, Bozi M, Varvaresos S, Ibáñez de Opakua A, Simitsi AM, Bougea A, Voumvourakis K, et al. (2021) A Novel SNCA A30G Mutation Causes Familial Parkinson's Disease. Mov Disord 36:1624–1633.

66. Appel-Cresswell S, Vilarino-Guell C, Encarnacion M, Sherman H, Yu I, Shah B, Weir D, Thompson C, Szu-Tu C, Trinh J, et al. (2013) Alpha-synuclein p.H50Q, a novel pathogenic mutation for Parkinson's disease: α- Synuclein p.H50q, A Novel Mutation For Pd. Mov Disord. 28:811–813.

67. Lesage S, Anheim M, Letournel F, Bousset L, Honoré A, Rozas N, Pieri L, Madiona K, Dürr A, Melki R, et al. (2013) G51D α-synuclein mutation causes a novel Parkinsonian-pyramidal syndrome: SNCA G51D in Parkinsonism. Ann Neurol. 73:459–471.

68. Pasanen P, Myllykangas L, Siitonen M, Raunio A, Kaakkola S, Lyytinen J, Tienari PJ, Pöyhönen M, Paetau A (2014) A novel α-synuclein mutation A53E associated with atypical multiple system atrophy and Parkinson's disease-type pathology. Neurobiology of Aging 35:2180.e1-2180.e5.

69. Chen Y, Gu X, Ou R, Zhang L, Hou Y, Liu K, Cao B, Wei Q, Li C, Song W, et al. (2020) Evaluating the Role of *SNCA* , *LRRK2* , and *GBA* in Chinese Patients With EARLY-ONSET Parkinson's Disease. Mov Disord 35:2046–2055.

70. Nishioka K, Hayashi S, Farrer MJ, Singleton AB, Yoshino H, Imai H, Kitami T, Sato K, Kuroda R, Tomiyama H, et al. (2006) Clinical heterogeneity of α-synuclein gene duplication in Parkinson's disease. Annals of Neurology 59:298–309.

71. Singleton AB, Farrer M, Johnson J, Singleton A, Hague S, Kachergus J, Hulihan M, Peuralinna T, Dutra A, Nussbaum R, et al. (2003) α-Synuclein Locus Triplication Causes Parkinson's Disease. Science 302:841–841.

72. Jensen PH, Nielsen MS, Jakes R, Dotti CG, Goedert M (1998) Binding of α-Synuclein to Brain Vesicles Is Abolished by Familial Parkinson's Disease Mutation. Journal of Biological Chemistry 273:26292–26294.

73. Fares M-B, Ait-Bouziad N, Dikiy I, Mbefo MK, Jovi i A, Kiely A, Holton JL, Lee S-J, Gitler AD, Eliezer D, et al. (2014) The novel Parkinson's disease linked mutation G51D attenuates in vitro aggregation and membrane binding of -synuclein, and enhances its secretion and nuclear localization in cells. Human Molecular Genetics 23:4491–4509.

74. Fusco G, Pape T, Stephens AD, Mahou P, Costa AR, Kaminski CF, Kaminski Schierle GS, Vendruscolo M, Veglia G, Dobson CM, et al. (2016) Structural basis of synaptic vesicle assembly promoted by α-synuclein. Nat Commun 7:12563.

75. Jo E, Fuller N, Rand RP, St George-Hyslop P, Fraser PE (2002) Defective membrane interactions of familial Parkinson's disease mutant A30P α-synuclein 1 1Edited by I. B. Holland. Journal of Molecular Biology 315:799–807.

76. Chou PY, Fasman GD (1978) Empirical Predictions of Protein Conformation. Annu. Rev. Biochem. 47:251–276.

77. Choi W, Zibaee S, Jakes R, Serpell LC, Davletov B, Anthony Crowther R, Goedert M (2004) Mutation E46K increases phospholipid binding and assembly into filaments of human α-synuclein. FEBS Letters 576:363–368.

78. Rovere M, Powers AE, Jiang H, Pitino JC, Fonseca-Ornelas L, Patel DS, Achille A, Langen R, Varkey J, Bartels T (2019) E46K-like α-synuclein mutants increase lipid interactions and disrupt membrane selectivity. Journal of Biological Chemistry 294:9799–9812.

79. Conway KA, Harper JD, Lansbury PT (1998) Accelerated in vitro fibril formation by a mutant α-synuclein linked to early-onset Parkinson disease. Nat Med 4:1318–1320.

80. Li J, Uversky VN, Fink AL (2001) Effect of Familial Parkinson's Disease Point Mutations A30P and A53T on the Structural Properties, Aggregation, and Fibrillation of Human α-Synuclein. Biochemistry 40:11604–11613.

81. Ghosh D, Mondal M, Mohite GM, Singh PK, Ranjan P, Anoop A, Ghosh S, Jha NN, Kumar A, Maji SK (2013) The Parkinson's Disease-Associated H50Q Mutation Accelerates α-Synuclein Aggregation *in Vitro*. Biochemistry 52:6925–6927.

82. Zhao K, Li Y, Liu Z, Long H, Zhao C, Luo F, Sun Y, Tao Y, Su X, Li D, et al. (2020) Parkinson's disease associated mutation E46K of α-synuclein triggers the formation of a distinct fibril structure. Nat Commun 11:2643.

83. Barrett PJ, Timothy Greenamyre J (2015) Post-translational modification of α-synuclein in Parkinson′s disease. Brain Research 1628:247–253.

84. Schmid AW, Fauvet B, Moniatte M, Lashuel HA (2013) Alpha-synuclein Post-translational Modifications as Potential Biomarkers for Parkinson Disease and Other Synucleinopathies. Molecular & Cellular Proteomics 12:3543–3558.

85. Burai R, Ait-Bouziad N, Chiki A, Lashuel HA (2015) Elucidating the Role of Site-Specific Nitration of α-Synuclein in the Pathogenesis of Parkinson's Disease via Protein Semisynthesis and Mutagenesis. J. Am. Chem. Soc. 137:5041–5052.

86. Dikiy I, Fauvet B, Jovičić A, Mahul-Mellier A-L, Desobry C, El-Turk F, Gitler AD, Lashuel HA, Eliezer D (2016) Semisynthetic and *in Vitro* Phosphorylation of Alpha-Synuclein at Y39 Promotes Functional Partly Helical Membrane-Bound States Resembling Those Induced by PD Mutations. ACS Chem. Biol. 11:2428–2437.

87. Hejjaoui M, Butterfield S, Fauvet B, Vercruysse F, Cui J, Dikiy I, Prudent M, Olschewski D, Zhang Y, Eliezer D, et al. (2012) Elucidating the Role of C-Terminal Post-Translational Modifications Using Protein Semisynthesis Strategies: α-Synuclein Phosphorylation at Tyrosine 125. J. Am. Chem. Soc. 134:5196–5210.

88. Levine PM, Galesic A, Balana AT, Mahul-Mellier A-L, Navarro MX, De Leon CA, Lashuel HA, Pratt MR (2019) α-Synuclein O-GlcNAcylation alters aggregation and toxicity, revealing certain residues as potential inhibitors of Parkinson's disease. Proc. Natl. Acad. Sci. U.S.A. 116:1511–1519.

89. Mahul-Mellier A-L, Fauvet B, Gysbers A, Dikiy I, Oueslati A, Georgeon S, Lamontanara AJ, Bisquertt A, Eliezer D, Masliah E, et al. (2014) c-Abl phosphorylates α-synuclein and regulates its degradation: implication for α-synuclein clearance and contribution to the pathogenesis of Parkinson's disease. Human Molecular Genetics 23:2858–2879.

90. Oueslati A, Schneider BL, Aebischer P, Lashuel HA (2013) Polo-like kinase 2 regulates selective autophagic α-synuclein clearance and suppresses its toxicity in vivo. Proc. Natl. Acad. Sci. U.S.A. [Internet] 110. Available from: https://pnas.org/doi/full/10.1073/pnas.1309991110

91. Paleologou KE, Oueslati A, Shakked G, Rospigliosi CC, Kim H-Y, Lamberto GR, Fernandez CO, Schmid A, Chegini F, Gai WP, et al. (2010) Phosphorylation at S87 Is Enhanced in Synucleinopathies, Inhibits α-Synuclein Oligomerization, and Influences Synuclein-Membrane Interactions. J. Neurosci. 30:3184–3198.

92. Fujiwara H, Hasegawa M, Dohmae N, Kawashima A, Masliah E, Goldberg MS, Shen J, Takio K, Iwatsubo T (2002) α-Synuclein is phosphorylated in synucleinopathy lesions. Nat Cell Biol 4:160–164.

93. Ghanem SS, Majbour NK, Vaikath NN, Ardah MT, Erskine D, Jensen NM, Fayyad M, Sudhakaran IP, Vasili E, Melachroinou K, et al. (2022) α-Synuclein phosphorylation at serine 129 occurs after initial protein deposition and inhibits seeded fibril formation and toxicity. Proc. Natl. Acad. Sci. U.S.A. 119:e2109617119.

94. Zhang S, Zhu R, Pan B, Xu H, Olufemi MF, Gathagan RJ, Li Y, Zhang L, Zhang J, Xiang W, et al. (2023) Post-translational modifications of soluble α-synuclein regulate the amplification of pathological α-synuclein. Nat Neurosci 26:213–225.

95. Zhao J, Pan B, Fina M, Huang Y, Shimogawa M, Luk KC, Rhoades E, Petersson EJ, Dong DW, Kashina A (2022) α-Synuclein arginylation in the human brain. Transl Neurodegener 11:20.

96. Periquet M, Fulga T, Myllykangas L, Schlossmacher MG, Feany MB (2007) Aggregated α-Synuclein Mediates Dopaminergic Neurotoxicity *In Vivo*. J. Neurosci. 27:3338–3346.

97. Johnson M, Geeves MA, Mulvihill DP Production of Amino-Terminally Acetylated Recombinant Proteins in E. coli. In: Hake SB, Janzen CJ, editors. Protein Acetylation. Vol. 981. Methods in Molecular Biology. Totowa, NJ: Humana Press; 2013. pp. 193–200. Available from: https://link.springer.com/10.1007/978-1-62703-305-3_15

98. Ysselstein D, Joshi M, Mishra V, Griggs AM, Asiago JM, McCabe GP, Stanciu LA, Post CB, Rochet J-C (2015) Effects of impaired membrane interactions on α-synuclein aggregation and neurotoxicity. Neurobiology of Disease 79:150–163.

99. Lázaro DF, Rodrigues EF, Langohr R, Shahpasandzadeh H, Ribeiro T, Guerreiro P, Gerhardt E, Kröhnert K, Klucken J, Pereira MD, et al. (2014) Systematic Comparison of the Effects of Alpha-synuclein Mutations on Its Oligomerization and Aggregation Kaganovich D, editor. PLoS Genet 10:e1004741.

100. JOHN CAVANAGH, WAYNE J. FAIRBROTHER, ARTHUR G. PALMER, III, MARK RANCE, NICHOLAS J. SKELTON Protein NMR Spectroscopy Principles and Practice. 2007.

101. Bodner CR, Maltsev AS, Dobson CM, Bax A (2010) Differential Phospholipid Binding of α-Synuclein Variants Implicated in Parkinson's Disease Revealed by Solution NMR Spectroscopy. Biochemistry 49:862–871.

102. Lima VDA, Do Nascimento LA, Eliezer D, Follmer C (2019) Role of Parkinson's Disease-Linked Mutations and N-Terminal Acetylation on the Oligomerization of α-Synuclein Induced by 3,4-Dihydroxyphenylacetaldehyde. ACS Chem. Neurosci. 10:690–703.

103. Brenner S (1974) THE GENETICS OF *CAENORHABDITIS ELEGANS*. Genetics 77:71–94.

104. Mello CC, Kramer JM, Stinchcomb D, Ambros V (1991) Efficient gene transfer in C.elegans: extrachromosomal maintenance and integration of transforming sequences. The EMBO Journal 10:3959–3970.

105. Chiti F, Dobson CM (2006) Protein Misfolding, Functional Amyloid, and Human Disease. Annu. Rev. Biochem. 75:333–366.

106. Ulamec SM, Maya-Martinez R, Byrd EJ, Dewison KM, Xu Y, Willis LF, Sobott F, Heath GR, Van Oosten Hawle P, Buchman VL, et al. (2022) Single residue modulators of amyloid formation in the N-terminal P1-region of α-synuclein. Nat Commun 13:4986.

107. Zhou W, Freed CR (2004) Tyrosine-to-Cysteine Modification of Human α-Synuclein Enhances Protein Aggregation and Cellular Toxicity. Journal of Biological Chemistry 279:10128–10135.

108. Kaylor J, Bodner N, Edridge S, Yamin G, Hong D-P, Fink AL (2005) Characterization of Oligomeric Intermediates in α-Synuclein Fibrillation: FRET Studies of Y125W/Y133F/Y136F α-Synuclein. Journal of Molecular Biology 353:357–372.

109. Zhu M, Rajamani S, Kaylor J, Han S, Zhou F, Fink AL (2004) The Flavonoid Baicalein Inhibits Fibrillation of α-Synuclein and Disaggregates Existing Fibrils. Journal of Biological Chemistry 279:26846–26857.

110. Aspholm EE, Matečko-Burmann I, Burmann BM (2020) Keeping α-Synuclein at Bay: A More Active Role of Molecular Chaperones in Preventing Mitochondrial Interactions and Transition to Pathological States? Life 10:289.

111. Brahmachari S, Karuppagounder SS, Ge P, Lee S, Dawson VL, Dawson TM, Ko HS (2017) c-Abl and Parkinson's Disease: Mechanisms and Therapeutic Potential. JPD 7:589–601.

112. Burmann BM, Gerez JA, Matečko-Burmann I, Campioni S, Kumari P, Ghosh D, Mazur A, Aspholm EE, Šulskis D, Wawrzyniuk M, et al. (2020) Regulation of α-synuclein by chaperones in mammalian cells. Nature 577:127–132.

113. Lokappa SB, Suk J-E, Balasubramanian A, Samanta S, Situ AJ, Ulmer TS (2014) Sequence and Membrane Determinants of the Random Coil–Helix Transition of α-Synuclein. Journal of Molecular Biology 426:2130–2144.

114. Sevcsik E, Trexler AJ, Dunn JM, Rhoades E (2011) Allostery in a Disordered Protein: Oxidative Modifications to α-Synuclein Act Distally To Regulate Membrane Binding. J. Am. Chem. Soc. 133:7152–7158.

115. Uversky VN, Yamin G, Munishkina LA, Karymov MA, Millett IS, Doniach S, Lyubchenko YL, Fink AL (2005) Effects of nitration on the structure and aggregation of α-synuclein. Molecular Brain Research 134:84–102.

116. Zhao K, Lim Y-J, Liu Z, Long H, Sun Y, Hu J-J, Zhao C, Tao Y, Zhang X, Li D, et al. (2020) Parkinson's disease-related phosphorylation at Tyr39 rearranges α-synuclein amyloid fibril structure revealed by cryo-EM. Proc. Natl. Acad. Sci. U.S.A. 117:20305–20315.

117. Gentile I, Garro HA, Delgado Ocaña S, Gonzalez N, Strohäker T, Schibich D, Quintanar L, Sambrotta L, Zweckstetter M, Griesinger C, et al. (2018) Interaction of Cu(I) with the Met-X $_3$ -Met motif of alpha-synuclein: binding ligands, affinity and structural features. Metallomics 10:1383–1389.

118. McLean PJ, Kawamata H, Hyman BT (2001) α-Synuclein–enhanced green fluorescent protein fusion proteins form proteasome sensitive inclusions in primary neurons. Neuroscience 104:901–912.

119. Bartels T, Ahlstrom LS, Leftin A, Kamp F, Haass C, Brown MF, Beyer K (2010) The N-Terminus of the Intrinsically Disordered Protein α-Synuclein Triggers Membrane Binding and Helix Folding. Biophysical Journal 99:2116–2124.

120. Man WK, Tahirbegi B, Vrettas MD, Preet S, Ying L, Vendruscolo M, De Simone A, Fusco G (2021) The docking of synaptic vesicles on the presynaptic membrane induced by α-synuclein is modulated by lipid composition. Nat Commun 12:927.

121. Cali F, Cantone M, Cosentino FII, Lanza G, Ruggeri G, Chiavetta V, Salluzzo R, Ragalmuto A, Vinci M, Ferri R (2019) Interpreting Genetic Variants: Hints from a Family Cluster of Parkinson's Disease. JPD 9:203–206.

122. Minafra, B., Buongarzone, G., Gana, S., Valente, M.L., Palmieri, I., Biagini, T., Plumari, M., Avenali, M, Zangaglia, R., Mazza, T., et al. A novel likely pathogenic SNCA variant associated with Parkinson's disease [abstract]. In: ; 2020. Available from: https://www.mdsabstracts.org/abstract/a-novel-likely-pathogenic-snca-variant-associated-with-parkinsons-disease/

123. Daida K, Shimonaka S, Shiba-Fukushima K, Ogata J, Yoshino H, Okuzumi A, Hatano T, Motoi Y, Hirunagi T, Katsuno M, et al. (2022) A-SYNUCLEIN V15A Variant in Familial Parkinson's Disease Exhibits a Weaker Lipid-Binding Property. Movement Disorders 37:2075–2085.

124. Bodner CR, Dobson CM, Bax A (2009) Multiple Tight Phospholipid-Binding Modes of α-Synuclein Revealed by Solution NMR Spectroscopy. Journal of Molecular Biology 390:775–790.

125. Didonna A, Benetti F, 1 Department of Neurology, University of California San Francisco, San Francisco, CA 94158, USA (2015) Post-translational modifications in neurodegeneration. AIMS Biophysics 3:27–49.

126. Sambataro F, Pennuto M (2017) Post-translational Modifications and Protein Quality Control in Motor Neuron and Polyglutamine Diseases. Front. Mol. Neurosci. [Internet] 10. Available from: http://journal.frontiersin.org/article/10.3389/fnmol.2017.00082/full

127. Son SM, Park SJ, Fernandez-Estevez M, Rubinsztein DC (2021) Autophagy regulation by acetylation—implications for neurodegenerative diseases. Exp Mol Med 53:30–41.

128. Vinueza-Gavilanes R, Íñigo-Marco I, Larrea L, Lasa M, Carte B, Santamaría E, Fernández-Irigoyen J, Bugallo R, Aragón T, Aldabe R, et al. (2020) N-terminal acetylation mutants affect alpha-synuclein stability, protein levels and neuronal toxicity. Neurobiology of Disease 137:104781.

129. Bartels T, Kim NC, Luth ES, Selkoe DJ (2014) N-Alpha-Acetylation of α-Synuclein Increases Its Helical Folding Propensity, GM1 Binding Specificity and Resistance to Aggregation Pastore A, editor. PLoS ONE 9:e103727.

130. Kang L, Moriarty GM, Woods LA, Ashcroft AE, Radford SE, Baum J (2012) N-terminal acetylation of α-synuclein induces increased transient helical propensity and decreased aggregation rates in the intrinsically disordered monomer. Protein Science 21:911–917.

131. Bu B, Tong X, Li D, Hu Y, He W, Zhao C, Hu R, Li X, Shao Y, Liu C, et al. (2017) N-Terminal Acetylation Preserves α-Synuclein from Oligomerization by Blocking Intermolecular Hydrogen Bonds. ACS Chem. Neurosci. 8:2145–2151.

132. Birol M, Wojcik SP, Miranker AD, Rhoades E (2019) Identification of N-linked glycans as specific mediators of neuronal uptake of acetylated α-Synuclein Bates GP, editor. PLoS Biol 17:e3000318.

133. De Oliveira RM, Vicente Miranda H, Francelle L, Pinho R, Szegö ÉM, Martinho R, Munari F, Lázaro DF, Moniot S, Guerreiro P, et al. (2017) The mechanism of sirtuin 2–mediated exacerbation of alpha-synuclein toxicity in models of Parkinson disease Bates G, editor. PLoS Biol 15:e2000374.

134. Strohäker T, Jung BC, Liou S-H, Fernandez CO, Riedel D, Becker S, Halliday GM, Bennati M, Kim WS, Lee S-J, et al. (2019) Structural heterogeneity of α-synuclein fibrils amplified from patient brain extracts. Nat Commun 10:5535.

135. Fantini J, Yahi N (2011) Molecular Basis for the Glycosphingolipid-Binding Specificity of α-Synuclein: Key Role of Tyrosine 39 in Membrane Insertion. Journal of Molecular Biology 408:654–669.

136. Park J, Kim KS, Lee S, Ryu J, Chung KC, Choo Y, Jou I, Kim J, Park SM (2009) On the mechanism of internalization of α-synuclein into microglia: roles of ganglioside GM1 and lipid raft. Journal of Neurochemistry 110:400–411.

137. Masaracchia C, Hnida M, Gerhardt E, Lopes Da Fonseca T, Villar-Pique A, Branco T, Stahlberg MA, Dean C, Fernández CO, Milosevic I, et al. (2018) Membrane binding, internalization, and sorting of alpha-synuclein in the cell. acta neuropathol commun 6:79.

138. Lan-Mark S, Miller Y (2022) Insights into the Interactions that Trigger the Primary Nucleation of Polymorphic α-Synuclein Dimers. ACS Chem. Neurosci. 13:370–378.

139. Zhang Y, Wang Y, Liu Y, Wei G, Ding F, Sun Y (2022) Molecular Insights into the Misfolding and Dimerization Dynamics of the Full-Length α-Synuclein from Atomistic Discrete Molecular Dynamics Simulations. ACS Chem. Neurosci. 13:3126–3137.

140. Kumari P, Ghosh D, Vanas A, Fleischmann Y, Wiegand T, Jeschke G, Riek R, Eichmann C (2021) Structural insights into α-synuclein monomer–fibril interactions. Proc. Natl. Acad. Sci. U.S.A. 118:e2012171118.

141. Zhou Y, Yao Y, Yang Z, Tang Y, Wei G (2023) Naphthoquinone–dopamine hybrids disrupt α-synuclein fibrils by their intramolecular synergistic interactions with fibrils and display a better effect on fibril disruption. Phys. Chem. Chem. Phys. 25:14471–14483.

142. Runwal G, Edwards RH (2021) The Membrane Interactions of Synuclein: Physiology and Pathology. Annu. Rev. Pathol. Mech. Dis. 16:465–485.

143. Shen J, Du T, Wang X, Duan C, Gao G, Zhang J, Lu L, Yang H (2014) α-Synuclein amino terminus regulates mitochondrial membrane permeability. Brain Research 1591:14–26.

144. Diaw SH, Borsche M, Streubel-Gallasch L, Dulovic-Mahlow M, Hermes J, Lenz I, Seibler P, Klein C, Brüggemann N, Vos M, et al. (2023) Characterization of the pathogenic α-Synuclein Variant V15A in Parkinson´s disease. npj Parkinsons Dis. 9:148.

145. Davidson WS, Jonas A, Clayton DF, George JM (1998) Stabilization of α-Synuclein Secondary Structure upon Binding to Synthetic Membranes. Journal of Biological Chemistry 273:9443–9449.

146. Chen SW, Drakulic S, Deas E, Ouberai M, Aprile FA, Arranz R, Ness S, Roodveldt C, Guilliams T, De-Genst EJ, et al. (2015) Structural characterization of toxic oligomers that are kinetically trapped during α-synuclein fibril formation. Proc. Natl. Acad. Sci. U.S.A. [Internet] 112. Available from: https://pnas.org/doi/full/10.1073/pnas.1421204112

147. Gram H, Theologidis V, Boesen T, Jensen PH (2023) Sarkosyl differentially solubilizes patient-derived alpha-synuclein fibril strains. Front. Mol. Biosci. 10:1177556.

148. Törnquist M, Michaels TCT, Sanagavarapu K, Yang X, Meisl G, Cohen SIA, Knowles TPJ, Linse S (2018) Secondary nucleation in amyloid formation. Chem. Commun. 54:8667–8684.

149. Gaspar R, Meisl G, Buell AK, Young L, Kaminski CF, Knowles TPJ, Sparr E, Linse S (2017) Secondary nucleation of monomers on fibril surface dominates *α* -synuclein aggregation and provides autocatalytic amyloid amplification. Quart. Rev. Biophys. 50:e6.

150. Cheon M, Chang I, Mohanty S, Luheshi LM, Dobson CM, Vendruscolo M, Favrin G (2007) Structural Reorganisation and Potential Toxicity of Oligomeric Species Formed during the Assembly of Amyloid Fibrils Shakhovich EI, editor. PLoS Comput Biol 3:e173.

151. Chakraborty P, Rivière G, Hebestreit A, De Opakua AI, Vorberg IM, Andreas LB, Zweckstetter M (2023) Acetylation discriminates disease-specific tau deposition. Nat Commun 14:5919.

152. Yang Y, Shi Y, Schweighauser M, Zhang X, Kotecha A, Murzin AG, Garringer HJ, Cullinane PW, Saito Y, Foroud T, et al. (2022) Structures of α-synuclein filaments from human brains with Lewy pathology. Nature 610:791–795.

153. Li L, Nguyen BA, Mullapudi V, Li Y, Saelices L, Joachimiak LA (2023) Disease-associated patterns of acetylation stabilize tau fibril formation. Structure 31:1025-1037.e4.

154. Kabir F, Atkinson R, Cook AL, Phipps AJ, King AE (2023) The role of altered protein acetylation in neurodegenerative disease. Front. Aging Neurosci. 14:1025473.

8. Appendix

8.1. Fasta sequence from UniProt

>sp|P37840|SYUA_HUMAN Alpha-synuclein OS=Homo sapiens OX=9606 GN=SNCA PE=1 SV=1

MDVFMKGLSK AKEGVVAAAE KTKQGVAEAA GKTKEGVLYV GSKTKEGVVH GVATVAEKTK EQVTNVGGAV VTGVTAVAQK TVEGAGSIAA ATGFVKKDQL GKNEEGAPQE GILEDMPVDP DNEAYEMPSE EGYQDYEPEA

8.2. Mass spectrometry of aSyn

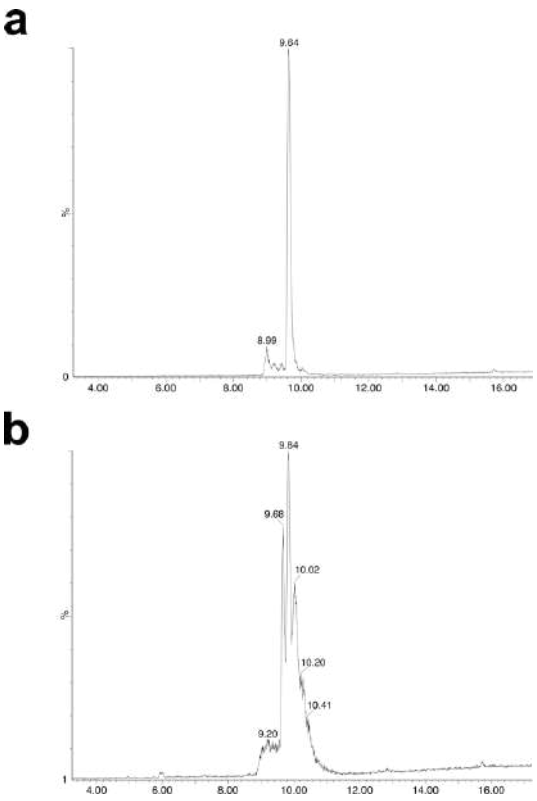

Figure 35: Mass spectrometry of aSyn. a) N-terminal acetylated protein. b) Acetylation of lysines in the monomer species of aSyn.

8.3. Molecule of phthalocyanine tetrasulfonate